Development and evaluation of PET tracers for imaging ÿØ-glucuronidase activity in cancer and inflammation

Antunes, Ines Farinha

Development and evaluation of PET tracers for imaging β-glucuronidase activity in cancer and inflammation

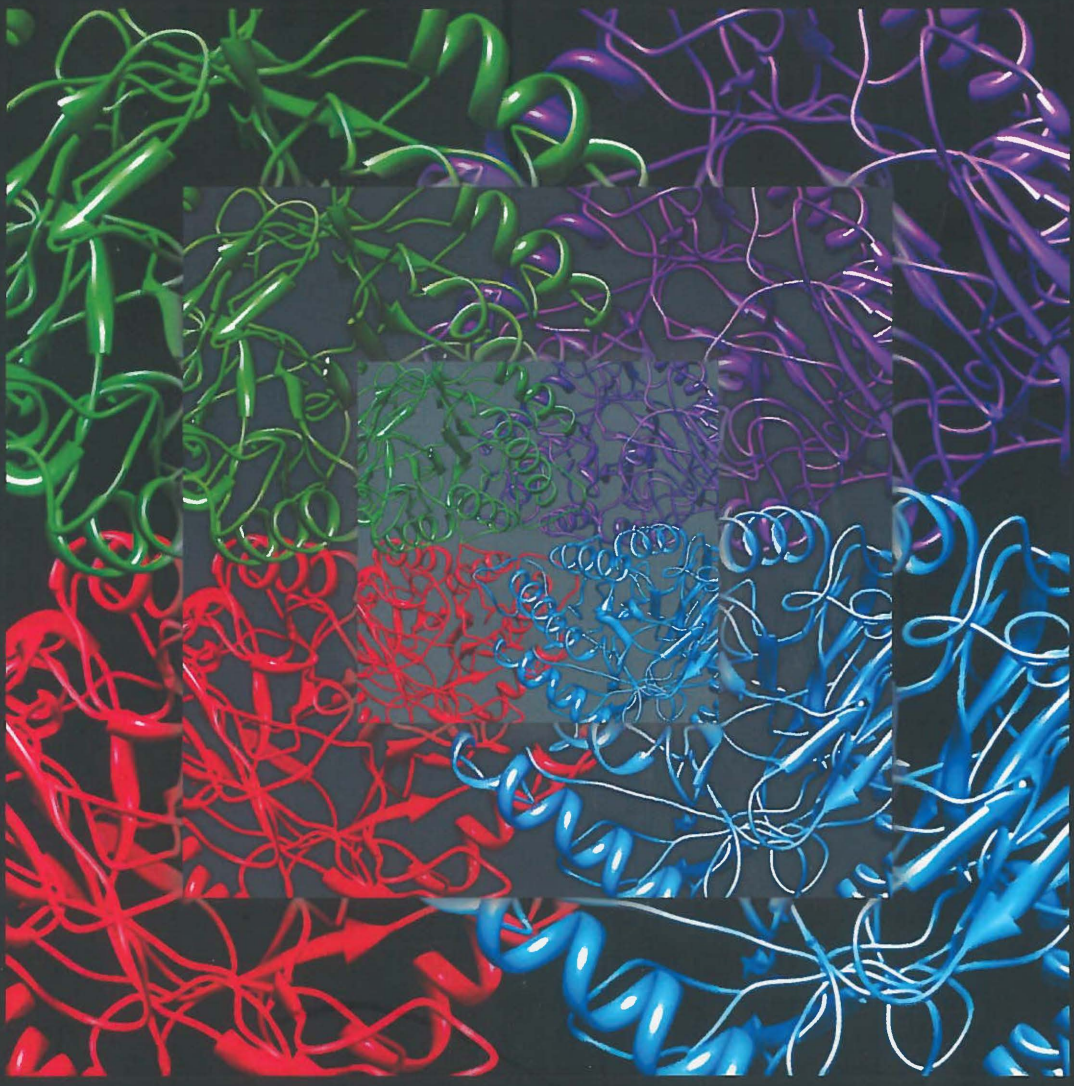

Inês Farinha Antunes

To Karol

Stellingen

Behorende bij het proefschrift

1. Prodrug research needs more imagination and less dependency on what has been tried in the past. (Valentino J. Stella; Advanced drug delivery reviews, 1996)
2. β-glucuronidase-based prodrug therapy can be applied in the treatment of cancer, but also in inflammatory disorders (this thesis, chapter 2)
3. PET can be an attractive tool to evaluate new enzyme-prodrug combinations and to optimize treatment strategies. (this thesis, chapter 3 and 4)
4. The best parameter to measure β-glucuronidase activity is the distribution volume of the PET tracer (this thesis, chapter 5)
5. The characteristics of a drug can not always be applied to predict the success of a PET tracer that is derived from this drug. (this thesis, chapter 6)
6. The release of β-glucuronidase accompanies the activation of microglia in neuroinflammation. (this thesis, chapter 7)
7. A single dose of a cytostatic drug can increase the release of β-glucuronidase in small tumors, resulting in enhanced extracellular levels of the prodrug-converting enzyme and therefore could improve the efficacy of glucuronide prodrug treatment. (this thesis, chapter 8)
8. All truths are easy to understand once they are discovered; the point is to discover them. (Galileo Galilei)
9. Being a PhD student is like becoming all of the Seven Dwarves. In the beginning you are Dopey and Bashful. In the middle, you are usually sick (Sneezy), tired (Sleepy), and irritable (Grumpy). But at the end, they call you Doc, and then you are Happy
10. I was taught that the way of progress is neither swift nor easy (Marie Curie; Pierre Curie, 1936, 167)
11. Like taxes, radioactivity has long been with us and in increasing amounts .... consider radiation as something to be treated with respect, avoided when practicable and accepted when inevitable. (Ralph Eugene Lapp, Must we Hide?, 1949, 44)

Printing of this thesis was financially supported by: University of Groningen, University Medical Center Groningen, Graduate School of Drug Exploration (GUIDE), Stichting Ina Veenstra-Rademaker, Von Gahlen, Waters, Covidien and Grace.

Cover: β-glucuronidase. Adapted from Nat. Struct. Biol. 3(4), 375-381, 1996
Cover design: ARTEFINAL, Lta, Portugal
Printed by: WÖHRMANN PRINT SERVICE

CMB.

RIJKSUNIVERSITEIT GRONINGEN

Development and evaluation of PET tracers for imaging β-glucuronidase activity in cancer and inflammation

Proefschrift

ter verkrijging van het doctoraat in de
Medische Wetenschappen
aan de Rijksuniversiteit Groningen
op gezag van de
Rector Magnificus, dr. E. Sterken,
in het openbaar te verdedigen op
woensdag 25 januari 2012
om 14.30 uur

door

Inês Farinha Antunes
geboren op 3 juni 1976
te Cartaxo, Portugal

Promotores:	Prof. dr. R.A.J.O. Dierckx
	Prof. dr. H.J. Haisma
	Prof. dr. P.H. Elsinga
Copromotor:	Dr. E.F.J. de Vries
Beoordelingscommissie:	Prof. dr. G.A.P. Hospers
	Prof. dr. A. Verbruggen
	Prof. dr. G.A.M.S. van Dongen

ISBN: 978-90-367-5228-2

CONTENTS

Chapter

General introduction

BACKGROUND

Dose-limiting side effects often restrict the therapeutic efficacy of drugs. To increase the therapeutic index, the drug could be modified to a less reactive or less cytotoxic prodrug that is converted to the active drug by an enzyme that is selectively expressed at the target site. The endogenous enzyme β-glucuronidase could be and attractive target for this prodrug monotherapy approach. β-Glucuronidase is a lysosomal enzyme which is involved in the degradation of glucosaminoglycans [1;2]. However, high levels of extracellular β-glucuronidase were also found in, for example, various tumor types [3-7], bacterial/viral infection [8;9], the synovial fluid of patients with rheumatoid arthritis [10-12] and neurological disorders [13-16]. Therefore, the high extracellular levels of β-glucuronidase could be exploited to develop a therapy based on a glucuronide prodrug that is selectively cleaved by β-glucuronidase to liberate the active drug at the site where it should exert its effect.

When prodrug therapy is based on elevated activity of β-glucuronidase at the target site, the localization and magnitude of expression of β-glucuronidase are probably the most important factors modulating the target-specificity of the release of the active drug from the glucuronide prodrug. The interindividual and intertissue variability in the activity of β-glucuronidase is high. Thus, the development of non-invasive clinically applicable technologies to monitor and evaluate β-glucuronidase based prodrug therapy has become desirable. A technique that seems especially suited for imaging β-glucuronidase expression is positron emission tomography (PET).

Positron emission tomography is a nuclear medicine imaging technique used to follow cellular and molecular events by injection of a positron-emitting radiolabeled molecular probe (tracer). A cyclotron is used to produce a sample of a positron-emitting radioisotope, which is then attached to the biologically interesting compound with known physiological properties. The most commonly used isotopes for PET imaging are ^{11}C, ^{13}N, ^{15}O and ^{18}F. These isotopes have relatively short half-lives (the time in which half of the radioactivity decays), varying from 2 to 110 min. Nowadays, other isotopes such as ^{68}Ga, ^{82}Rb, ^{89}Zr, ^{124}I and ^{64}Cu are applied as well. Isotopes used for PET imaging have a highly

unstable nucleus, which decays by the conversion of a proton to a neuron, during which a positron is emitted. A positron (β^+) is the anti-particle of an electron, i.e. the positron has the same mass as an electron, but the opposite charge. Because of the abundance of electrons in the tissue, the emitted positron will soon meet an electron and interact. This interaction results in annihilation of the positron and electron. The total mass (m) of both particles is converted to energy (E) according to Einstein's formula $E=mc^2$, where c is the speed of light. The energy is emitted in the form of two photons (γ-rays) of 511 keV each, that travel at opposite directions from the site of annihilation. This characteristic of positron emission is exploited by PET cameras using the principle of coincidence detection. The PET cameras consist of multiple detectors, which are located in a ring around the individual. When two emitted photons are detected simultaneously by two detectors on opposite sides of the PET scanner, a signal will be generated. All the signals together are used to create a 3D image of the radioactivity distribution.

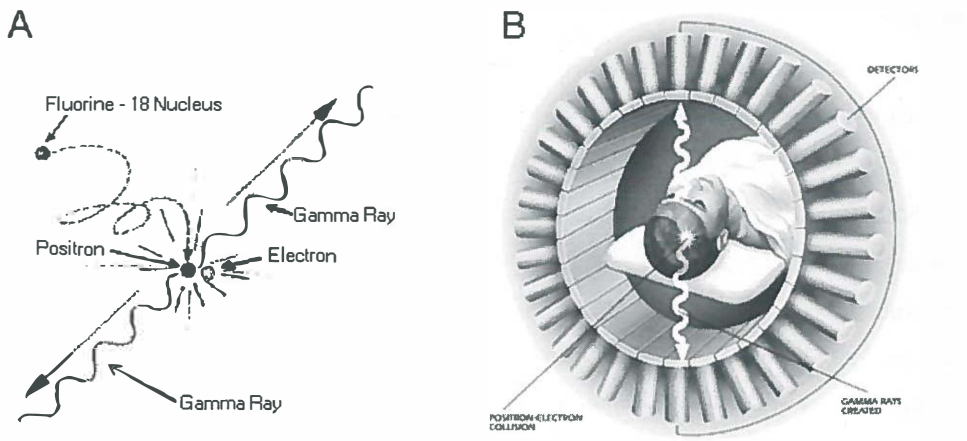

Figure 1. Basic principle of PET. **A)** Positron emission by an unstable nucleus, followed by annihilation with an electron. Adapted from: http://miac.unibas.ch/PMI/07-NuclearMedicine Imaging media/figs/PET_scanner_principle.jpg. **B)** Coincidence detection of photons by the detectors in the PET cameras. Adapted from: http://physiology-physics.blogspot.com/2008/12/pet-scan-particle-physics-and.html.

A PET tracer for imaging β-glucuronidase activity would allow monitoring of the location, magnitude and persistence of β-glucuronidase expression over time. Therefore, PET might give important information about diseases where high levels of extracellular β-glucuronidase are present and it might be used to predict which patients would benefit from β-glucuronidase prodrug therapy, thus improving treatment efficacy.

AIM AND OUTLINE OF THE THESIS

Driven by the lack of PET tracers suitable to monitor extracellular β-glucuronidase, the aim of this thesis was to develop PET tracers for extracellular β-glucuronidase enzyme activity and to use this tracer for evaluation of β-glucuronidase expression in different animal models for various disorders.

Chapter 2 reviews the biological role of β-glucuronidase and its expression in different pathologies. In addition, the applications of β-glucuronidase prodrug therapy are described.

In **chapter 3**, an overview is presented about the use of PET or SPECT tracers for monitoring gene/enzyme expression for prodrug therapy.

In order to evaluate extracellular β-glucuronidase activity a PET tracer had to be developed. In **chapter 4** the synthesis and the *in vitro* cleavage of [^{18}F]FEAnGA by β-glucuronidase was evaluated. [^{18}F]FEAnGA was also tested in mice bearing both CT26 and transfected murine colon adenocarcinoma that expresses membrane-anchored β-glucuronidase on the outer cell membrane (CT26mβGUS). These pilot experiments aimed to demonstrate that the PET tracer could detect extracellular β-glucuronidase *in vitro* and *in vivo*.

Next, an *in vivo* evaluation of [^{18}F]FEAnGA was performed in a less artificial model: i.e. rats bearing C6 gliomas with different dimensions and a sterile muscle inflammation. In the necrotic tumor areas, β-GUS is released by the necrotic tumor cells and infiltrating white blood cells. The C6 glioma is a rapidly growing tumor that becomes necrotic when it grows larger than 1 g. Thus, the large C6 tumors and the inflamed muscle,

both having increased extracellular β-GUS levels, are expected to show enhanced [^{18}F]FEAnGA accumulation. The results of these experiments are described in **chapter 5**.

In an attempt to obtain a PET tracer for β-glucuronidase with better pharmacokinetics, a more lipophilic PET tracer called [^{18}F]FEAnGA-Me was synthesized. [^{18}F]FEAnGA-Me is the methyl ester of [^{18}F]FEAnGA and is activated by a two-step process. First, the methyl ester is hydrolyzed by esterases in plasma, yielding the original tracer [^{18}F]FEAnGA, which is activated by β-glucuronidase at the target site. [^{18}F]FEAnGA-Me was evaluated in the same C6 tumor & inflammation rodent model as [^{18}F]FEAnGA, which is described in **chapter 6**.

The work in chapter 5 suggested that [^{18}F]FEAnGA could be used in inflammatory disorders where high levels of β-glucuronidase are released to the extracellular domain. In **chapter 7,** we investigated the potential of [^{18}F]FEAnGA as novel tracer for β-glucuronidase imaging in neuroinflammation.

The work in chapter 5 also indicated that, the most fast growing forms of cancer are likely to be the best targets β-glucuronidase prodrug therapy, because in these tumors high levels of β-glucuronidase are present in necrotic areas. However in small tumors the efficacy of prodrug therapy is smaller due to the low levels of extracellular β-glucuronidase within these tumors. In **chapter 8** we investigated whether a single dose of a cytostatic drug could induce the release of β-glucuronidase in small tumors, resulting in a higher efficacy of the prodrug treatment.

Finally, in **chapter 9** a summary of the studies performed in this thesis is given and **chapter 10** describes the future perspectives with concluding remarks.

REFERENCES

1. Chen X, Wu B, and Wang PG (2003) Curr. Med. Chem. Anticancer Agents 3:139-150.
2. De Graaf M, Boven E, Scheeren HW, Haisma HJ, and Pinedo HM (2002) Curr. Pharm. Des 8:1391-1403.
3. Bauer HG, Asp NG, Oste R, Dahlqvist A, and Fredlund PE (1979) Cancer Res. 39:3752-3756.
4. Beratis NG, Kaperonis A, Eliopoulou MI, Kourounis G, and Tzingounis VA (2005) J. Cancer Res. Clin. Oncol. 131:371-376.
5. Kim DH and Jin YH (2001) Arch. Pharm. Res. 24:564-567.
6. Sperker B, Werner U, Murdter TE, Tekkaya C, Fritz P, Wacke R, Adam U, Gerken M, Drewelow B, and Kroemer HK (2000) Naunyn Schmiedebergs Arch. Pharmacol. 362:110-115.
7. Whitaker BL (1960) Br. J. Cancer 14:471-477.
8. Selvaraj P, Kannapiran M, Reetha AM, Uma H, Xavier T, and Narayanan PR (1997) Int. J. Tuberc. Lung Dis. 1:265-269.
9. Vishwanath V, Meera R, Puvanakrishnan R, and Narayanan PR (1997) Mol. Cell Biochem. 175:169-175.
10. Moro L, de BB, and Gonano F (1975) Clin. Chim. Acta 65:371-377.
11. Ortutay Z, Polgar A, Gomor B, Geher P, Lakatos T, Glant TT, Gay RE, Gay S, Pallinger E, Farkas C, Farkas E, Tothfalusi L, Kocsis K, Falus A, and Buzas EI (2003) Arthritis Rheum. 48:2163-2172.
12. Vijayan V, Shyni GL, and Helen A (2010) Inflammation.
13. Cross AJ, Crow TJ, Dawson JM, Ferrier IN, Johnson JA, Peters TJ, and Reynolds GP (1986) J. Neurochem. 47:882-889.
14. Cuzner ML, Barnard RO, MacGregor BJ, Borshell NJ, and Davison AN (1976) J. Neurol. Sci. 29:323-334.
15. McGeer EG, McGeer PL, Akiyama H, and Harrop R (1989) Can. J. Neurol. Sci. 16:511-515.
16. McGeer EG, McGeer PL, Harrop R, Akiyama H, and Kamo H (1990) J. Neurosci. Res. 27:612-619.

Chapter

β-Glucuronidase in health and disease: Opportunities for therapy

Inês F. Antunes, Hidde J. Haisma,
Philip H. Elsinga, Rudi A. Dierckx, Erik F. J. de Vries

Submitted for publication

ABSTRACT

β-Glucuronidase (EC 3.2.1.31), is a hydrolytic enzyme present mainly in lysosomes that is involved in intralysosomal protein-turnover and degradation of the extracellular matrix once secreted. In recent years, however, β-glucuronidase has also been accredited with more specific functions, including roles in bone remodeling, healing of tissue injuries, inflammation and infection, cell death and cancer cell invasion. Importantly, in certain conditions there can be either a lack or an excess of β-glucuronidase expression leading to a pathological state. This review offers an overview of the different expression levels of β-glucuronidase present in diseases and how the enzyme can be exploited for therapy.

1. β-Glucuronidase

β-Glucuronidase is a lysosomal enzyme which catalyses the hydrolysis of β-D-glucuronic acid residues of mucopolysaccharides (also referred to as glycosaminoglycans, GAGs), such as heparin sulfate, chondroitin sulfate and dermatan sulfate. β-Glucuronidase is localized in the cell in the lysosomes, but it was also found in microsomes [1;2]. The optimal pH for activity of human β-glucuronidase is 4 to 5, which resembles the pH in lysosomes. At physiological tissue pH, the enzyme displays only 10% activity. β-Glucuronidase is resistant to denaturation and proteolytic attack and is stable at temperatures up to 70 °C [3].

1.1. Structure

β-Glucuronidase is a homotetramer of 332 kDa (Fig. 1) which contains four identical monomers of 77 kDa with a single chain of 651 amino acids localized in lysosomes of cells [4]. Each polypeptide chain undergoes several post-translational modifications (signal sequence cleavage, N-linked glycosylation, disulfide bond formation and tetramerization) following their synthesis on membrane-bound ribosomes. During transit to the Golgi the newly synthesized enzyme is phosphorylated via a 2 step process catalyzed by N-acetylglucosamine 1–phosphotransferase and N-acetylglucosamine phosphodiester glycosidase to generate a common recognition marker, mannose-6-phosphate (M6P). These M6P residues are then recognized in the trans-Golgi network by specific receptors that transport lysosomal enzymes to lysosomes. In addition, β-glucuronidase is reduced by 2-3 kDa at its C-terminus in endosomes during transport to the lysosomes [5;6].

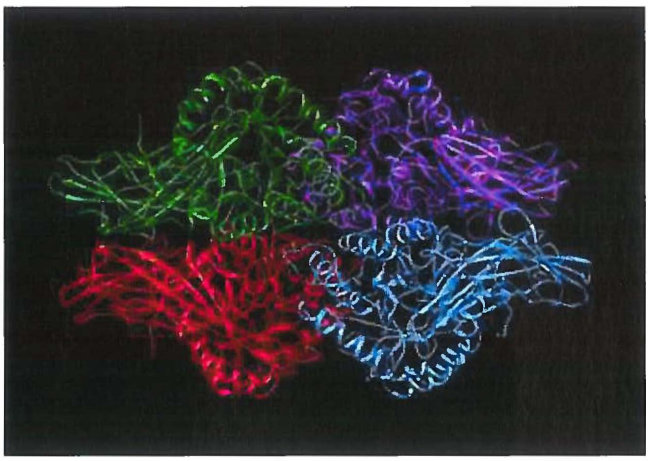

Figure 1. Stereo ribbon diagrams of human β-glucuronidase in the homotetramer. Adapted from: Nat. Struct. Biol. 3(4), 375-381, 1996.

1.2. Mechanism of catalysis

β-Glucuronidase is a glycohydrolase, member of a β-glycosidases family (Family 2) known to hydrolyze their substrates with net retention of anomeric configuration, presumably via a double displacement mechanism involving the action of active site carboxylic acid residues. Three amino acid residues within the active site cavity have been associated with catalytic activity. Glu^{540} acts as a nucleophile, Glu^{451} as an acid-base catalyst and Tyr^{504} is also involved, although its role is unclear [7].

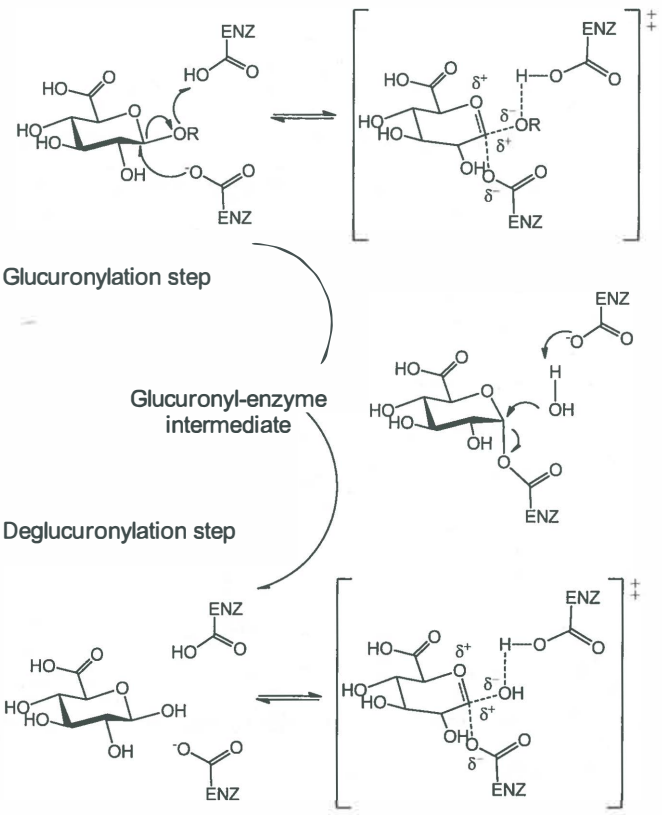

Figure 2. Proposed mechanism for β-glucuronidase catalyzed hydrolysis of glucuronides.

The proposed mode of action of β-glucuronidase in the hydrolysis of the sugar moiety of glucuronide conjugates is depicted in figure 2. The first step involves nucleophilic attack by one of the carboxylate residues within the active site of the enzyme on the sugar anomeric center. In the second step, the intermediate is hydrolyzed by the base-catalyzed attack of water at the anomeric center, resulting in cleavage of the glycosydic bond with net retention of the anomeric configuration [7].

2. β-Glucuronidase assays

In general, the most favored method of detecting and assaying glycosidase hydrolases is to incubate the enzyme with a substrate that is as close to the natural substrate as possible, but which will liberate a molecule that can be quantified on the basis of its color, fluorescence, or chemiluminescence. The usual assays involve incubation with a substrate glycoside. Phenolphthalein-β-glucuronide and 4-nitrophenyl-β-glucuronide [8;9] are the most commonly used substrates in colorimetrical tests, whereas the more sensitive fluorometric assay has mostly been used with the substrate 4-methylumbelliferyl-β-glucuronide [10]. For *in situ* functional assays, a variety of enzymatic histochemical methods have been described using substrates like 8-hydroxyquinoline-β-glucuronide, naphtol AS-BI-β-glucuronide and 5-bromo-4-chloro-3-indolyl-β-glucuronide [11-13]. In addition, polymerase chain reaction (PCR) and reverse-transcription polymerase chain reaction (RT-PCR) have been used to detect mRNA expression of β-glucuronidase [14]. This last technique has been found to be most useful in determining β-glucuronidase expression for Gene Therapy. However, PCR and RT-PCR do not give any information about the protein levels or the enzyme activity.

3. Physiological role

β-Glucuronidase is an acid hydrolase. Its main physiological role is glycosaminoglycan degradation in the lysosome by removing terminal β-glucuronosyl residues from oligosaccharadies. However, the function of β-glucuronidase is not limited to intralysosomal protein-turnover. It has become apparent that this enzyme (among other hydrolases) has a role in cartilage degradation, bone resorption and bone remodeling [15;16]. In addition, since β-glucuronidase is present in leukocytes, one can expect a vital function in protecting the body against infection and inflammation [17;18]

4. Pathological role

For numerous reasons, including predisposition and external stimulation, expression of β-glucuronidase can be altered leading to pathological conditions. In pathological

conditions, β-glucuronidase expression can either be upregulated or downregulated. In the following paragraphs, we present an overview of the disorders, in which altered β-glucuronidase expression has been observed.

4.1. Low expression of β-glucuronidase

Mucopolysaccharidosis (MPS) VII (Sly syndrome) is caused by the mutation in the GUSB gene. This gene provides instructions for producing the lysosomal enzyme β-glucuronidase, which is involved in the degradation of large sugar molecules called glycosaminoglycans (GAGs). Mutation in the GUSB gene reduce or completely eliminates the function of β-glucuronidase. This lack in β-glucuronidase results in an inability to metabolize the GAGs, such as dermatan sulfate (DS), heparan sulfate (HS) and chondroitin sulfate (CS). Accumulation of intact GAGs affects a number of organ systems, including the liver, spleen, skeletal system, eye, heart and brain. The clinical features of MPS VII vary from patient to patient, but all have short stature due to growth retardation and some have mental retardation. Survival into adulthood is common with milder cases and osteoarthritis is a common complication [19;20].

4.2. High expression of β-glucuronidase

There are three discrete situations, in which β-glucuronidase (among other lysosomal hydrolases) and other inflammatory substances, ordinarily sequestered in membrane-bounded granules, can gain access to the exterior of cells [21;22]. The first circumstance is *cell death*, resulting in damage of the cell membrane. Under these circumstances, cytoplasmic enzymes, potassium, cellular constituents and lysosomal hydrolases find their way into the surrounding tissues. The cell does not die, because lysosomal hydrolases are released into its cytoplasm, but because injury to other parts of the cell, especially the cell membrane, cannot be reversed. The second mechanism, *Endocytosis*, is perhaps more common in pathology. Whenever cells engage in phagocytosis, pinocytosis or receptor-mediated endocytosis, they release a portion of their hydrolases (acid phosphatase and β-glucuronidase) into the surrounding medium, unassociated with damage to the cells. This

appears to be due to the extrusion of lysosomal materials from, as yet, incompletely closed phagosomes, open at their internal border by lysosomes actively discharging β-glucuronidase into the vacuole. The third mechanism of β-glucuronidase release is called *exocytosis,* where intracellular vesicles in the cytoplasm fuse with the plasma membrane and release or "secrete" their contents into the extracellular space (Fig. 3).

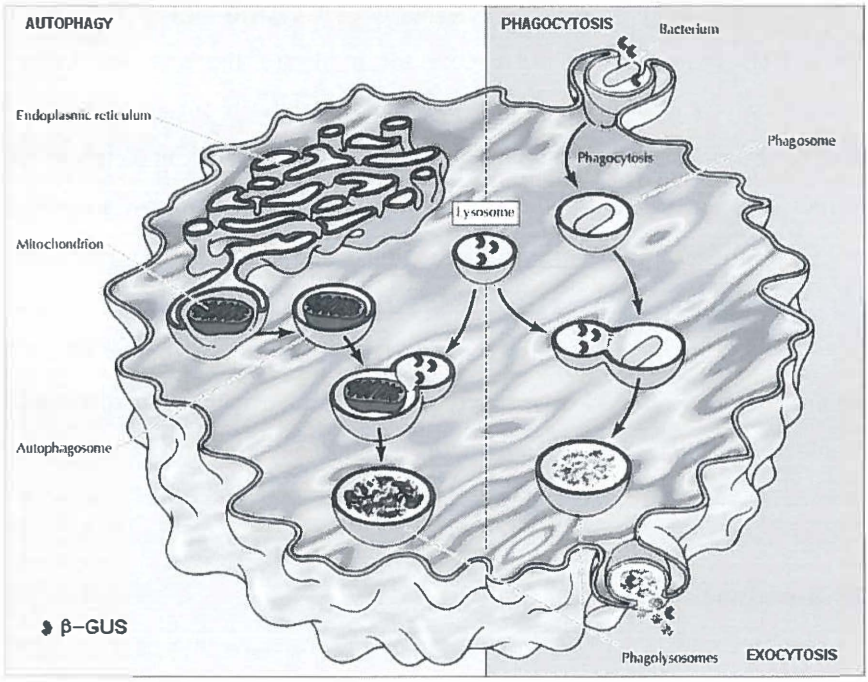

Figure 3. A schematic example of β-glucuronidase secretion during endocytosis or exoxytosis. Adapted from www.ncbi.nlm.nih.gov/books/NBK9953/bin/ch9f37.jpg

4.2.1. Inflammation

Since the description of lysosomes by de Duve in 1955 as a new group of cytoplasmic organelles, they have been assigned a central role in many processes involving intracellular digestion, autolysis, and tissue injury. In the 1960s β-glucuronidase was introduced into the field of inflammation, when high levels of β-glucuronidase were found in inflammatory lesions. It was hypothesized that these high levels of extracellular β-glucuronidase could be due to pathogenic or lysosomal origin [23]. It has been shown that

patients with active granulomatous diseases, such as tuberculosis, sarcoidosis as well as some patents with Crohn´s disease have elevated levels of β-glucuronidase that appears to correlate with the degree of severity of the clinical illness [24].Increased activity of β-glucuronidase in extracellular fluids has been found in synovial fluid (SF) of rheumatoid arthritis, gingival crevicular fluid (GCF) of periodontitis, CSF of bacterial meningitis and in plasma of patients with acquired immunodeficiency syndrome (Table1).

Inflammation of the lungs

Pneumotoxicans exposure or the presence of pathogens in the lung results in activation of phagocytic alveolar macrophages (AMs) followed by an acute inflammatory response and damage to the respiratory epithelial cells and interstitial matrix. During the phagocytic process the activated macrophages generate superoxide anions and release lysosomal hydrolytic enzymes such as β-glucuronidase, which are involved in the killing and/or degradation of the engulfed pathogen or pneumotoxicans. β-glucuronidase was found to be increased in bronchoalveolar lavage fluid (BALF) of rodents after inhalation of respirable pneumotoxicants (mineral dust and diesel) [25]. β-Glucuronidase was also found to be increased in serum of patients with Coal workers' pneumoconiosis (CWP), which is usually complicated by a chronic inflammatory response and progressive massive fibrosis due to prolonged exposure to coal dust [26]. Moreover, high levels of β-glucuronidase were found in the lungs of patients suffering from tuberculosis [27].

Periodontitis

Periodontitis is a set of inflammatory diseases, affecting the tissues that surround and support the teeth. Periodontitis is caused by microorganisms that adhere to and grow on the tooth's surface, and is associated with an overly aggressive immune response against these microorganisms. During periodontal destruction, host cells (mainly PMNs) release granular enzymes that are capable of attacking all extracellular matrix components. β-Glucuronidase is an important component of the primary granules of PMN that contributes to non-collagenous matrix degradation in periodontal diseases. As a result,

salivary levels of β-glucuronidase in gingival crevicular fluid (GCF) are increased, which was suggested to be a good indicator or predictor of periodontal diseases activity [28-30].

Rheumatoid arthritis

Rheumatoid arthritis (RA) is a chronic progressive autoimmune disorder, which is characterized by the irreversible destruction of hyaline cartilage. During arthritis, the nature of the lysosomal membrane gets altered, causing lysosomes to fuse with the cell membrane and extrude an array of enzymes like β-glucuronidase, β-hexosaminidase, cathesin D and collagenolytic enzymes. These enzymes solubilize collagen, destroy structural macromolecules of connective tissues and alter the metabolism of glycosaminoglycans (GAGs) and glycoproteins, causing disruption of cellular activities [31]. In the 1970s Moro *et al*. reported elevated levels of β-glucuronidase in the synovial fluid of arthritic patients [32]. In addition, Ortutay *et al*. found that β-glucuronidase, β-hexosaminidase alone or in combination with matrix metalloproteinases, proved to be effective in depleting glycosaminiglycans from cartilage and thereby facilitating the invasion of synovial cells and their attachment to cartilage in RA. They concluded that β-glucuronidase or β-hexosaminidase may be useful markers in assessing the degree and type of join destruction [33].

Neurological disorders

Many neurological disorders, such as Alzheimer's disease, Huntington's disease, Parkinson's disease and multiple sclerosis, are associated with neurodegenerative processes. Despite the large differences between these disorders, they are all accompanied by neuronal loss and the increase of hydrolase enzymes, such as β-glucuronidase. Therefore, β-glucuronidase has been suggested as biomarker for gliosis or glial proliferation. Cross *et al*. found a significant increase in the activity of β-glucuronidase in both temporal cortex of patients with Alzheimer's disease and putamen of patients with Huntington's disease, suggesting that β-glucuronidase could be a biochemical indicator of cellular damage in the central nervous system [34]. While McGeer *et al*.

indicated that the apparent correlation between low brain metabolism ([^{18}F]FDG uptake in the PET scan) in patients with Alzheimer's disease and β-glucuronidase activity determined post-mortem is consistent with previous suggestions that the decrease in metabolism reflects local neuronal loss and gliosis [35;36].

Table 1. Release of β-glucuronidase in different disorders associated with inflammation/infection. PMNs= Polymorphonuclear leucocytes; MNs=Mononuclear leukocytes; MPGs=Macrophages; AMPGs=Alveolar macrophages; CSF= cerebral spinal fluid; PF=peritoneal fluid; GCF=gingival crevicular fluid; AIDS=acquired immune deficiency syndrome; MS= multiple sclerosis and RA= rheumatoid arthritis.

	Sample	Origin of β-glucuronidase	Reference
Infection			
Leprosy	serum	PMNs	[37-39]
Tuberculosis	macrophages	MPGs	[27,40]
AIDS	serum	PMNs	[41;42]
Gallstone	Bile samples	Hepatocytes/PMNs	[43-46]
Bacterial meningitis	CSF	PMNs	[47;48]
Peritonitis	PF	PMNs and MNs	[49]
Inflammation			
Periodontitis	GCF	PMNs	[28-30]
Pneumoconiosis	serum	AMPGs and PMNs	[26]
MS	CSF	Phagocytic cells and/or astroglia	[50;51]
RA	Synovial fluid	PMNs and MNs	[31-33]
Other disorders			
Myocardial infarction	Tissue samples/Serum/Urine	Ischemic necrosis of cardiac muscle	[52-55]
Epilepsy	Serum	Derangement of GAG metabolism	[52;56]
Alzheimer's disease	Tissue samples	gliosis	[34-36]
Huntington's disease	Tissue samples	gliosis	[34]

4.2.2. Cancer

High β-glucuronidase activity was first found in white blood cells of human leukemia patients and Hodgkin's disease patients in 1950 [57]. In subsequent years, high β-glucuronidase activity was found in serum, urine or tissue of breast cancer patients, uterine cancer patients, genital cancer, colon cancer and many other cancers (Table2).

Increased activity of β-glucuronidase in tumor tissue, as opposed to normal tissues, has been shown to be due to increased expression of the enzyme. The high expression of β-glucuronidase in a wide range of malignancies, such as gastrointestinal, lung and breast carcinomas, and melanomas, is particularly localized in necrotic areas. When tumors grow to a certain size, blood supply to the tumor will become insufficient and some regions of the tumor will become deprived from nutrients, resulting in the induction of an autophagosomal process. When the deprived cells die, β-glucuronidase is released from the lysosomes, which stimulates the aseptic autolysis and could contribute to inflammatory effects. The inflammatory changes that are seen, including edema and tissue liquefaction, are accompanied by infiltration of immune cells, which have a high content of β-glucuronidase [58;59]. Studies in human tumor tissue biopsies indicated that the release of β-glucuronidase in necrotic areas can be mainly ascribed to secretion of the enzyme by monocytes and granulocytes [60].

Not only necrotic tumors, but also invasive tumors are associated with increased release of β-glucuronidase. In order for the tumor to grow, malignant cells must invade normal tissue by penetrating through the connective tissues, including basement membranes, and between host cells. The β-glucuronidase released by tumor cells is responsible for the degradation of the proteoglycan matrix as well as the collagen fibers of connective tissues, including those in basement membranes.

Table 2. High levels of extracellular β-glucuronidase in various oncological disorders. NS= Not specified, PhG= Phenolphthalein-β-glucuronide and MuG= 4-methylumbelliferyl-β-glucuronide; ELISA= Enzyme-linked immunosorbent assay

Cancer	Detection	sample	Reference
Head and Neck	qRC-PCR	Lymph nodes	[61]
Renal carcinoma	Chromatic assay (NS)	Urine sample	[62]
Gastric carcinoma	Chromatic assay (PhG)	Gastric aspirate	[63;64]
Ovarian cancer	Chromatic assay (MuG)	Pelvic peritoneal fluid	[65]
Breast cancer	Chromatic assay (PhG)	Serum	[66]
Pancreatic adenocarcinoma	Chromatic assay (MuG)	Pancreatic tissue	[67]
Colon cancer	Chromatic assay (PhG)	Fecal specimens	[68;69]
Hepatocellular carcinoma	ELISA	Serum	[70]
Prostatic cancer	Chromatic assay (PhG)	Tissue	[71]
Bladder carcinoma	Chromatic assay (PhG)	Urine samples	[72]
Hodgkin's disease	Chromatic assay (PhG)	Serum	[57]

5. β-glucuronidase as target for therapy

As follows from the above, the levels of β-glucuronidase can be either downregulated or upregulated, depending on the pathology. In Mucopolysaccharidosis VII (MPS VII) where β-glucuronidase is lacking, the classic treatment consists of organ transplantation, such as liver (an organ highly affected in most MPS VII patients), as well as bone marrow transplantation [73;74]. A related approach is the implantation or transplantation of healthy cells (bone marrow or mesenchymal stem cells) obtained from healthy subjects. These healthy cells, which express wild type or normal copies of the β-glucuronidase, are grown in culture and then implanted in patients who lack the enzyme, hence correcting the defect. Some of these therapies resulted in dramatic reductions of lysosomal storage, improvements in skeletal development, and increased life span [75-80]. However, these therapies are not applicable for an unlimited number of times, due to the lack of

compatible donors and graft-versus-host diseases. Gene therapy using viral vectors has also been under development as a treatment option for MPS VII. Some strategies include somatic gene transfer in animal models using adenovirus, adeno-associated virus, herpesvirus and, more recently, retrovirus and lentivirus vectors which are capable of integrating the exogenous gene sequences into the host genome for prolonged enzyme expression. This last strategy proved to be inefficient in the CNS [81-85]. Currently, enzyme replacement therapy (ERT) is one of the most viable treatments for several lysosomal storage diseases. In the ERT, an injection of small amounts of the active lysosomal enzyme (such as β-glucuronidase) is given to a lysosomal storage disease patient, resulting in reduced amounts of the stored substrates, attenuating the clinical phenotype of the disease. However, this strategy is hampered by the lack of effective delivery of the enzyme into the CNS, underlying the need to improve current strategies.

In the pathological conditions where there is an increase of β-glucuronidase, a prodrug-based therapy has been proposed. Several systems have been developed for enzyme-mediated prodrug therapy. The prodrug-converting enzymes can either be endogenous proteins that are expressed selectively in high concentrations at the target site or exogenous proteins that have been selectively delivered to the target.

Glucuronide-drug conjugates exhibit improved water solubility, stability and lower toxicity towards normal cells than the native drug. However, glucuronide-drug conjugates are susceptible to enzymatic cleavage by β-glucuronidase, resulting in the *in situ* generation of the active drug that can subsequently selectively accumulate into targeted cells. A number of prodrugs for β-glucuronidase have been designed (Table 3) and extensively reviewed elsewhere [86;87]. These prodrugs generally consist of three distinct parts: a trigger, a linker and an effector unit. For β-glucuronidase targeted prodrugs, the trigger and effector units consist of a glucuronide moiety and the active drug, respectively. They are joined together by the linker unit, which should release the drug as fast as possible after prodrug activation via a chemical breakdown [88-90].

Table 3. List of some important glucuronide conjugates studied for Prodrug therapy. MDR= Multidrug Resistance.

Prodrug	Drug	Pharmacology	Reference
Budesonide-β-O-glucuronide 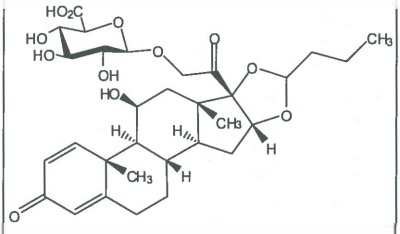	Budesonide	Anti-inflammatory	[91-93]
Quercetin-3-O-glucuronide 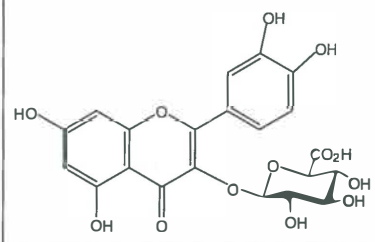	Quercetin Quertecin glucuronide	Anti-inflammatory, antiviral	[94;95]
retinoyl-O-β-glucuronide 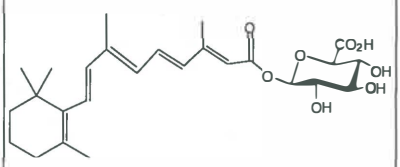	Retinoyl Retinoyl-glucuronide	Cell differentiation	[96;97]
Morphine-6-glucuronide 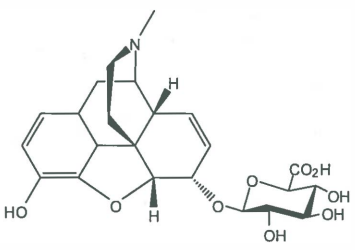	Morphine Morphine-6-glucuronide	Analgesic	[98;99]

Hydroxyaniline mustard glucuronide 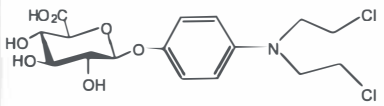 (BHAMG)	p-Hydroxyaniline mustard	DNA intercalation, inhibition of Topoisomerase II redox cycling (Oxidative stress).	[100]
Epirubicin-glucuronide 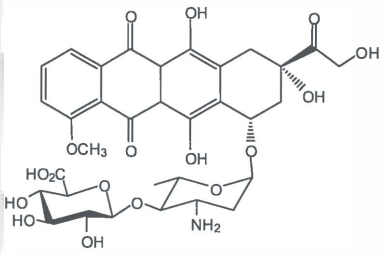	Epirubicin	DNA intercalation, inhibition of Topoisomerase II redox cycling (Oxidative stress).	[101]
Doxorubicin-glucuronides 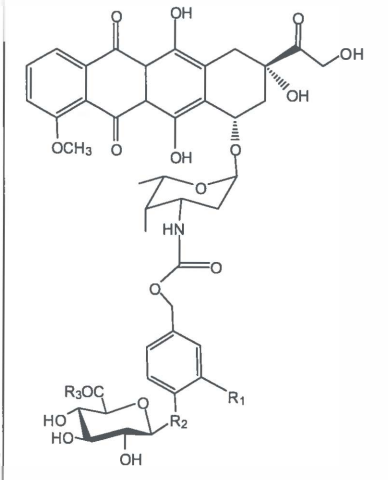 HMR 1826; R_1=NO_2, R_2=O and R_3=OH DOX-GA_3; R_1=H, R_2=OCONH and R_3=OH DOX-mGA_3; R_1=H, R_2=OCONH and R_3=OCH_3	Doxorubicin	DNA intercalation, inhibition of Topoisomerase II redox cycling (Oxidative stress).	[102-104]

Daunorubicin glucuronide 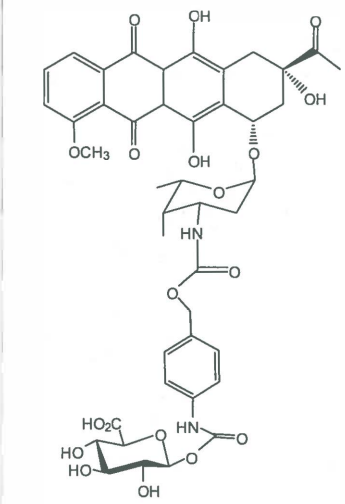 (DNR-GA3)	Daunorubicin	DNA intercalation, inhibition of Topoisomerase II redox cycling (Oxidative stress).	[105]
Paclitaxel glucuronide 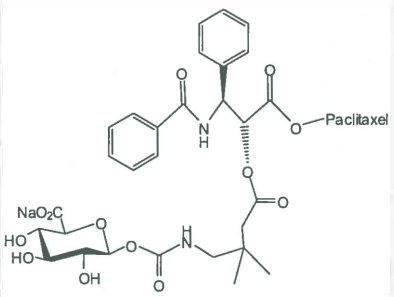	Paclitaxel	Microtubule-binding	[106;107]

9-Aminocamptothecin glucuronide (9-ACG) 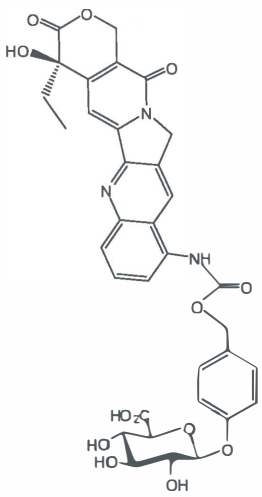	Campthotecin	Inhibition of Topoisomerase I	[108]
5-Fluorouracil glucuronide 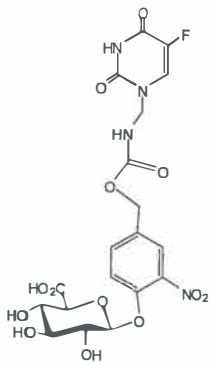 (5-FUG)	9-Fluorouracil	Thymidylate synthase inhibitor	[109]
Verapamil glucuronide 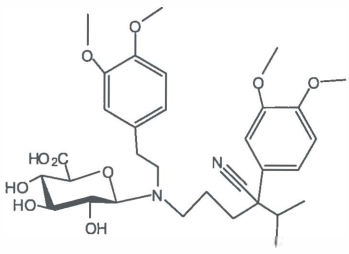	Verapamil	Modulator of Pgp-mediated MDR	[110]

Duocarmycin glucuronide 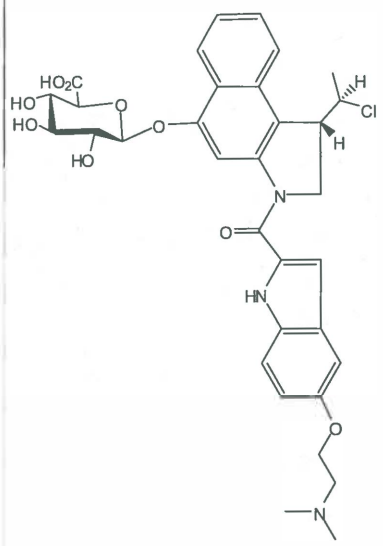	Duocarmycin	DNA-alkylation	[111;112]
Cl-994 glucuronide 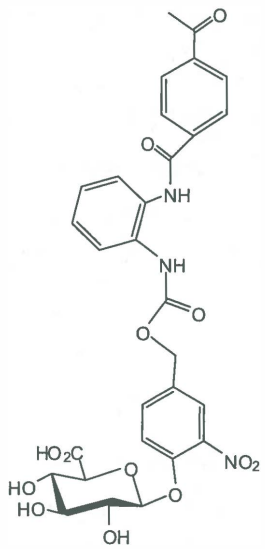	Cl-994	Inhibition of histone deacetylases	[113;114]

Cyclopamine glucuronide 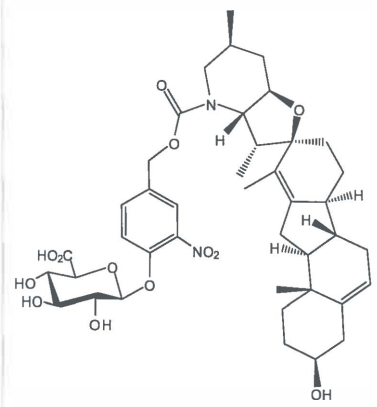	Cyclopamine	Inhibition of cell proliferation and differentiation	[115]

5.1 β-Glucuronidase as target in inflammation treatment

Few studies have been devoted to glucuronide-conjugates as intervention for inflammatory disorders. The orally administered budesonide-β-O-glucuronide, improved the healing of experimentally induced colitis in rats that produced dose limiting side-effects (adrenal suppression) after treatment with the parent drug [82].

Topically applied retinoyl-O-β-glucuronide was found to be highly effective in treating patients with moderate to moderately severe acne without producing the typical side-effects of retinoic acid [97]. However, it is unclear whether retinoyl-O-β-glucuronide is biologically active per se or by its hydrolysis to retinoic acid by β-glucuronidase released during inflammation [116;117].

In another study, Kawai *et al.* found that lipopolysaccharide (LPS)-stimulated macrophages enhanced β-glucuronidase activity, which lead to the generation of quercetin when the cells were exposed to quercetin-3-O-β-glucuronide [118]. Furthermore, Mochizuki *et al.* found that the vascular permeability of quercetin-3-O-β-glucuronide in cultured human aortic endothelial cell inserts was increased by the stimulation of interleukin IL-1, an inflammatory cytokine originating from macrophages [119]. Together, these findings suggest that quercetin-3-O-β-glucuronide can be effectively translocated into the vascular intima if endothelial cells are subjected to

oxidative stress (e.g. exposure to oxidized low-density lipoprotein (LDL)). The translocated glucuronide conjugates can subsequently exert their biological effect as such or after hydrolysis by the increased levels of β-glucuronidase [111].

5.2 Glucuronide prodrugs for cancer treatment

Because glucuronide conjugates of cytotoxic drugs exert much less toxicity to normal tissue than the parent drug, these prodrugs have the potential to become a treatment for cancer with less side effects than conventional chemotherapy. A number of the glucuronide prodrugs have been shown to be more effective antitumor agents in animal models than the corresponding parent drugs. Initially, Connors and Whisson reported a correlation between therapeutic response to aniline mustard in tumor bearing mice and β-glucuronidase activity in tumors [120]. This correlation was further proven, where a mouse tumor with high levels of β-glucuronidase was cured with a single dose of aniline mustard [121]. A clinical trial of aniline mustard in patients with several different types of advanced cancer has shown that only patients with tumors with high β-glucuronidase activity had a therapeutic response [122].

Anthracyclines, like epirubicin, daunorubicin and doxorubicin, are cytostatic agents used in patients with ovarian cancer, breast cancer, lymphomas and soft-tissue sarcomas. Commonly used therapeutic doses of these cytostatics can induce myelosuppression and cardiotoxicity. Therefore, the development of relatively non-toxic glucuronides prodrugs of these active anthracyclines has been extensively studied. Epirubicin-glucuronide was found to be inefficient for enzyme prodrug therapy due to its low conversion to the active drug by β-glucuronidase. However, daunorubicin-glucuronide (DNR-GA3) and doxorubicin-glucuronides: DOX-GA3 (Which contain a bicarbamate spacer) or HMR 1826 (which contained a nitrobenzene spacer), are efficiently hydrolyzed by β-glucuronidase. For these three anthracycline-based glucuronide prodrugs, concentrations of the parent drug in plasma and normal tissue (except kidneys) were significantly lower than after administration of the parent drug itself. Overall, these prodrugs exhibit a superior safety profile compared to the parent drug, particularly with regards to

cardiotoxicity. For example, HMR 1826 is 100 times less cardiotoxic than DOX in animal models. Treatment of OVCAR-3 xenografts with DNR-GA3 resulted in about 70% higher tumor growth inhibition than treatment with daunorubicin. The two glucuronide prodrugs based on doxorubicin, DOX-GA3 and HMR 1826 given in equitoxic doses of DOX, have also been shown to be effective in tumor growth inhibition (in average 87 % and 25 %, against the 65 % and 54 % when treated with DOX itself), when compared to untreated animals [60,104]. The therapeutic index was enhanced due to increased levels of the active drug in tumor tissue after administration of the glucuronide prodrug as compared to the levels after administration of the active drug itself.

9-Aminocampthotecin, and analogue of 20(S)-Camptothecin (inhibitor of topoisomerase I), has displayed promising activity in preclinical tumors and early clinical trials. However, its clinical use has been hindered by its low solubility in water. Therefore, a glucuronide prodrug of 9-aminicapthotecin was synthesized (9ACG). This prodrug was found to be 20-80 times less toxic than 9-aminocampthotecin. In addition, *in vivo* studies have shown that both 9-ACG and 9-AC inhibited LS174T tumor growth by about 80 % [108].

Despite these promising preclinical results, glucuronide prodrugs have not been introduced into the clinic yet. There are some major limitations in the prodrug monotherapy strategy that still need to be overcome. Due to hydrophilic characteristics of the glucuronide prodrugs, their clearance rate is much faster than their conversion rate. Therefore, very high doses of the prodrug are required to achieve a therapeutic effect. This could present a problem for patients under an inflammatory condition where β-glucuronidase is also released. The other potential limitation of glucuronide prodrugs in monotherapy is that they are not activated homogenously throughout the tumor tissue, but only at the site of necrosis and inflammatory cell infiltration. As in small tumors that do not yet contain necrotic areas, the activation of the glucuronide prodrugs will not be possible.

6. Conclusion

Human β-glucuronidase is a very good candidate for selective activation of relatively non toxic prodrugs. First, β-glucuronidase is a human enzyme which is preferred for immunogenicity reasons. Second, it is normally localized in the lysosomes of cells and, therefore, not available for the extracellular glucuronide prodrug. Third, it has been recognized that high levels of β-glucuronidase activity are present extracellularly in necrotic tumor tissue and in inflammatory lesions making prodrug monotherapy a feasible approach. In fact, several successful proof-of-concept studies in animal tumor and inflammation models have been published. Despite these promising preclinical results, however, glucuronide prodrugs have not found extensive use in humans yet. Some major hurdles still need to be taken, before prodrug strategies can be successfully translated from the preclinical proof-of-concept studies to the clinic.

References

1. Bartalos M and Gyorkey F (1963) J. Am. Geriatr. Soc. 11:21-34.
2. Fishman WH, Goldman SS, and DeLellis R (1967) Nature 213:457-460.
3. Brot FE, Bell CE, Jr., and Sly WS (1978) Biochemistry 17:385-391.
4. Jain S, Drendel WB, Chen ZW, Mathews FS, Sly WS, and Grubb JH (1996) Nat. Struct. Biol. 3:375-381.
5. Gabel CA and Foster SA (1986) J. Cell Biol. 102:943-950.
6. Shipley JM, Grubb JH, and Sly WS (1993) J. Biol. Chem. 268:12193-12198.
7. Wong AW, He S, Grubb JH, Sly WS, and Withers SG (1998) J. Biol. Chem. 273:34057-34062.
8. Fishman WH, Springer B, and Brunettei R (1948) J. Biol. Chem. 173:449-456.
9. Szasz G (1967) Clin. Chem. 13:752-759.
10. Omene JA, Adamson I, Okolo AA, and Glew RH (1979) Clin. Chim. Acta 91:213-219.
11. Billett F (1954) Biochem. J. 57:159-162.
12. Schmitz UK, Lonsdale DM, and Jefferson RA (1990) Curr. Genet. 17:261-264.
13. Vaquero C, Masson C, Guigon M, and Hewitt J (1975) Eur. J. Cancer 11:739-742.
14. Beaud D, Tailliez P, and nba-Mondoloni J (2005) Microbiology 151:2323-2330.
15. Mankin HJ (1982) J. Bone Joint Surg. Am. 64:460-466.
16. Rath NC, Hand AR, and Reddi AH (1981) Dev. Biol. 85:89-98.
17. Shimoi K and Nakayama T (2005) Methods Enzymol. 400:263-272.
18. Wright DG and Malawista SE (1972) J. Cell Biol. 53:788-797.
19. Berges BK, Yellayi S, Karolewski BA, Miselis RR, Wolfe JH, and Fraser NW (2006) Mol. Ther. 13:859-869.
20. Sly WS, Quinton BA, McAlister WH, and Rimoin DL (1973) J. Pediatr. 82:249-257.
21. Weissmann G (1967) Annu. Rev. Med. 18:97-112.
22. Weissmann G, Zurier RB, and Hoffstein S (1972) Am. J. Pathol. 68:539-564.
23. Bang J, Cimasoni G, and Held AJ (1970) Arch. Oral Biol. 15:445-451.
24. Perrotto JL, Falchuk KR, Pelly RP, and Warren KS (1976) Ann. N. Y. Acad. Sci. 278:592-598.
25. Henderson RF, Benson JM, Hahn FF, Hobbs CH, Jones RK, Mauderly JL, McClellan RO, and Pickrell JA (1985) Fundam. Appl. Toxicol. 5:451-458.
26. Cobben NA, Drent M, De VJ, Wouters EF, Van Dieijen-Visser MP, and Henderson RF (1999) Clin. Biochem. 32:659-664.
27. Selvaraj P, Kannapiran M, Reetha AM, Uma H, Xavier T, and Narayanan PR (1997) Int. J. Tuberc. Lung Dis. 1:265-269.

28. Lamster IB and Ahlo JK (2007) Ann. N. Y. Acad. Sci. 1098:216-229.
29. Layik M, Yamalik N, Caglayan F, Kilinc K, Etikan I, and Eratalay K (2000) J. Periodontol. 71:618-624.
30. Albandar JM, Kingman A, and Lamster IB (1998) J. Clin. Periodontol. 25:630-639.
31. Vijayan V, Shyni GL, and Helen A (2010) Inflammation.
32. Moro L, de BB, and Gonano F (1975) Clin. Chim. Acta 65:371-377.
33. Ortutay Z, Polgar A, Gomor B, Geher P, Lakatos T, Glant TT, Gay RE, Gay S, Pallinger E, Farkas C, Farkas E, Tothfalusi L, Kocsis K, Falus A, and Buzas EI (2003) Arthritis Rheum. 48:2163-2172.
34. Cross AJ, Crow TJ, Dawson JM, Ferrier IN, Johnson JA, Peters TJ, and Reynolds GP (1986) J. Neurochem. 47:882-889.
35. McGeer EG, McGeer PL, Akiyama H, and Harrop R (1989) Can. J. Neurol. Sci. 16:511-515.
36. McGeer EG, McGeer PL, Harrop R, Akiyama H, and Kamo H (1990) J. Neurosci. Res. 27:612-619.
37. George J, Rajendran M, and Bhatia VN (1990) Indian J. Med. Res. 91:106-110.
38. Ha DK, Lawton JW, and Gardner ID (1984) Exp. Mol. Pathol. 40:177-194.
39. Nandan D, Venkatesan K, Katoch K, and Dayal RS (2007) Lepr. Rev. 78:243-247.
40. Vishwanath V, Meera R, Puvanakrishnan R, and Narayanan PR (1997) Mol. Cell Biochem. 175:169-175.
41. O'Neil WM, Drobitch RK, MacArthur RD, Farrough MJ, Crane LR, and Svensson CK (2003) AIDS 17:269-270.
42. Saha AK, Glew RH, Kotler DP, and Omene JA (1991) Clin. Chim. Acta 199:311-316.
43. Ho KJ, Hsu SC, Chen JS, and Ho LH (1986) Eur. J. Clin. Invest 16:361-367.
44. Ho KJ (1996) Dig. Dis. Sci. 41:2409-2416.
45. Nakai K, Tazuma S, Nishioka T, and Chayama K (2003) Biochim. Biophys. Acta 1632:48-54.
46. Su Y, Wu SD, Jin JZ, Zhang ZH, and Fan Y (2006) Hepatobiliary. Pancreat. Dis. Int. 5:443-448.
47. Beratis NG, Mavrommatis T, Hatiris I, Kavaliotis J, Tsagaropoulou-Stiga H, and Syrogiannopoulos GA (1997) Pediatr. Res. 41:235-241.
48. Beratis NG, Eliopoulou MI, and Syrogiannopoulos GA (2003) Acta Paediatr. 92:1272-1276.
49. Beratis NG, Georgiou G, and Eliopoulou M (2002) Pediatrics 109:E44.
50. Cuzner ML, Barnard RO, MacGregor BJ, Borshell NJ, and Davison AN (1976) J. Neurol. Sci. 29:323-334.
51. Halonen T, Kilpelainen H, Pitkanen A, and Riekkinen PJ (1987) J. Neurol. Sci. 79:267-274.

52. Miller BF, Keyes FP, and Curreri PW (1967) J. Atheroscler. Res. 7:591-600.
53. Ravichandran LV, Puvanakrishnan R, and Joseph KT (1991) Biochem. Med. Metab Biol. 45:6-15.
54. Sathish V, Ebenezar KK, and Devaki T (2003) Biomed. Pharmacother. 57:309-313.
55. Abedin Z, Daniel W, and Bloomfield DK (1982) Jpn. Heart J. 23:897-903.
56. Varma R, Michos GA, Mesmer RE, Varma RS, and Shirey RE (1983) Neurosci. Lett. 39:105-111.
57. Nlyan AJ, Gamble J, and Hoster HA (1950) Cancer 3:116-123.
58. Allison AC (1974) J. Clin. Pathol. Suppl (R. Coll. Pathol.) 7:43-50.
59. Kirkegaard T and Jaattela M (2009) Biochim. Biophys. Acta 1793:746-754.
60. Bosslet K, Straub R, Blumrich M, Czech J, Gerken M, Sperker B, Kroemer HK, Gesson JP, Koch M, and Monneret C (1998) Cancer Res. 58:1195-1201.
61. Ferris RL, Xi L, Seethala RR, Chan J, Desai S, Hoch B, Gooding W, and Godfrey TE (2011) Clin. Cancer Res. 17:1858-1866.
62. Ho KJ and Kuo SH (1995) Cancer 76:473-478.
63. Russell RI and Watts C (1968) Gut 9:585-589.
64. Sulochana G, Sadagopan T, and Padmanabhan L (1982) Clin. Chim. Acta 119:115-119.
65. Beratis NG, Kaperonis A, Eliopoulou Ml, Kourounis G, and Tzingounis VA (2005) J. Cancer Res. Clin. Oncol. 131:371-376.
66. Whitaker BL (1960) Br. J. Cancer 14:471-477.
67. Sperker B, Werner U, Murdter TE, Tekkaya C, Fritz P, Wacke R, Adam U, Gerken M, Drewelow B, and Kroemer HK (2000) Naunyn Schmiedebergs Arch. Pharmacol. 362:110-115.
68. Bauer HG, Asp NG, Oste R, Dahlqvist A, and Fredlund PE (1979) Cancer Res. 39:3752-3756.
69. Kim DH and Jin YH (2001) Arch. Pharm. Res. 24:564-567.
70. Ohta H, Ono M, Sekiya C, and Namiki M (1992) Clin. Chim. Acta 208:9-21.
71. Pearson JP, Pretlow TP, Bradley EL, Jr., McGinnis MC, and Pretlow TG (1989) Cancer 64:911-915.
72. Kerr WK, Barkin M, D'aloisio J, and Menczykz (1963) Cancer 16:633-638.
73. Krivit W (2002) Adv. Pediatr. 49:359-378.
74. Malatack JJ, Consolini DM, and Bayever E (2003) Pediatr. Neurol. 29:391-403.
75. Li T and Davidson BL (1995) Proc. Natl. Acad. Sci. U. S. A 92:7700-7704.
76. Sands MS, Barker JE, Vogler C, Levy B, Gwynn B, Galvin N, Sly WS, and Birkenmeier E (1993) Lab Invest 68:676-686.
77. Snyder EY, Taylor RM, and Wolfe JH (1995) Nature 374:367-370.

78. Taylor RM and Wolfe JH (1997) Nat. Med. 3:771-774.
79. Taylor RM and Wolfe JH (1997) J. Neurochem. 68:2079-2085.
80. Wolfe JH, Sands MS, Barker JE, Gwynn B, Rowe LB, Vogler CA, and Birkenmeier EH (1992) Nature 360:749-753.
81. Ellinwood NM, Vite CH, and Haskins ME (2004) J. Gene Med. 6:481-506.
82. Eto Y and Ohashi T (2000) J. Inherit. Metab Dis. 23:293-298.
83. Haskins M (2009) ILAR. J. 50:112-121.
84. Hodges BL and Cheng SH (2006) Curr. Gene Ther. 6:227-241.
85. Sands MS and Davidson BL (2006) Mol. Ther. 13:839-849.
86. Chen X, Wu B, and Wang PG (2003) Curr. Med. Chem. Anticancer Agents 3:139-150.
87. De GM, Boven E, Scheeren HW, Haisma HJ, and Pinedo HM (2002) Curr. Pharm. Des 8:1391-1403.
88. Denny WA (2003) J. Biomed. Biotechnol. 2003:48-70.
89. Papot S, Tranoy I, Tillequin F, Florent JC, and Gesson JP (2002) Curr. Med. Chem. Anticancer Agents 2:155-185.
90. Rivault F, Tranoy-Opalinski I, and Gesson JP (2004) Bioorganic & Medicinal Chemistry 12:675-682.
91. Cui N, Friend DR, and Fedorak RN (1994) Gut 35:1439-1446.
92. Nolen H, III, Fedorak RN, and Friend DR (1995) J. Pharm. Sci. 84:677-681.
93. Nolen HW, III, Fedorak RN, and Friend DR (1997) Biopharm. Drug Dispos. 18:681-695.
94. Bartholome R, Haenen G, Hollman CH, Bast A, Dagnelie PC, Roos D, Keijer J, Kroon PA, Needs PW, and Arts CW (2010) Drug Metab Pharmacokinet. 25:379-387.
95. Fan D, Zhou X, Zhao C, Chen H, Zhao Y, and Gong X (2011) Fitoterapia 82:805-810.
96. Formelli F, Barua AB, and Olson JA (1996) FASEB J. 10:1014-1024.
97. Goswami BC, Baishya B, Barua AB, and Olson JA (1999) Skin Pharmacol. Appl. Skin Physiol 12:167-173.
98. Osborne R, Thompson P, Joel S, Trew D, Patel N, and Slevin M (1992) Br. J. Clin. Pharmacol. 34:130-138.
99. Peterson GM, Randall CT, and Paterson J (1990) Eur. J. Clin. Pharmacol. 38:121-124.
100. Lougerstay-Madec R, Florent JC, Monneret C, Nemati F, and Poupon MF (1998) Anticancer Drug Des 13:995-1007.
101. Haisma HJ, Boven E, Van MM, de JJ, van d, V, and Pinedo HM (1992) Br. J. Cancer 66:474-478.
102. Bakina E, Wu Z, Rosenblum M, and Farquhar D (1997) J. Med. Chem. 40:4013-4018.

103. De GM, Nevalainen TJ, Scheeren HW, Pinedo HM, Haisma HJ, and Boven E (2004) Biochem. Pharmacol. 68:2273-2281.

104. Houba PH, Boven E, van der Meulen-Muileman IH, Leenders RG, Scheeren JW, Pinedo HM, and Haisma HJ (2001) Br. J. Cancer 84:550-557.

105. Houba PH, Boven E, van der Meulen-Muileman IH, Leenders RG, Scheeren JW, Pinedo HM, and Haisma HJ (1999) Biochem. Pharmacol. 57:673-680.

106. Alaoui AE, Saha N, Schmidt F, Monneret C, and Florent JC (2006) Bioorg. Med. Chem. 14:5012-5019.

107. De Bont DB, Leenders RG, Haisma HJ, van dM-M, I, and Scheeren HW (1997) Bioorg. Med. Chem. 5:405-414.

108. Prijovich ZM, Chen BM, Leu YL, Chern JW, and Roffler SR (2002) Br. J. Cancer 86:1634-1638.

109. Guerquin-Kern JL, Volk A, Chenu E, Lougerstay-Madec R, Monneret C, Florent JC, Carrez D, and Croisy A (2000) NMR Biomed. 13:306-310.

110. Desbene S, Van HD, Michel S, Tillequin F, Koch M, Schmidt F, Florent JC, Monneret C, Straub R, Czech J, Gerken M, and Bosslet K (1999) Anticancer Drug Des 14:93-106.

111. Tietze LF, Schuster HJ, Schmuck K, Schuberth I, and Alves F (2008) Bioorg. Med. Chem. 16:6312-6318.

112. Tietze LF, Schmuck K, Schuster HJ, Muller M, and Schuberth I (2011) Chemistry. 17:1922-1929.

113. Thomas M, Rivault F, Tranoy-Opalinski I, Roche J, Gesson JP, and Papot S (2007) Bioorg. Med. Chem. Lett. 17:983-986.

114. Thomas M, Clarhaut J, Tranoy-Opalinski I, Gesson JP, Roche J, and Papot S (2008) Bioorg. Med. Chem. 16:8109-8116.

115. Hamon F, Renoux B, Chadeneau C, Muller JM, and Papot S (2010) Eur. J. Med. Chem. 45:1678-1682.

116. Lin HS, Barua AB, Olson JA, Low KS, Chan SY, Shoon ML, and Ho PC (2001) J. Pharm. Sci. 90:2023-2031.

117. Zile MH, Cullum ME, Simpson RU, Barua AB, and Swartz DA (1987) Proc. Natl. Acad. Sci. U. S. A 84:2208-2212.

118. Kawai Y, Nishikawa T, Shiba Y, Saito S, Murota K, Shibata N, Kobayashi M, Kanayama M, Uchida K, and Terao J (2008) J. Biol. Chem. 283:9424-9434.

119. Mochizuki M, Kajiya K, Terao J, Kaji K, Kumazawa S, Nakayama T, and Shimoi K (2004) Biofactors 22:201-204.

120. Connors TA and Whisson ME (1966) Nature 210:866-867.

121. Whisson ME and Connors TA (1965) Nature 206:689-691.

122. Young CW, Yagoda A, Bittar ES, Smith SW, Grabstald H, and Whitmore W (1976) Cancer 38:1887-1895.

Chapter

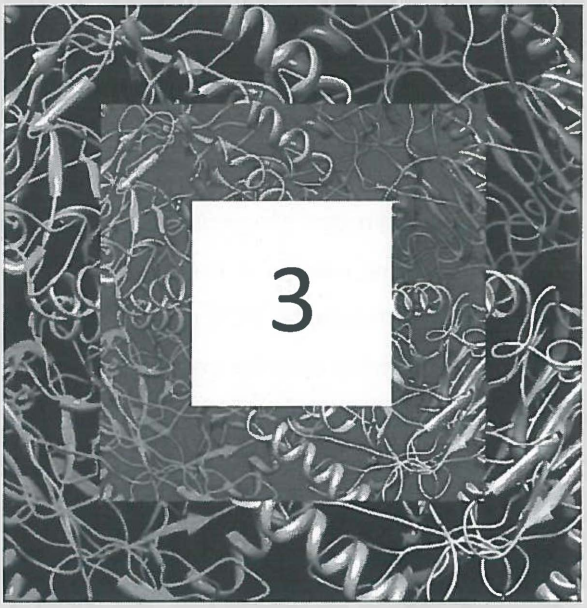

Tumor-specific activation of prodrugs: Is there a role for nuclear medicine?

Inês F. Antunes, Hidde J. Haisma, Erik F. J. de Vries

Nucl Med Commun 2008; 29, 845-846

Chemotherapy is an important strategy for treatment of advanced cancer, but it is often associated with severe side-effects. The difficulty of chemotherapy is to deliver high concentrations of cytotoxic drug to the target site in order to completely eradicate the tumor. Due to the physiological similarities between normal cells and tumor cells, the therapeutic index of chemotherapeutic drugs is often small, resulting in dose-limiting toxicity or insufficient drug concentrations at the tumor site. For better selectivity and efficacy of chemotherapy, local conversion of a non-toxic prodrug into an active cytotoxic agent by enzymes that are selectively expressed at the tumor site could be an attractive approach [1;2]. For such specific strategies, knowledge of the expression levels and the distribution of the prodrug-converting enzyme is vital. Therefore non-invasive imaging techniques like positron emission tomography (PET) can be attractive tools to evaluate new enzyme-prodrug combinations and to optimize treatment strategies [3-5].

Several systems have been developed for enzyme-mediated prodrug therapy. The prodrug-converting enzymes can either be endogenous proteins that are expressed selectively in high concentrations at the tumor site or exogenous proteins that have been selectively delivered to the tumor.

Among the most frequently studied prodrug strategies is gene–directed enzyme prodrug therapy (GDEPT) or "suicide" gene therapy. In this two-step strategy, a so-called suicide gene encoding the desired exogenous enzyme is transfected into the tumor, enabling the conversion of a relatively non-toxic prodrug into the cytotoxic drug. Various GDEPT systems have been developed, using a number of different prodrug/enzyme combinations, such as: i) herpes simplex virus type 1 thymidine kinase (HSVtk)/ganciclovir (GCV), ii) bacterial or yeast cytosine deaminase/5-fluorocytosine, or iii) bacterial nitroreductase/CB1954. So far, adenoviral transfer of the HSVtk gene followed by GCV administration has been the most extensively studied both in the laboratory and in the clinic. Several PET and SPECT (single-photon emission computed tomography) tracers have been developed and successfully tested as probes for monitoring the expression of the transferred HSVtk gene in the tumor, like [^{18}F]FIAU, [$^{123/124}$I]FIAU and [^{18}F]FHBG. Despite the fact that imaging methods for monitoring and optimization of gene delivery of HSVtk

and other genes are available now, widespread clinical application of GDEPT is still beyond reach, because of the low efficiency of *in vivo* gene delivery into the target cells and the immune response induced by the non-human enzymes [6-9].

Antibody-directed enzyme prodrug therapy (ADEPT) is a technique that is related to GDEPT. The ADEPT approach shows many similarities with radioimmunotherapy. In ADEPT, a monoclonal antibody-enzyme (mAb-Enz) conjugate, targeted to a tumor-associated antigen, is used to deliver the enzyme to the tumor site, where it can convert the prodrug to the cytotoxic agent. Compared to standard chemotherapy, the ADEPT approach can reduce peripheral toxicity and improve efficacy of the therapeutic agent, provided that the mAb-Enz conjugate selectively accumulates in the tumor. For optimal ADEPT treatment, *in vivo* monitoring of the distribution of the conjugate would be required before administration of the prodrug is started. Like in radioimmunotherapy, where the mAb is labeled with a therapeutic and/or diagnostic radionuclide, the mAb-Enz conjugate can be labeled with a radioactive isotope for imaging of the distribution of the conjugate. Alternatively, the prodrug could be labeled provided that it is trapped in the tissue after conversion by the conjugate. The latter approach was used by Brady *et al.*, who labeled a glutamic acid mustard derived prodrug with carbon-11 for monitoring the ADEPT with PET [10]. Although imaging of mAb for radioimmunotherapy is commonplace, to our knowledge, no examples of labeled mAb-Enz conjugates for ADEPT have been published so far. There are several disadvantages in the ADEPT strategy, such as immunogenicity of the antibody-enzyme conjugate. The mAb-Enz conjugate does not always localize in the target tissue to the desired extent, mAbs penetrate poorly into tumors, tumor cells express only a limited number of antigens, the clearance of unbound mAb-Enz conjugate is often inadequate and antigen expression levels vary between individuals and between tumors. Nuclear imaging may help to overcome these obstacles by using a suitable PET tracer to quantify distribution of the prodrug or the mAb-Enz conjugate, providing information on the selectivity between tumors and normal tissues and aiding the appropriate timing of therapy [11].

Despite the improvements in specific drug-targeting systems such as ADEPT and GDEPT, these systems are still far from introduction into the clinic. A more feasible approach could be the use of a simpler, but possibly less selective one step prodrug activation system, called prodrug monotherapy (PMT). PMT involves the activation of a non-toxic prodrug by an endogenous enzyme that is exclusively (or at least preferentially) expressed in high quantities by the tumor itself, thus avoiding potential immunogenicity problems. Several classes of endogenous enzymes have been investigated as prodrug converting enzymes such as *Oxidoreductases*, *Transferases*, *Hydrolases* and *Lyases* [12-14]. Since PMT depends on the activity of an endogenous gene, it is of paramount importance for the assessment of therapy efficacy and safety to have insight in the expression levels of the enzyme, not only in the tumor, but also in other tissues. Remarkably, nuclear imaging techniques for monitoring PMT are currently lacking.

For example, β-glucuronidase is a promising prodrug-converting enzyme for PMT. It is localized intracellularly in microsomes and lysosomes and its activity is not detectable in human blood. Under normal circumstances, β-glucuronidase is not available for a prodrug that can not enter the cell. However, large amounts of endogenous β-glucuronidase are present extracellularly in tumors, which would allow the selective activation of a glucuronide-based prodrug to a cytotoxic agent at the tumor site [15;16]. Encouraging results have already been obtained in animal studies [17-20]. For imaging purposes, glucuronide-based tracers could be developed with similar structures as the prodrug. So far, only a few glucuronide prodrug have been radiolabeled with [^{125}I] and [^{211}At] to enhance the efficacy of these prodrug by adding radiotoxicity of an appropriate radionuclide in the same prodrug [21;22]. When other isotopes are applied these labeled compound might be suitable tracers for imaging. For MRI, a glucuronide has been labeled with gadolinium, but *in vivo* evaluation of this probe has not been published yet [23]. This probe could be radiolabeled with a radioactive isotope for nuclear imaging. To our knowledge, however, there are still no glucuronide PET or SPECT tracers available to monitor tumor-specific activation of prodrugs by β-glucuronidase or another endogenous prodrug converting enzymes.

Despite the appealing concept of prodrug therapy and the encouraging preclinical results, the quest for a clinical applicable strategy is continuing. Nuclear medicine could provide valuable information on the expression of endogenous and exogenous prodrug-converting enzymes and thus could assist the development and optimization of these new interventions. However, suitable tracers for monitoring ADEPT and especially PMT are virtually absent. In the last decade, the development of tracers for GDEPT has received a lot of attention, but so far these tracers have not led to a suitable therapy yet. Since successful PMT and ADEPT seem to be within reach now, this could be the time for the nuclear medicine society to expand their focus from GDEPT to these other prodrug approaches. Nuclear medicine can provide crucial information regarding prodrug-converting enzyme expression and prodrug pharmacology, which will lead to a better understanding of the mechanisms of action and metabolic conversion of the prodrug and therefore nuclear medicine could induce an impetus for the development of prodrug therapy.

REFERENCES

1. Chen X, Wu B, and Wang PG (2003) Curr. Med. Chem. Anticancer Agents 3:139-150.
2. De GM, Boven E, Scheeren HW, Haisma HJ, and Pinedo HM (2002) Curr. Pharm. Des 8:1391-1403.
3. Brady F, Luthra SK, Brown GD, Osman S, Aboagye E, Saleem A, and Price PM (2001) Curr. Pharm. Des 7:1863-1892.
4. Gupta N, Price PM, and Aboagye EO (2002) Eur. J. Cancer 38:2094-2107.
5. Unak T (2000) Curr. Pharm. Des 6:1127-1142.
6. Dachs GU, Dougherty GJ, Stratford IJ, and Chaplin DJ (1997) Oncol. Res. 9:313-325.
7. De Vries EF, Buursma AR, Hospers GA, Mulder NH, and Vaalburg W (2002) Curr. Pharm. Des 8:1435-1450.
8. Greco O and Dachs GU (2001) J. Cell Physiol 187:22-36.
9. Wang HE, Yu HM, Liu RS, Lin M, Gelovani JG, Hwang JJ, Wei HJ, and Deng WP (2006) J. Nucl. Med. 47:1161-1171.
10. Malik N, Luthra SK, Burke P, Price PM, Aboagye EO, Latigo J, Zhao Y, and Brady F (2004) Appl. Radiat. Isot. 60:825-834.
11. De Groot FM, Damen EW, and Scheeren HW (2001) Curr. Med. Chem. 8:1093-1122.
12. De Groot FM, Damen EW, and Scheeren HW (2001) Curr. Med. Chem. 8:1093-1122.
13. Rooseboom M, Commandeur JN, and Vermeulen NP (2004) Pharmacol. Rev. 56:53-102.
14. Yoon KJ, Potter PM, and Danks MK (2005) Curr. Med. Chem. Anticancer Agents 5:107-113.
15. Chen X, Wu B, and Wang PG (2003) Curr. Med. Chem. Anticancer Agents 3:139-150.
16. De GM, Boven E, Scheeren HW, Haisma HJ, and Pinedo HM (2002) Curr. Pharm. Des 8:1391-1403.
17. De GM, Pinedo HM, Oosterhoff D, van der Meulen-Muileman IH, Gerritsen WR, Haisma HJ, and Boven E (2004) Hum. Gene Ther. 15:229-238.
18. Heine D, Muller R, and Brusselbach S (2001) Gene Ther. 8:1005-1010.
19. Houba PH, Boven E, van der Meulen-Muileman IH, Leenders RG, Scheeren JW, Pinedo HM, and Haisma HJ (2001) Int. J. Cancer 91:550-554.
20. Weyel D, Sedlacek HH, Muller R, and Brusselbach S (2000) Gene Ther. 7:224-231.
21. Unak T, Unak P, Ongun B, and Duman Y (1997) Appl. Radiat. Isot. 48:777-783.
22. Unak T (2000) Curr. Pharm. Des 6:1127-1142.
23. Duimstra JA, Femia FJ, and Meade TJ (2005) J. Am. Chem. Soc. 127:12847-12855.

Chapter

Synthesis and evaluation of [^{18}F]FEAnGA as a PET tracer for β-glucuronidase activity

Inês F. Antunes, Hidde J. Haisma, Philip H. Elsinga,
Rudi A. Dierckx, Erik F. J. de Vries

Parts of this chapter have been published in Bioconjug Chem 2010; 21(5), 911-20

ABSTRACT

To increase the therapeutic index of chemotherapeutic drugs, prodrugs have been investigated as anti-cancer agents, as they may present less cytotoxic side effects than conventional cytotoxic drugs, while therapeutic efficacy is maintained or even increased. Extracellular β-glucuronidase (β-GUS) in the tumors has been investigated as a target-enzyme for prodrug therapy, as it can convert nontoxic prodrugs into cytostatic drugs. To optimize β-GUS-based prodrug therapies, PET imaging could be a useful tool by providing information regarding the localization and expression levels of β-GUS. Here we describe the first PET tracer for extracellular β-GUS, [^{18}F]FEAnGA, which consists of a 2-[^{18}F]fluoroethylamine ([^{18}F]FEA) group bound to a glucuronic acid via a self-immolative nitrophenyl spacer. [^{18}F]FEAnGA was synthesized by alkylation of its imidazole carbamate precursor with [^{18}F]FEA, followed by deprotection of the sugar moiety with NaOH in 10-20% overall radiochemical yield. [^{18}F]FEAnGA is about 10-fold more hydrophilic than the cleavage product [^{18}F]FEA and it is stable in PBS and rat plasma for at least 3 h. In the presence of either *Escherichia coli* β-GUS or bovine liver β-GUS, *in vitro* cleavage of [^{18}F]FEAnGA with complete release of [^{18}F]FEA was observed within 30 min. Incubation of CT26 murine colon adenocarcinoma cells or the genetically engineered CT26mβGUS cells, which expressed membrane-anchored GUS on the outer cell membrane, with the tracer resulted in a 3 fold higher tracer uptake into GUS expressing cells as compared to control cells. A microPET study in mice bearing both CT26 and CT26mβGUS tumors, [^{18}F]FEAnGA exhibited a 2 times higher retention of radioactivity in the tumor expressing β-GUS than in the control tumor. [^{18}F]FEA did not show any difference in tracer uptake between tumors. Metabolite analysis of [^{18}F]FEAnGA in mice revealed that the conversion of [^{18}F]FEAnGA to [^{18}F]FEA was 2 times higher in CT26mβGUS tumors then in CT26 tumors and only 10% of the radioactivity in plasma consisted of the metabolized [^{18}F]FEAnGA at 60 min p.i. These results suggest that [^{18}F]FEAnGA may be a suitable PET tracer for evaluation of β-GUS activity, since it is specifically cleaved by β-GUS and the released [^{18}F]FEA remains attached to targeted cells.

INTRODUCTION

To overcome the limitation of toxicity associated with chemotherapeutic drugs, local conversion of a non-toxic prodrug to the active cytotoxic drug in or in the vicinity of tumors provides a means for delivering active drugs selectively to tumor cells while sparing the normal cells of a host.

β-Glucuronidase (β-GUS) (EC 3.2.1.31) belongs to a group of isoenzymes that catalyze the hydrolysis of β-D-glucuronides to the corresponding alcohol and D-glucuronate. The enzyme is present in virtually all tissues and can be found in microsomes (endoplasmic reticulum) and lysosomes. The human enzyme has a pH optimum of 4 to 5. Under normal tissue pH, only about 10% the maximum activity is retained. β-GUS concentrations are low in human serum and the extracellular compartment of normal tissue [1]. However, increased levels of extracellular β-GUS have been reported in a number of pathological conditions, such as rheumatoid arthritis, leprosy, myocardial infarction, liver fibrosis, bacterial infection and various inflammatory processes [2]. It is also known that tumors have high extracellular levels of β-GUS, due to invading monocytes and granulocytes [3]. Extracellular β-GUS is also associated with tumor invasiveness and metastatic potential [3]. Therefore, β-GUS seems to be a promising candidate for a prodrug-converting enzyme.

Glucuronide-drug conjugates exhibit improved water solubility, stability and lower toxicity towards normal cells than the native drug. However, glucuronide-drug conjugates are susceptible to enzymatic cleavage by β-GUS, resulting in the in-situ generation of highly cytotoxic drugs that can selective accumulate into targeted tumor cells [1;4;5]. A number of prodrugs for β-GUS have been designed. These prodrugs generally consist of three distinct parts: a trigger, a linker and an effector unit. For β-GUS targeted prodrugs, the trigger and effector units consist of a glucuronide moiety and the cytostatic drug, respectively. They are joined together by the linker unit, which should release the drug as fast as possible after prodrug activation via a chemical breakdown [6-8].

Encouraging results were obtained with the prodrugs DOX-GA3 and HMR 1826 both carrying para-substituted aromatic spacers, which were able to release doxorubicin after enzymatic cleavage of the glucuronide moiety by extracellular β-GUS (Scheme 1).

Scheme 1. Mechanism of activation of the prodrugs HMR 1826 and DOX-GA3 by β-GUS

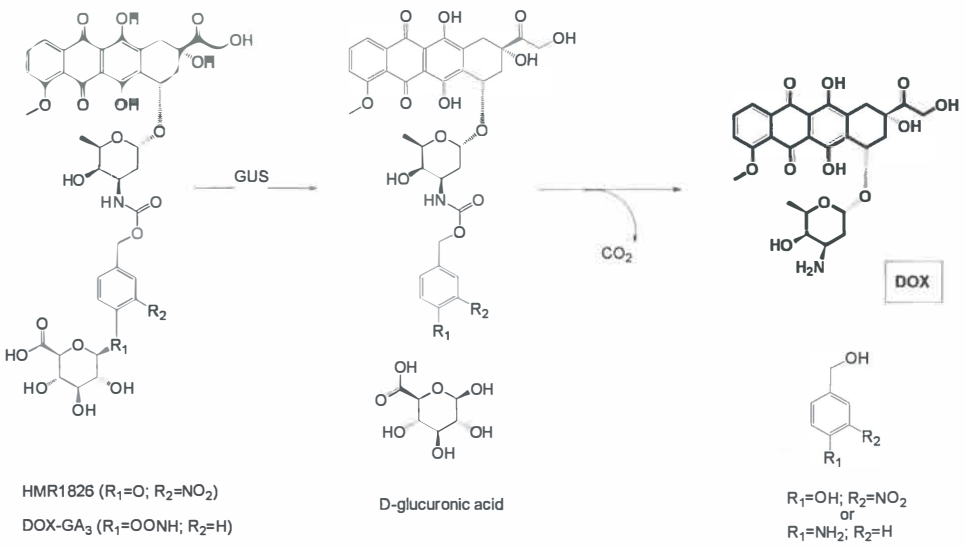

As follows from the above, bioactivation of the glucuronide prodrug by β-GUS is an attractive approach in prodrug therapy. However, interindividual and intertissue variability of β-GUS activity as well as factors modulating the enzyme's expression and activity are key determinants for the success of these therapeutic strategies [9;10].

For a better understanding of the mechanisms of action and metabolic conversion of these prodrugs, some *in vivo* optical measurements of gene/enzyme expression have been done using substrates with fluorescent or bioluminescent properties. These optical imaging modalities are useful in superficial tissues and have extensive application in small animals, but application to larger animals or humans is limited by the depth of light penetration [11-13]. Monitoring enzyme or gene expression in larger animals and ultimately in humans is possible with the use of specific radiotracers

combined with nuclear imaging techniques like PET or SPECT [14-17]. Among these techniques, PET is of particular interest for drug development because of its high sensitivity and ability to provide quantitative kinetic data [18;19].

For PET imaging of β-GUS activity, a suitable tracer is necessary [20]. Therefore, we aimed to develop a PET tracer that allows repetitive non-invasive imaging of β-GUS activity in living subjects. Thus, we designed a potential PET tracer with a structure based on HMR 1826. In the PET tracer, the doxorubicin moiety was replaced by a [^{18}F]-fluoroalkylamine group.

Due to the highly hydrophilic character of the glucuronide, the intact tracer will be rapidly cleared from plasma and from tissues that do not have extracellular β-GUS. However, in tissues with high levels of β-GUS, the enzyme should cleave the glucuronic acid moiety from the PET tracer. As a result, the less hydrophilic [^{18}F]fluoroethylamine will be released after self-immolation of the spacer and we hypothesized that [^{18}F]fluoroethylamine will be trapped in the target tissue (Scheme 2).

Scheme 2. General structure of the PET tracer and its mechanism of activation

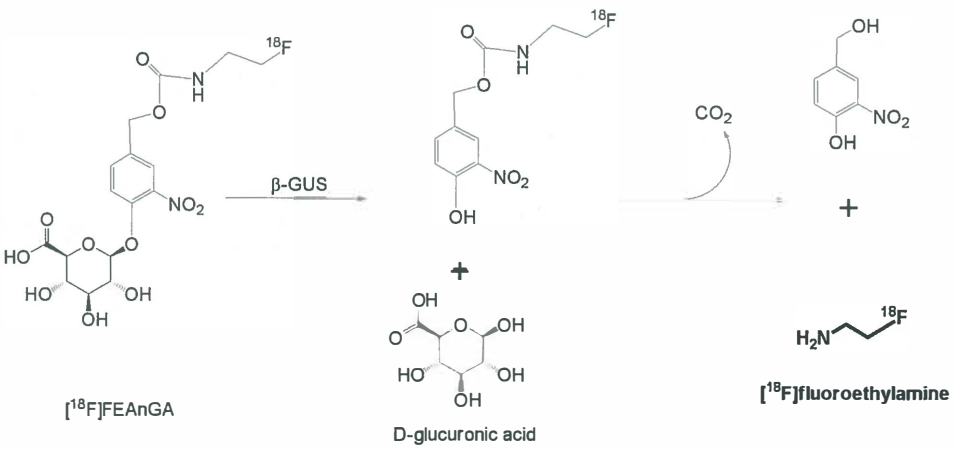

This study aimed to provide a proof of principle of this tracer design. The tracer may be further optimized by replacing the [^{18}F]fluoroethylamine moiety with, for example,

a more lipophilic or targeted moiety in order to increase trapping efficiency as a result of increased non-specific binding.

MATERIALS AND METHODS

Reagents and solvents were obtained from commercial suppliers (Aldrich, Fluka, Sigma and Merck) and used without further purification. A glucose, magnesium and calcium solution (GMC-PBS) was prepared by adding 5.6 mM D-glucose, 0.49 mM $MgCl_2$ and 0.68 mM $CaCl_2$ to 100 mL phosphate-buffered saline (PBS). Flash chromatography was performed on silica gel 60 (0.040-0.063, Merck). All reactions were monitored by thin layer chromatography on Merck F-254 silica gel plates. Detection of the compounds on the TLC plates was performed with UV light (254 nm). Sugar compounds were additionally visualized by staining the TLC strip with 8% H_2SO_4 followed by heating. For radiolabeled compounds, the detection on the TLC was performed with Cyclone phosphor storage screens (multisensitive, Packard). These screens were exposed to the TLC strips for a few seconds and subsequently read out using a Cyclone phosphor storage imager (PerkinElmer) and analyzed with OptiQuant software. ^{1}H- and ^{19}F- NMR were recorded on a Varian 300 MHz and 200 MHz respectively. Chemical shifts were determined relative to the signal of the solvent, converted to the TMS scale and expressed in δ units (ppm) downfield from TMS. Coupling constants were reported in Hertz (Hz). Splitting patterns are defined as s (singlet), d (doublet), dd (double-doublet), t (triplet), dt (double-triplet) or m (multiplet). HPLC purifications were performed with an Elite LaChrom VWR Hitachi L-2130 pump system using a Phenomenex Prodigy C18-column (5µ, 10×250 mm), connected to a UV-spectrometer (Elite LaChrom VWR Hitachi L-2400 UV detector) set at 254 nm and a Bicron frisk-tech radiation detector. Radioactivity measurements for log D determination and cell studies were done using an automated gamma counter (Compugamma, LKB Wallac). Absorbance measurements in the enzyme assays were obtained with a UV-spectrophotometer (Waters 2487 dual wavelength absorbance detector). CT26mβGUS murine colon adenocarcinoma were kindly provided by Steve Roffler [11], Institute of

Biomedical Science, Academia Sinica, Academia Road, Section 2 No128, 11529 Taipei, Taiwan.

Synthesis. *Methyl 1-O-(4-((2-fluoroethylcarbamoyloxy)methyl)-2-nitrophenyl)-2,3,4-tri-O-acetyl-β-D-glucopyronuronate* **(2)**. Methyl 1-O-(4-(1*H*-imidazole-carbamoyloxymethyl)-2-nitrophenyl)-2,3,4-tri-*O*-acetyl-β-D-glucopyronuronate **1** was synthesized in 3 steps according to the procedure described by Duimstra *et al.* [21]. Carbamate **1** (0.2 g, 0.35 mmol) was dissolved in 3 mL anhydrous CH_2Cl_2 under a N_2 atmosphere and cooled to 0 °C. Methyl triflate (45 µl, 0.40 mmol) was added to the reaction mixture. After stirring for 30 min at 0 °C, the reaction mixture was diluted with 2 mL Et_2O and cooled to -20 °C to allow the methylated product to precipitate. The white solid was collected by filtration, washed with Et_2O and dried *in vacuo*. The methylated compound was resuspended in 2.5 mL CH_2Cl_2 under a N_2 atmosphere and 2-fluoroethylamine hydrochloride (0.05g, 0.54 mmol) and triethylamine (75µL, 0.54 mmol) were added. The slurry was stirred for 5 h at room temperature and then washed with water and brine. The organic layer was dried on Na_2SO_4, concentrated *in vacuo* and purified by flash chromatography (silica, EtOAc-Hexane 1:1 + 0.1% Et_3N) to give 18 mg (41%) of 2 as a white solid. ^{1}H NMR (300 MHz, DMSO-*d6*) δ 1.97 (s, 3H, OAc), 1.99 (s. 6H, OAc), 3.23 (m, 2H, CH_2N), 3.61 (s, 3H, $COOCH_3$), 4.38 (dt, 2H, *J* = 47.2 Hz, *J* = 10 Hz, CH_2F), 4.71 (d, 1H, J = 9.5 Hz, H-5), 5.01-5.12 (m, 4H, benzylic CH_2, H-2, H-4), 5.43 (t, 1H, J = 19 Hz, H-3), 5.71 (d, 1H, J = 7.7 Hz, H-1), 7.40 (d, 1H, J = 8.4 Hz, ArH), 7.56 (m, 1H, NH), 7.65 (d, 1H, J = 9.5 Hz, ArH), 7.87 (s. 1H, ArH); ^{19}F NMR (200 MHz, DMSO-*d6*) δ -217.84; ESI-MS *m/z* 592.3 $[M+NH_4]^+$, 597.3 $[M+Na]^+$.

Methyl 1-O-(4-((2-fluoroethylcarbamoyloxy)methyl)-2-nitrophenyl)-β-D-glucopyronuronate **(3)**. 12.6 µL 30% w/v NaOMe in MeOH was added to a solution of **2** (50 mg, 0.087 mmol) in anhydrous MeOH at 0 °C. After 2 hours of stirring under nitrogen atmosphere, the reaction was quenched with acetic acid and concentrated in *vacuo*. The crude residue was purified by flash column chromatography (silica, 10% MeOH in CH_2Cl_2). The resulting solid was dissolved in acetone and filtered through a 0.2 µm PTFE filter to

remove any remaining silica. Trituration of the solid in diethyl ether yielded 30.3 mg of **3** (78%) as a white solid.

^{1}H NMR (300 MHz, DMSO-*d6*) δ 3.2 (m, 2H, CH_2N, 3.63 (s, 3H, $COOCH_3$), 4.10 (d, 1H, J = 9.1 Hz, H-5), 4.38 (dt, 2H, *J* = 47.6 Hz, *J* = 10 Hz, CH_2F), 5.00 (s, 2H, benzylic CH_2), 5.3 (d, 2H,J = 7 Hz,H-2, H-4), 5.51 (s, 2H, H-3, H-1), 7.42 (d, 1H, J = 8.8 Hz, ArH), 7.56 (m, 1H, NH), 7.65 (m, 2H, NH, ArH), 7.84 (s. 1H, ArH); ^{19}F NMR (200 MHz, DMSO-*d6*) δ -232 ESI-MS *m/z* 455.3 $[M+Li]^+$.

1-O-(4-(2-Fluoroethyl-carbamoyloxymethyl)-2-nitrophenyl)-O-β-D-glucopyronuronate (FEAnGA)(**4**). A solution of **3** (20 mg, 0.047 mmol) in acetone (1 mL) was stirred in the presence of a 1M NaOH (380 μL) solution at 0 °C. After 10 min, the mixture was neutralized with 1M HCl, concentrated in *vacuo* and purified by flash column chromatography (Silica, MeCN/H_2O 7:3) to give 17.3 mg of a light yellow solid (91%).

^{1}H NMR (300 MHz, DMSO-*d6*) δ 3.2 (m, 2H, CH_2N), 3.55 (d, 1H, J = 9.4 Hz, H-5), 4.38 (dt, 2H, *J* = 47.6 and 10 Hz, CH_2F), 5.01 (s, 2H, benzylic CH_2), 5.11 (d, 2H, J = 6.8 Hz, H-2, H-4), 5.30 (d, 2H, J = 4.4 Hz, H-3, H-1), 7.41 (d, 1H, J = 9.1 Hz, ArH), 7.60 (m, 2H, NH, ArH), 7.83 (s. 1H, ArH); ^{19}F NMR (200 MHz, DMSO-*d6*) δ -225; *m/z* 457.2 $[M+Na]^+$.

Radiolabeling. *Radiosynthesis of [^{18}F]FEAnGA* (**[^{18}F]-4**). Aqueous [^{18}F]fluoride was produced by irradiation of [^{18}O] water with a Scanditronix MC-17 cyclotron via the ^{18}O (p,n)^{18}F nuclear reaction. The [^{18}F]fluoride solution was passed through an activated SepPak Light Accell plus QMA anion exchange cartridge (Waters) to recover the ^{18}O-enriched water. The [^{18}F]fluoride was eluted from the cartridge with 1 mL of K_2CO_3 (5 mg/mL) and collected in a vial with 20 mg Kryptofix [2.2.2]. To this solution, 1 mL acetonitrile was added and the solvents were evaporated at 130 °C. The [^{18}F]KF/Kryptofix complex was dried 3 times by the addition of 0.5 mL acetonitrile, followed by evaporation of the solvent.

[^{18}F]FEA (**[^{18}F]-7**) was prepared by [^{18}F]fluorination of N-[2-(toluene-4-sulfonyloxy)-ethyl]-phtalimide (30 mg, 0.09 mmol) in acetonitrile at 110 °C, followed by deprotection with hydrazine hydrate (50μl, 1.03 mmol) as described in literature [22]. The resulting amine was distilled at 75 °C into an ice cold solution of **1** (5 mg, 0.009 mmol) in

acetonitrile (0.2 mL). The mixture was allowed to react at room temperature for 30 min. The product was diluted with 20 mL of water and passed through a tC18 cartridge (activated with 5 mL EtOH and 10 mL H_2O). Deprotection of the hydroxyl groups was done on the tC18 cartridge by addition of 1 mL 2M NaOH and incubation for 7 min at room temperature. The product was eluted from the cartridge with 4 mL of water and purified by HPLC (10 % EtOH in NaH_2PO_4 0.025 M (pH 6.3); 4 mL/min; retention time: [^{18}F]FEAnGA= 12 min).

The radiolabeled compound [^{18}F]FEAnGA (**[^{18}F]-4**) was obtained in 5-20 % radiochemical yield from [^{18}F]fluoride (decay corrected) in 150 min. At the end of synthesis (EOS) the specific activity was 50-100 GBq/μmol and the radiochemical purity > 95%.

Stability of [$^{18/19}$F]FEAnGA. Samples of [$^{18/19}$F]FEAnGA were taken for stability testing. A sample of FEAnGA was dissolved in PBS (1 mL) and incubated at 37 °C. After 60 minutes, the solution was analyzed by HPLC (retention time: FEAnGA= 3.2 min, HNBA= 10.4 min) (20% CH_3CN/NaH_2PO_4 0.025 M (pH 6.3); 4 mL/min).

A sample of radiolabeled [^{18}F]FEAnGA was dissolved in PBS (1mL) and rat plasma (1 mL) and incubated at 37 °C. After 1hour and 3 hours of incubation, respectively, the stability of the radiolabeled [^{18}F]FEAnGA was followed by Radio-TLC (R_f FEA= 0.0, R_f FEAnGA= 0.4) (eluent: MeOH/CH_2Cl_2 2:8 + 0.1 % Et_3N). After elution, the TLCs were analyzed by phosphor storage imaging. The screens were scanned with Cyclone phosphor storage system (PerkinElmer) and the percentage of conversion of [^{18}F]FEAnGA as a function of the incubation period was calculated by ROI analysis using OptiQuant software.

In order to not underestimate the amounts of [^{18}F]FEA due to its volatile nature, we created a calibration curve of the amount of [^{18}F]FEA evaporated over time from the radio TLC ($y = -0.2141x + 103.11$, $r^2 = 0.72$, $p = 0.03$) and corrected all values. [^{18}F]FEA was prepared as mentioned above and purified by HPLC (10 % EtOH in NaH_2PO_4 0.025 M (pH 6.3); 4 mL/min; retention time: [^{18}F]FEA= 5.5 min). The calibration curve was prepared by pipetting 1.5 μL of a stock [^{18}F]FEA purified solution at different time points in a TLC plate.

The TLC was read out by storage phosphorous imaging. Images were analyzed by Optiquant software and the percentage of evaporated activity was calculated. At 60 min, approximately 10% of [^{18}F]FEA has evaporated.

Distribution Coefficient (Log $D_{7.4}$). To determine the Log $D_{7.4}$ of [^{18}F]FEA and [^{18}F]FEAnGA, an aliquot of 1 mL of HPLC purified [^{18}F]FEA or [^{18}F]FEAnGA solution was added to a mixture of n-octanol/PBS (5mL:5mL) at pH 3 and 7 for [^{18}F]FEAnGA and at pH 7 and 10 for [^{18}F]FEA. The tubes were vortexed at room temperature for 1 min, followed by 30 min shaking in a water bath at 37 °C. Aliquots of 1000 μL and 25 μL were drawn from the n-octanol and aqueous phase, respectively, and the radioactivity was counted using an automated gamma counter. The experiments were performed in triplicate.

***In Vitro* Hydrolysis of FEAnGA**. To assess the kinetic parameters for the β-GUS-catalyzed hydrolysis of FEAnGA, aliquots of FEAnGA were prepared with concentrations ranging from 0.001M to 0.01 M in PBS buffer (pH 7.4). To a 0.950 mL solution containing 0.1% BSA in PBS (pH=7.4), 3.7 μg (74U) *Escherichia coli* β-GUS (E.C.3.2.1.31, 20,000 U /mg Aldrich) and 50 μL of FEAnGA were added. The solution was incubated at 37 °C in a water bath and 75 μL samples were collected at different time points ranging from 30 s to 30 min after the start of incubation. Each sample was immediately added to 500 μL acetonitrile in ice to stop the reaction. The release of 4-hydroxy-3-nitrobenzyl alcohol (HNBA) (ε= 3460 $M^{-1}cm^{-}1$) was monitored by measuring the UV absorbance at 420 nm. The initial velocities of the reactions were determined from the slope of the absorbance curve at time= 0. The kinetic parameters K_M and V_{max} were obtained from a Lineweaver-Burk plot [12;23;24]

The kinetic parameters of the hydrolysis of FEAnGA by bovine liver β-GUS were determined as described above, but with minor modifications. Briefly, to a 0.8 mL solution containing 0.1% BSA in PBS (pH=5), 95.2 μg (952U) bovine liver β-GUS (B-10, E.C.3.2.1.31, 10,000U/mg Sigma) and 200 μL of FEAnGA were added. The same assay was also performed for a control sample solution (without enzyme) under the same conditions and it showed negligible absorption for the duration of the experiment. For comparison, the kinetic parameters of a reference substrate, p-nitrophenyl-β-D-glucuronide (PNPG) (ε=

7578 $M^{-1}cm^{-1}$) were determined using the same conditions as for FEAnGA. The experiment was performed in triplicate.

***In Vitro* Hydrolysis of [^{18}F]FEAnGA**. To a 0.6 mL solution of 0.1% BSA in PBS (pH=7), 3.7 μg (74U) *Escherichia coli* β-GUS or 95.2 μg (952U) bovine liver β-GUS and 0.4 mL of HPLC purified [^{18}F]FEAnGA (0.68 - 1.28 MBq) were added. The solutions were incubated in a water bath at 37 °C and 75 μL samples were collected at different time points ranging from 30 s to 30 min after the start of incubation. The enzymatic activity was stopped by dilution of the samples in 0.5 mL of acetonitrile and cooling of the samples in ice. The degradation of the radiolabeled [^{18}F]FEAnGA was followed by Radio-TLC (eluent: MeOH/CH_2Cl_2 2:8 + 0.1% Et_3N). After elution, the TLCs were analyzed by phosphor storage imaging as described above.

Cellular uptake of [^{18}F]FEAnGA in CT26 adenocarcinoma cells. CT26 control cells as well as the genetically engineered CT26mβGUS murine colon adenocarcinoma cells that expresses membrane-anchored GUS on the outer cell membrane were maintained in 10 mL DMEM medium supplemented with 10% FBS and 1% Penicillin-Streptomycin in 75 cm^3 culture flasks. Cells were grown in a humidified atmosphere containing 5% CO_2 and were passaged every 3-4 days. For uptake experiments, cells were plated in triplicate in a 12-well plate at a density of 7×10^5 cells per well. After 24 h, the medium was discarded and 1 mL of PBS-GMC buffer per well was added, followed by the addition of 200 μL [^{18}F]FEAnGA (ca. 250 kBq) or 10 μL [^{18}F]FEA (ca. 125 kBq). After 60 min of incubation at 37 °C, the medium was collected, the cells washed with cold PBS (3×1 mL/well), harvested with trypsin (250 μL) and resuspended in 1750 μL of DMEM. The cell suspensions as well as the supernatant fractions were collected separately for each well and the radioactivity was measured using a gamma counter. For each well, the medium was analyzed for conversion of [^{18}F]FEAnGA to [^{18}F]FEA by Radio-TLC (R_f [^{18}F]FEA= 0.37, R_f ^{18}F]FEAnGA= 0.54) (eluent: MeOH/CH_2Cl_2 2:8 + 0.1% Et_3N). After elution, the TLCs were analyzed by phosphor storage imaging as described above.

MicroPET Imaging in a β-GUS expressing tumor (CT26mβGUS) mouse model. The animals were provided with standard laboratory chow and tap water *ad libitum*. All

studies were carried out in compliance with the local ethical guidelines for animal experiments. The protocol was approved by the local Animal Ethics Committee. CT26 and CT26mβGUS cells [1-1.6 × 10^6, in a 1:1 mixture of Matrigel and DMEM with 10 % FBS)] were subcutaneously injected into the right and left shoulders of two male Balb/c mice (6-8 weeks old), respectively. On day 7 after inoculation of the mice with CT26 and CT26mβGUS cells, the mice were anesthetized with 2% Isoflurane, positioned in the small animal PET camera in a transaxial position. A 20 minutes transmission scan with a Co-57 point source was obtained for the correction of attenuation of 511 keV photons by tissue. After the transmission scan was completed, [^{18}F]FEAnGA (3.91 ± 4.04 MBq, n=7) or [^{18}F]FEA (3.90 ± 1.05 MBq, n=3) was injected via the penile vein of the mice. Simultaneously with the injection of the PET tracer, an emission scan of 60 minutes was acquired with a Focus 220 rodent scanner (CTI Siemens, Munich, Germany). After completion of the PET scan, a CT scan was performed in a few animals to verify the accuracy of the drawing of the ROI's drawn around the tumors. Therefore, the animal fixed to the bed of the PET camera was positioned in the microCT scanner (MicroCT II, CTI Siemens) and a microCT image (exposure time= 1050 msec; X-Ray voltage= 55 kvp; Anode current= 500 µA; number of rotation steps= 500; total rotation= 360 degrees) was acquired for 15 min to allow anatomic localization of the tumor. From the difference in bed positions between PET and CT, a transformation matrix was constructed, which describes the translation between both images. This transformation matrix was used for precise fusion of both images, using Inveon Research Workplace (Siemens) software.

The list mode data of the emission scans was separated into 17 frames (2×30, 4×60, 5×120, 3×300, 3×600 s). Emission sinograms were iteratively reconstructed (OSEM2D) after being normalized, corrected for attenuation, and corrected for radioactive decay.

Three-dimensional regions of interest (3D-ROIs) were manually drawn around the tumors. Time-activity curves (TACs) for the ROIs were calculated, using standard software (Inveon, Siemens, USA). Tracer accumulation is expressed as standardized uptake values

(SUV), which was defined as: [Tissue activity concentration (MBq/g) × body weight (g) / injected dose (MBq)].

Biodistribution (BD) studies. After the last scan, anesthetized mice were terminated by cervical dislocation. Blood was collected, and plasma and red cells were obtained from the blood sample by centrifugation (20 min at 6000 g). Several tissues (see Table 2) were excised. The complete tumor was removed and separated from muscle and skin. All tissue samples and plasma were weighed and the amount of radioactivity was determined with a gammacounter (LKB Wallac, Turku, Finland). Tracer uptake is expressed as SUV.

Metabolite analysis of [^{18}F]FEAnGA in tumors and plasma. In a group of Balb/c mice 3.90 ± 3.16 MBq of [^{18}F]FEAnGA (n= 10) was injected into the penile vein. The animals were sacrificed at different time points (15, 30 and 75 min) and tumors and blood samples were collected. The blood samples were centrifuged to acquire a plasma sample. Tumors and plasma were weighed and the amount of radioactivity was determined with the gamma counter. Tracer uptake is expressed as SUV. The tumors were homogenized in 0.50 mL of 2% $HClO_4$ and centrifuged (5 min, 3000 g). The acid-soluble fraction of tumors and plasma samples was analyzed by Radio-TLC (R_f [^{18}F]FEA= 0.57, R_f [^{18}F]FEAnGA= 0.89) (eluent: MeCN/H_2O 3:7). After elution, radioactivity on TLC plates was analyzed by phosphor storage imaging. Exposed screens were scanned with a Cyclone phosphor storage system (PerkinElmer) and the percentage of conversion of [^{18}F]FEAnGA as a function of the tracer distribution time was calculated by ROI analysis using OptiQuant software.

Data analysis. Apparent kinetic constants (V_{max} and K_M) were determined from Lineweaver-Buck plots of the initial rates ($1/V_0$) against the reciprocal substrate concentration 1/[S] generated in Sigmaplot software. The comparison between cells with and without β-GUS was performed using a two-sided t-test that was paired for the different conditions in a single experiment. In all cases, a $p \leq 0.05$ was considered significant.

RESULTS AND DISCUSSION

Prior studies with DOX-GA3 and HMR 1826, which have a β-glucuronyl group attached to doxorubicin via a *para* substituted aromatic group showed promising preclinical results for prodrug therapy. Their low general toxicity has been clearly demonstrated in mice and rats studies with human tumor xenografts such as lungs, colon, breast, ovary, stomach, and pancreatic cancer. Experiments in *ex vivo* human lung tumour specimens have demonstrated that HMR 1826 leads to increased levels of free DOX in tumour tissues and decreased levels in normal tissues compared to native DOX. DOX-GA3 showed enhanced efficacy in ovarian cancer xenografts in comparison to native DOX. Inspired by the structures of these doxorubicin prodrugs, we designed an ^{18}F-labeled PET tracer for imaging of β-GUS (Scheme 2). In this PET tracer the DOX moiety is replaced by a lipophilic labeled molecule. After cleavage of the PET tracer by β-GUS, the labeled lipophilic part of the molecule is supposed to be trapped at the cleavage site by non-specific binding.

Compound **1** was prepared in 3 steps from methyl 1-bromo-2,3,4-tri-O-acetyl-α-D-glucopyronuronate according to the procedure described by Duimstra *et al.* [21]. Activation of the imidazole intermediate with methyltriflate followed by the reaction with fluoroethylamine gave compound **2** in 30 % yield. It was observed that the amount of methyl triflate used was critical in this step, since higher amounts than 1.1 mol equivalent led to lower yields of compound **2**. This could be due to the reaction of fluorethylamine with the excess of methyl triflate instead of compound **1**. The deprotection of the sugar moiety in **2** in a single step did not give product **4** in the desired yield, as the reaction was incomplete and led to the formation of multiple side-products. Moreover, the purification of product FEAnGA by flash chromatography proved difficult and consequently it was decided to perform the synthesis of FEAnGA by a two steps procedure as depicted in scheme 3. First, deacetylation of the hydroxyl groups was achieved using sodium methoxide. Then, the basic hydrolysis of the carboxylic ester was performed with NaOH, which afforded the unlabeled reference compound FEAnGA in 50 % yield. The overall yield of this procedure was 23 %. The identity of the compound was confirmed by low

resolution mass spectroscopy (LRMS) and the disappearance of the methoxy and acetyl groups of the glucuronic moiety in ^{1}H NMR.

Scheme 3. Synthesis of compound FEAnGA.

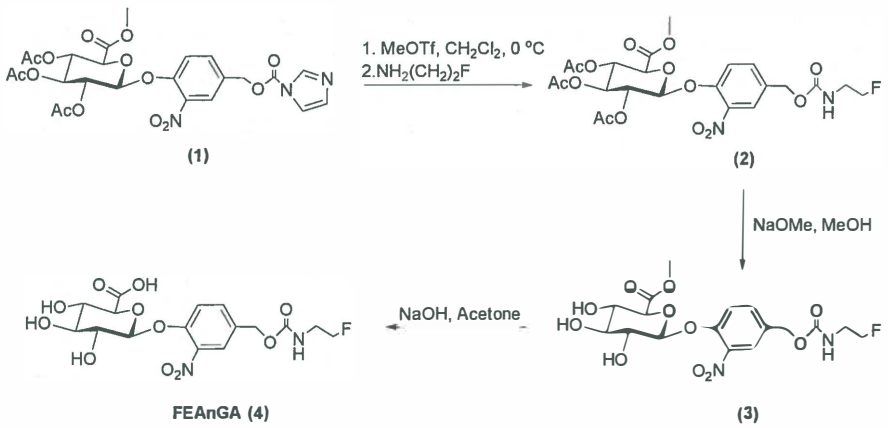

The anomeric β-configuration, essential for substrate affinity for β-GUS, was confirmed by the NMR, which showed the H-1 proton as a doublet at a chemical shift δ_{H-1} of 5.71 ppm with a characteristic coupling constant J_{H1-H2} of 7.7 Hz. Typically, the H1-H2 coupling constants of the α anomer is 2-5 Hz, whereas the coupling constant of the β anomer is between 6 and 10 Hz [19;25;26].

The synthesis of [^{18}F]FEAnGA is a 3 step procedure consisting of the preparation of [^{18}F]FEA followed by the coupling of the amine with compound **1** and the removal of the protecting groups. [^{18}F]FEA was prepared according to the procedure described by Tewson [22] by reaction of tosylate **5** with [^{18}F]fluoride and subsequent removal of the phthalimide group in **6** with hydrazine. This last step is of critical importance with regard to the final labeling yield. In order to obtain distilled [^{18}F]FEA in 48 ± 9 % (n= 8) yield, it is necessary to use hydrated hydrazine in a reaction mixture that is free of acetonitrile to avoid the evaporation of the hydrazine associated water, which is required for the hydrolysis of the phthalimide moiety. On the other hand, distillation should not be performed at higher temperatures than 75 °C or longer than 15 minutes to avoid the

distillation of hydrazine into the second reaction vial. Hydrazine competes with [^{18}F]FEA in the carbamate formation reaction, thus decreasing the final yield. The carbamate formation of compound **1** with the distilled [^{18}F]FEA gives compound [^{18}F]FEAnGA in 33 ± 19 % (n= 8) yield after 30 minutes of reaction at room temperature. Deprotection of the hydroxyl groups was done on the tC18 cartridge by addition of 1 mL 2M NaOH and incubation for 7 min at room temperature. The product was eluted from the cartridge with 4 mL of water and was purified by HPLC in 79 ± 9 % (n= 8) yield. In contrast to the deprotection of the reference compound **2** which was obtained in 2 steps, surprisingly it was possible to deprotect **[^{18}F]-2** in a single step giving our final product in good yield. Thus, the final product [^{18}F]FEAnGA was obtained in 13 ± 7 % (n= 8) overall radiochemical yield (corrected for decay, based on [^{18}F]fluoride) with a total synthesis time of 150 min (Scheme 4). The identity of the tracer was confirmed by coelution with an authentic sample of the non-radioactive compound by RP-HPLC.

Scheme 4. Radiosynthesis of compound [^{18}F]FEAnGA

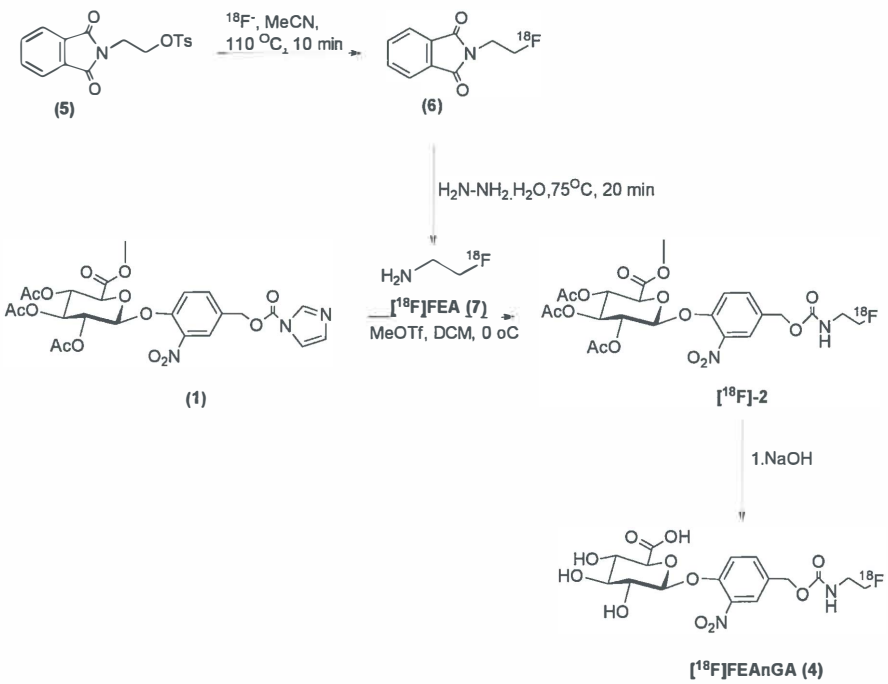

The stability of [$^{18/19}$F]FEAnGA in PBS was determined at 37 °C. After 1 hour of incubation, HPLC analysis showed that 98% of the tracer was still intact. The stability of [^{18}F]FEAnGA in PBS and rat plasma were also determined at 37 °C. After 1 and 3 hours of incubation, 98% and 99% (Radio-TLC) of the radioactivity still corresponded to the intact tracer, respectively. This indicates that the tracer is highly stable *in vitro*.

The lipophilicities of [^{18}F]FEAnGA and [^{18}F]FEA were determined by measuring their n-octanol/water distribution coefficient at pH 7.4, the Log D was found to be -1.61 ± 0.01 for [^{18}F]FEAnGA and -0.69 ± 0.02 for [^{18}F]FEA. As expected, [^{18}F]FEAnGA is about 10 times more hydrophilic than [^{18}F]FEA due to the presence of the glucuronic acid moiety. Moreover, [^{18}F]FEAnGA is less hydrophilic at pH 3 (Log $D_{3.0}$ -1.01 ± 0.03) than at pH 7.4, because the glucuronic acid is partially protonated at acidic pH ($pK_a \approx 3$). In contrast, the log D of [^{18}F]FEA was increased at pH 10 (-0.42 ± 0.03) as compared to pH 7.4, due to the fact that [^{18}F]FEA is not protonated anymore at basic pH ($pK_a \approx 8.8$)[15;19;27-30].

The enzymatic processing of FEAnGA was studied using commercially available bacterial *Escherichia coli* β-GUS and mammalian bovine liver β-GUS. The water-soluble FEAnGA is stable in aqueous buffer in the absence of β-GUS and as a result a solution of FEAnGA remains colorless. However, in the presence of β-GUS it undergoes rapid hydrolysis, resulting in the spontaneous release of [^{18}F]FEA and the self immolating spacer, which immediately colors the solution yellow. The liberation of 4-hydroxy-3-nitrobenzyl alcohol (HNBA) can be measured with a UV-spectrophotometer at 412 nm. In a similar manner, the commercially available reference substrate, PNPG, is cleaved by β-GUS, producing p-nitrophenol (PNP) which can also be measured by UV-spectrophotometer at 402 nm (Fig. 1)

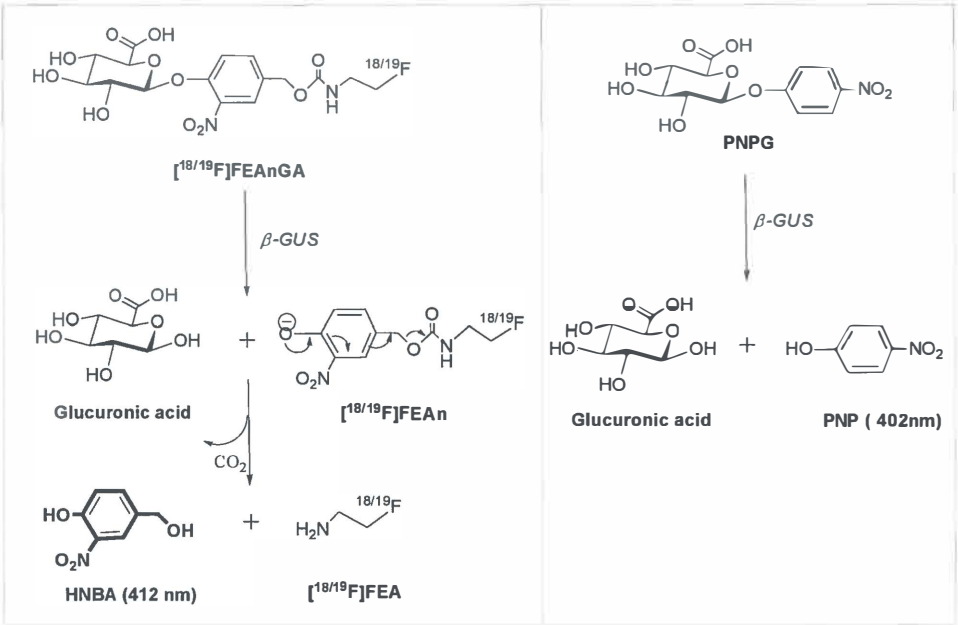

Figure 1. Mechanism of activation of [$^{18/19}$F]FEAnGA and PNPG by β-GUS.

Thus, the kinetic parameters for the hydrolysis of FEAnGA were determined by measuring the release of HNBA under physiological conditions. The kinetic parameters of PNPG were also determined under the same conditions for comparison. In general, the kinetic parameters of FEAnGA are in the same order of magnitude as those of PNPG, which indicates that FEAnGA is a good substrate of β-GUS as well. The maximum hydrolysis rate (V_{max}) of PNPG by *Escherichia coli* β-GUS and bovine liver β-GUS was 4 and 2 times higher than that of FEAnGA, respectively (Table 1). FEAnGA and PNPG show similar affinity for E.coli β-GUS ($K_M \approx 7$ μM). However, FEAnGA (K_M = 5.8 μM) has 6 times higher affinity towards bovine liver- β-GUS than PNPG (K_M = 34 μM). Thus, despite the slightly lower turn over (K_{cat}) of FEAnGA by bovine liver- β-GUS as compared to PNPG, FEAnGA will still undergo relatively fast hydrolysis at low concentrations of substrate and enzyme, as is demonstrated by a higher catalytic efficiency, K_{cat}/K_M. Although FEAnGA is a slightly less efficient substrate for E. coli β-GUS compared to PNPG, it proves to be a better substrate for bovine liver β-GUS (higher K_{cat}/K_M) (Table 1). In a control experiment under identical

conditions, but in absence of β-GUS no hydrolysis of FEAnGA was observed. These results indicate that FEAnGA is specifically hydrolyzed by β-GUS [21;27;31;32].

Table 1. Enzyme Kinetic Parameters for FEAnGA represented by the mean values of triplicate samples ± SD.

Enzyme	Substrate	K_M (μM)	V_{max} (μmol.min^{-1}mg^{-1})	k_{cat} (s^{-1})	k_{cat}/K_M (10^6 $M^{-1}s^{-1}$)
E.coli β-GUS	PNPG	8.2 ± 1.6	1366 ± 68	660	80.3
	FEAnGA	7.1 ± 0.9	348 ± 24	134	24.6
Bovine liver β-GUS	PNPG	34.0 ± 16.5	56.9 ± 23	19	0.6
	FEAnGA	5.7 ± 2.7	25.8 ± 9	10	1.8

Radiolabeled [^{18}F]FEAnGA was rapidly cleaved by both *Escherichia coli* β-GUS and bovine liver β-GUS. Radio-TLC analysis confirmed that the cleavage of [^{18}F]FEAnGA by both enzymes is a two-step process [33]. The consumption of [^{18}F]FEAnGA leads to the formation of an intermediate which we hypothesized being the 4-(hydroxymethyl)-2-nitrophenol self-immolative spacer attached to [^{18}F]FEA ([^{18}F]FEAn). The intermediate ([^{18}F]FEAn) is subsequently converted to [^{18}F]FEA resulting in almost complete cleavage of the tracer into [^{18}F]FEA within 10 min of incubation with *Escherichia coli* β-GUS (95 % conversion) and 30 min of incubation with bovine liver β-GUS (86% conversion) (Fig. 2).

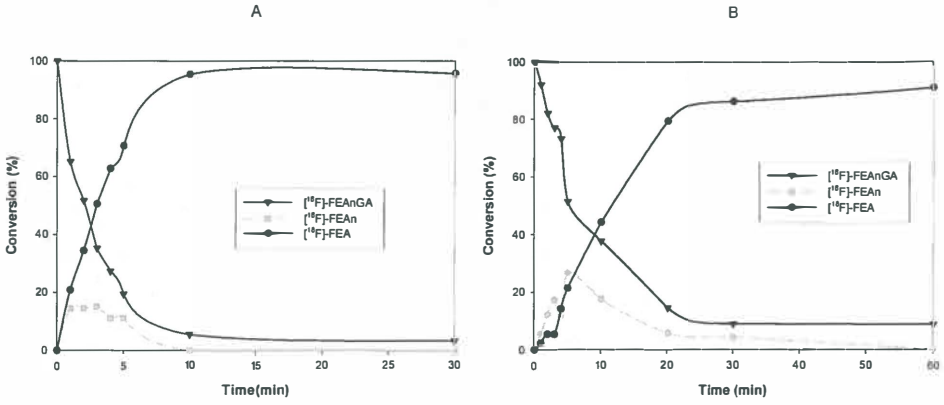

Figure 2. Cleavage of [^{18}F]FEAnGA by **A)** E.Coli β-GUS (n= 1), **B)** bovine liver β-GUS (n= 1)

[^{18}F]FEAnGA and [^{18}F]FEA were evaluated in genetically engineered CT26mβGUS murine colon adenocarcinoma cells that expressed membrane-anchored β-GUS on the outer cell membrane. Therefore, CT26 cells and CT26mβGUS were incubated with [^{18}F]FEAnGA or [^{18}F]FEA for 60 minutes at 37 °C. Incubation with [^{18}F]FEA resulted in a 14 times higher cell associated radioactivity in control CT26 cells than incubation with [^{18}F]FEAnGA. This increase in uptake is most likely due to the small size of [^{18}F]FEA that enables the crossing of the cell membrane by passive diffusion and nonspecific binding to the cell membrane. There was no significant difference between CT26 and CT26mβGUS associated radioactivity when incubated with [^{18}F]FEA, while incubation with [^{18}F]FEAnGA caused 3 times higher uptake in β-glucuronidase expressing cells (CT26mβGUS) than control CT26 cells (Fig. 3). Radio-TLC of the medium showed that [^{18}F]FEAnGA was converted to [^{18}F]FEA (20% conversion) by the enzyme expressing cells only.

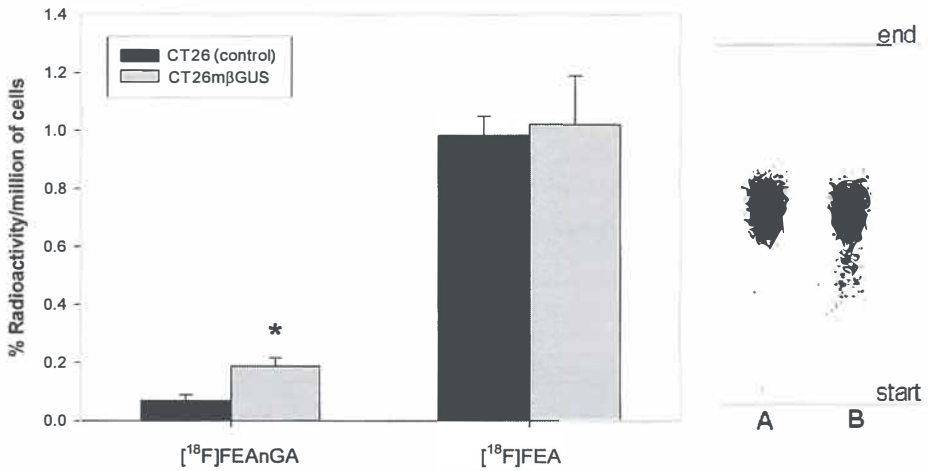

Figure 3. Cell associated radioactivity of [^{18}F]FEAnGA and [^{18}F]FEA in control (CT26) and CT26mβGUS cells. Data are expressed as % Radioactivity/million cells and are mean values of triplicate samples ± SD. *p<0.05, unpaired bidirectional Student *t* test (left side). Radio-TLC of (A) medium sample of CT26 cells; (B) medium sample of CT26mβGUS. The upper spot represents the intact [^{18}F]FEAnGA and the lower spot represents [^{18}F]FEA.

To test the potential of [^{18}F]FEAnGA as a PET tracer probe for detecting β-GUS expression *in vivo*, a PET study was performed in mice bearing CT26 and CT26mβGUS tumors. Mice were injected with either [^{18}F]FEAnGA or [^{18}F]FEA and a microPET scan was acquired for 60 min followed by a 15 min microCT scan. After injection of the mice with [^{18}F]FEAnGA, the CT26mβGUS tumor produced a much stronger signal than the control tumor (CT26). The uncleaved [^{18}F]FEAnGA was rapidly cleared out of the body leading to a very clear image with a good tumor-to-background ratio. High accumulation of radioactivity was observed only in the bladder and the kidney, as result of the rapid renal clearance of the intact tracer. On the other hand, animals injected with [^{18}F]FEA revealed a homogeneous distribution, indicating no specific accumulation in the tumors (Fig. 4). Therefore, it was only possible to discriminate the tumor in the [^{18}F]FEA images, in particular the control CT26 tumors, using the fused PEC/CT images.

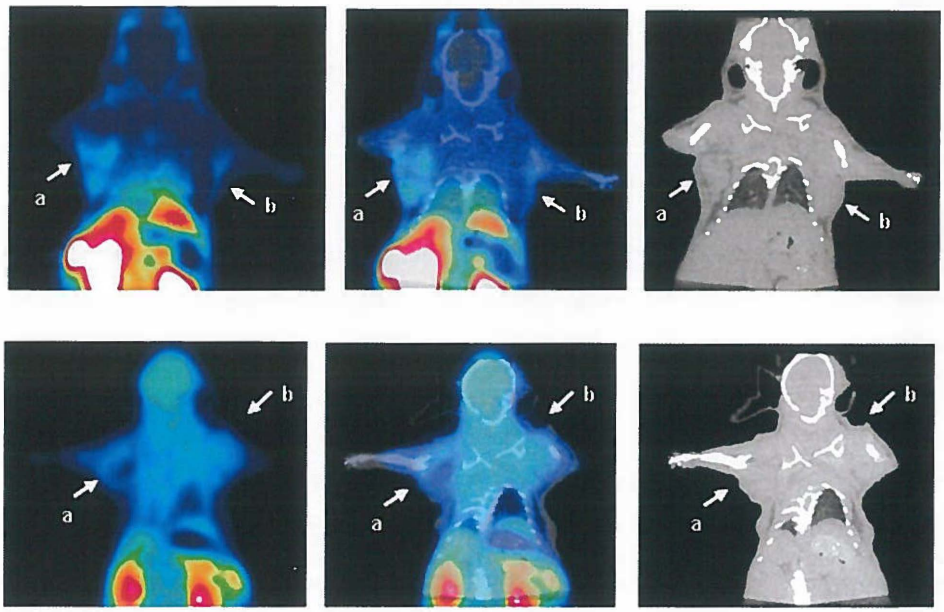

Figure 4. MicroPET image (left), microPET/CT fusion image (middle) and microCT image (right) of a mouse bearing a CT26mβGUS tumor (a) and a CT26 tumor (b) injected with either [^{18}F]FEAnGA (upper row) or [^{18}F]FEA (lower row).

The time activity curves of [^{18}F]FEAnGA revealed different kinetics between the tumors. In the CT26mβGUS tumors, maximum accumulation of the tracer was reached within 12 min post injection. Subsequently, tumor activity decreased exponentially with a half-life of 61 ± 30 min. In the control tumor (CT26), the maximum accumulation of the tracer was reached within 6 min post injection, after which activity decreased more rapidly with a half-life of 43 ± 29 min (Fig. 5). These differences in accumulation of radioactivity between both tumors are statistically significant at intervals ≥14 min (n= 7; $p<0.05$) after the injection of [^{18}F]FEAnGA.

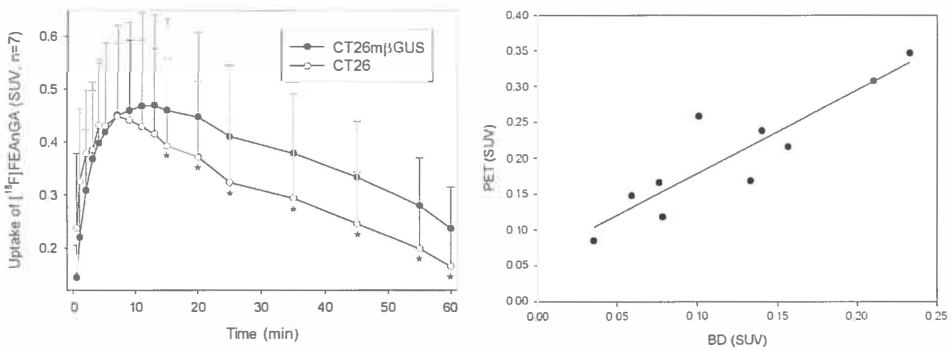

Figure 5. Time activity curves of [^{18}F]FEAnGA accumulation (SUV) in mice bearing both CT26mβGUS and CT26 tumors (left side). Correlation between the uptake (SUV) of the excised tumors and the uptake (SUV) obtain obtained from PET imaging at 60 minutes post injection ($y=1.1651x + 0.0626$, $r^2= 0.81$, $p= 0.0004$) (right side).

Ex vivo biodistribution of [^{18}F]FEAnGA and [^{18}F]FEA performed at 75 min post injection are shown in table 2. [^{18}F]FEAnGA uptake in CT26mβGUS tumors was 2 fold higher than in CT26 tumors (0.15 ± 0.06 and 0.07 ± 0.04, respectively; p= 0.001; n= 7) and correlated well with the SUV obtained from PET imaging (Fig. 5). In contrast, injection of [^{18}F]FEA did not result in differential accumulation of radioactivity between CT26mβGUS (0.42 ± 0.06) and CT26 (0.48 ± 0.09; p= 0.34; n= 3) tumors.

Table 2. *Ex vivo* biodistribution of [^{18}F]FEAnGA and [^{18}F]FEA 75 min p.i in BALB/c mice bearing CT26 and CT26mβGus tumors, expressed as standardized uptake values (SUV; mean ± SD).

	[^{18}F]FEAnGA (n= 7)	[^{18}F]FEA (n=3)
Bone	0.04 ± 0.03	0.22 ± 0.05
Colon	0.14 ± 0.06	0.95 ± 0.37
Heart	0.08 ± 0.03	0.38 ± 0.14
Kidney	0.50 ± 0.17	1.08 ± 0.27
Liver	0.25 ± 0.10	0.64 ± 0.18
Lung	0.14 ± 0.06	0.50 ± 0.17
Pancreas	0.08 ± 0.06	0.48 ± 0.14
Spleen	0.10 ± 0.06	0.73 ± 0.12
R.B.C	0.07 ± 0.03	0.37 ± 0.22
Plasma	0.26 ± 0.13	0.33 ± 0.16
Muscle	0.10 ± 0.12	0.45 ± 0.12
CT26	0.07 ± 0.04	0.48 ± 0.09
CT26mβGUS	0.15 ± 0.06	0.42 ± 0.06

[^{18}F]FEAnGA also displayed a faster blood clearance and low uptake in non-target tissues, resulting in better tumor-to-muscle ([^{18}F]FEAnGA: 2.41 ± 1.10; [^{18}F]FEA: 0.95 ± 0.09; p= 0.01) ratios in CT26mβGUS tumors, as compared to CT26 tumors ([^{18}F]FEAnGA: 1.11 ± 0.46; [^{18}F]FEA: 1.08 ± 0.22, p= 0.87). Both tracers, [^{18}F]FEAnGA and [^{18}F]FEA, had relatively high uptake in the kidneys (0.50 ± 0.17 and 1.08 ± 0.27) and moderate uptake in the liver (0.25 ± 0.10 and 0.64 ± 0.18).

To investigate whether the radioactivity accumulation in the tumors was specifically due to the conversion of [^{18}F]FEAnGA into [^{18}F]FEA by extracellular β-GUS, metabolite analysis of CT26mβGUS and CT26 control tumors was performed. Plasma analysis of the mice injected with [^{18}F]FEAnGA revealed that 90 % of the activity was present as intact tracer at 60 min, indicating high *in vivo* stability. Figure 6 indicates that 80% of [^{18}F]FEAnGA in CT26mβGUS tumors was converted into [^{18}F]FEA over time, while in CT26 control tumors this conversion reached 40%.

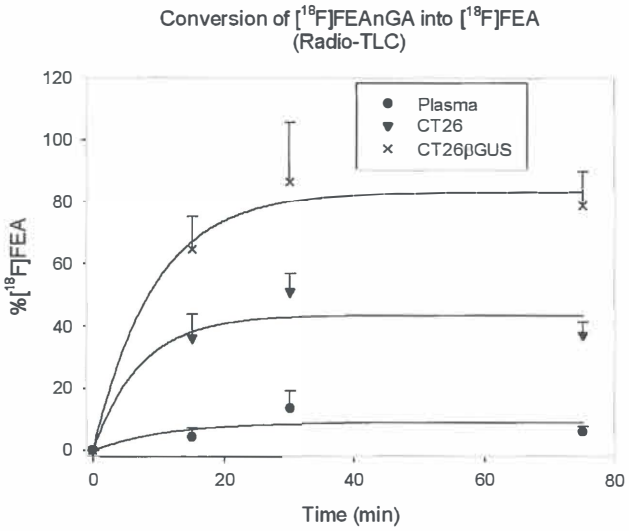

Figure 6. [^{18}F]FEAnGA metabolite analysis by Radio-TLC of acid-soluble fractions of CT26mβGUS tumors, CT26 tumors and plasma.

Metabolite analysis of the tumors suggests that the enhanced radioactivity in CT26mβGUS tumors is due to conversion of [^{18}F]FEAnGA into [^{18}F]FEA by β-GUS present in the extracellular domain. It seems likely that some of the radioactivity present in the control CT26 tumor was also due to extracellular β-GUS, as metabolite analysis showed up to 40% conversion of the tracer in control tumors as well. In this study, CT26 tumors were relatively large and contained some necrotic regions which are known to contain extracellular β-GUS. Plasma analysis revealed that [^{18}F]FEAnGA is highly stable *in vivo* during the scanning time, presenting no more than 10% of metabolites one hour after tracer injection. Although β-GUS enzyme assays could be performed in both tumors to evaluate the excess of β-GUS present in CT26mβGUS tumors compared to the control CT26 tumors, it would be difficult to discriminate the extracellular enzyme concentration in a tumor from the intracellular enzyme. Thus it would be not possible to correlate the amount of extracellular β-GUS with the conversion of [^{18}F]FEAnGA to [^{18}F]FEA and ultimately with the uptake in the tumor.

This *in vivo* study suggest that extracellular β-GUS efficiently cleaves the tracer, resulting in the formation of [^{18}F]FEA, which is retained in the tumor. The increased

retention of radioactivity in the tumor that expresses β-glucuronidase extracellularly can be visualized in the PET images.

CONCLUSION

[^{18}F]FEAnGA was efficiently labeled with [^{18}F]fluoride in good yield. [$^{18/19}$F]FEAnGA showed high *in vitro* stability in PBS and rat plasma. Kinetic studies indicate that [$^{18/19}$F]FEAnGA is a good substrate for *Escherichia coli* β-GUS and bovine liver β-GUS. Cleavage of the tracer by β-GUS caused an increase in cell associated radioactivity in CT26/CT26mβGUS cells. The *in vivo* study showed that [^{18}F]FEAnGA is specially retained in CT26mβGUS tumors with high tumor uptake and good tumor-to-background ratio. Therefore [^{18}F]FEAnGA has proven to be a promising PET tracer for imaging of extracellular β-glucuronidase activity.

ACKNOWLEDGMENT

We gratefully thank Annie van Dam and Margot Jeronimus-Stratingh for performing all LRMS analysis, Katica Stojanov for her help in the C6 glioma cell studies, Dr. Steve Roffler for providing the CT26mβGUS cells and Jurgen Sijbesma for the help in the *in vivo* study.

REFERENCES

1. De Graaf M, Boven E, Scheeren HW, Haisma HJ, and Pinedo HM (2002) Curr. Pharm. Des 8:1391-1403.
2. George J (2008) Biochem. Cell Biol. 86:235-243.
3. Boyer MJ and Tannock IF (1993) Adv. Cancer Res. 60:269-291.
4. Chen X, Wu B, and Wang PG (2003) Curr. Med. Chem. Anticancer Agents 3:139-150.
5. De Groot FM, Damen EW, and Scheeren HW (2001) Curr. Med. Chem. 8:1093-1122.
6. Denny WA (2003) J. Biomed. Biotechnol. 2003:48-70.
7. Papot S, Tranoy I, Tillequin F, Florent JC, and Gesson JP (2002) Curr. Med. Chem. Anticancer Agents 2:155-185.
8. Rivault F, Tranoy-Opalinski I, and Gesson JP (2004) Bioorganic & Medicinal Chemistry 12:675-682.
9. Sperker B, Murdter TE, Schick M, Eckhardt K, Bosslet K, and Kroemer HK (1997) J. Pharmacol. Exp. Ther. 281:914-920.
10. Sperker B, Werner U, Murdter TE, Tekkaya C, Fritz P, Wacke R, Adam U, Gerken M, Drewelow B, and Kroemer HK (2000) Naunyn Schmiedebergs Arch. Pharmacol. 362:110-115.
11. Chen KC, Cheng TL, Leu YL, Prijovich ZM, Chuang CH, Chen BM, and Roffler SR (2007) Cancer Gene Ther. 14:187-200.
12. Ho NH, Weissleder R, and Tung CH (2007) Chembiochem 8:560-566.
13. Su YC, Chuang KH, Wang YM, Cheng CM, Lin SR, Wang JY, Hwang JJ, Chen BM, Chen KC, Roffler S, and Cheng TL (2007) Gene Ther. 14:565-574.
14. Biber FZ, Unak P, Ertay T, Medine El, Zihnioglu F, Tasci C, and Durak H (2006) Applied Radiation and Isotopes 64:778-788.
15. Celen S, Deroose C, de Groot T, Chitneni SK, Gijsbers R, Debyser Z, Mortelmans L, Verbruggen A, and Bormans G (2008) Bioconjugate Chemistry 19:441-449.
16. Ertay T, Unak P, Biber FZ, Tasci C, Zihnioglu F, and Durak H (2007) Applied Radiation and Isotopes 65:170-175.
17. Kumar P, Wiebe LI, Mannan RH, Zhang Z, Xia HY, and Mcewan AJ (2002) Applied Radiation and Isotopes 57:719-728.
18. Brady F, Luthra SK, Brown GD, Osman S, Aboagye E, Saleem A, and Price PM (2001) Current Pharmaceutical Design 7:1863-1892.
19. Rukhman I and Gutman AL (2000) Tetrahedron Letters 41:6889-6892.
20. Antunes IF, Haisma HJ, and de Vries EF (2008) Nucl. Med. Commun. 29:845-846.
21. Duimstra JA, Femia FJ, and Meade TJ (2005) Journal of the American Chemical Society 127:12847-12855.
22. Tewson TJ (1997) Nuclear Medicine and Biology 24:755-760.

23. Combaud D, Thomas M, Papot S, and Gesson JP (2005) Letters in Drug Design & Discovery 2:631-637.
24. Tomasic J and Keglevic D (1973) Biochemical Journal 133:789-795.
25. Chittaboina S, Hodges B, and Wang Q (2006) Letters in Organic Chemistry 3:35-38.
26. Stachulski AV and Jenkins GN (1998) Natural Product Reports 15:173-186.
27. Houba PH, Leenders RG, Boven E, Scheeren JW, Pinedo HM, and Haisma HJ (1996) Biochem. Pharmacol. 52:455-463.
28. Huwyler J, Drewe J, Klusemann C, and Fricker G (1996) British Journal of Pharmacology 118:1879-1885.
29. Huwyler J, Drewe J, Gutmann H, Thole M, and Fricker G (1998) International Journal of Clinical Pharmacology and Therapeutics 36:69-70.
30. Leu YL, Chen CS, Wu YJ, and Chern JW (2008) Journal of Medicinal Chemistry 51:1740-1746.
31. Bosslet K, Czech J, and Hoffmann D (1994) Cancer Res. 54:2151-2159.
32. Wei GP, Loktionova NA, Pegg AE, and Moschel RC (2005) Journal of Medicinal Chemistry 48:256-261.
33. Bakina E, Wu Z, Rosenblum M, and Farquhar D (1997) J. Med. Chem. 40:4013-4018.

Chapter

In vivo evaluation of [^{18}F]FEAnGA: a PET tracer for imaging β-glucuronidase (β-GUS) activity in a tumor & inflammation rodent model

Inês F. Antunes, Hidde J. Haisma, Philip H. Elsinga,
Aren van Waarde, Antoon T. M. Willemsen,
Rudi A. Dierckx, Erik F. J. de Vries

Parts of this chapter have been published in Bioconjug Chem 2010; 21(5), 911-20 and in Molecular imag 2011, in press

ABSTRACT

β-Glucuronidase (β-GUS) plays an important role in inflammation and degenerative processes. The enzyme has also been investigated as a target in prodrug therapy for cancer. To investigate the role of β-GUS in pathologies and to optimize β-GUS-based prodrug therapies, we developed a PET tracer,1-O-(4-(2-fluoroethyl-carbamoyloxymethyl)-2-nitrophenyl)-O-β-D-glucopyronuronate ([^{18}F]FEAnGA) that proved to be selectively cleaved by β-GUS. Here we present the evaluation of [^{18}F]FEAnGA for imaging of β-GUS in a tumor & inflammation model. C6 glioma cells incubated with the tracer and *Escherichia coli* β-GUS or bovine liver β-GUS showed a 4 and 1.5-fold higher uptake of radioactivity respectively, as compared to control C6 cells without β-GUS. *Ex vivo* biodistribution of [^{18}F]FEAnGA was conducted in healthy rats. PET imaging and pharmacokinetic modeling was performed in Wistar rats bearing C6 tumors of different sizes and a sterile inflammatory lesion. The biodistribution studies of [^{18}F]FEAnGA indicated low uptake in major organs and rapid excretion through the renal pathway. MicroPET studies revealed 3 times higher uptake in the viable part of larger C6 gliomas than in smaller C6 gliomas. Uptake in inflamed muscle was significantly higher than in control muscle. The distribution volume of [^{18}F]FEAnGA in the viable part of the tumor correlated well with the cleavage of the tracer to [^{18}F]fluoroethylamine and the spacer 4-hydroxy-3-nitrobenzyl alcohol. [^{18}F]FEAnGA is a PET tracer able to detect an increased activity of β-GUS in large solid tumors as well as in inflamed tissues.

INTRODUCTION

β-Glucuronidase (β-GUS) (EC 3.2.1.31) is a lysosomal enzyme that catalyzes the hydrolysis of the β-glucuronic acid residue from the glycosaminoglycans. Therefore, β-GUS is an essential enzyme for the normal restructuring of the extracellular matrix. The enzyme is localized intracellularly in lysosomes and microsomes and its activity is hardly detectable in human blood in normal conditions [1]. However, increased levels of extracellular β-GUS have been reported in various inflammatory pathologies, where it plays a role in the degenerative processes [2]. It is known that tumors also have high extracellular levels of β-GUS, due to release of the enzyme by invading monocytes and granulocytes, as well as release from necrotic tumor cells [3].

The extracellular β-GUS in tumors has been exploited as target for new anticancer therapies. Conventional cancer chemotherapy is associated with severe dose-limiting side-effects, which often restrict the therapeutic efficacy of drugs. To increase the therapeutic index, the drug could be modified into a non-toxic prodrug that is converted *in situ* to the active drug by an enzyme that is selectively expressed at the target site. β-GUS has been investigated as an endogenous prodrug-converting enzyme.

Glucuronide prodrugs exhibit low toxicity due to their hydrophilic nature, which prevents them from entering normal cells and thus from being activated by lysosomal β-GUS. However, in large tumors the intracellular enzyme is released from necrotic tumor cells and macrophages resulting in activation of glucuronide prodrugs by the extracellular β-GUS present at the tumor site [4-6]. Encouraging *in vivo* results were obtained with the prodrugs such as DOX-GA3, HMR 1826 and 9ACG [7-9]. These prodrugs were able to release the active drug (either doxorubicin or camptothecin) after enzymatic cleavage of the glucuronide moiety by extracellular β-GUS inducing superior or equal tumor growth inhibition (70 to 80%) over the toxic parent drug (40% to 80%) in human tumor xenografts. These results suggest that bioactivation of glucuronide prodrugs by β-GUS is an attractive approach in prodrug therapy.

However, interindividual and intertissue variability of β-GUS activity as well as factors modulating the enzyme's expression and activity are key determinants for the

success of these prodrug therapeutic strategies [10;11]. Therefore, monitoring enzyme activity in larger animals and ultimately in humans, using specific radiotracers combined with nuclear imaging techniques like PET would lead to a better understanding of the metabolic conversion of prodrugs and improvement of β-GUS targeted therapy [12;13].

Recently Roffler *et al.* designed a PET tracer, [^{124}I]-phenolphthalein glucuronide ([^{124}I]-PTH-G), for β-GUS imaging. This tracer selectively accumulated in a genetically modified β-GUS expressing tumor, as compared to a control tumor [14]. Fluorine-18 has superior imaging properties over iodine-124, therefore we designed a ^{18}F-labeled PET tracer for β-GUS, [^{18}F]FEAnGA [15]. This tracer has a structure similar to the HMR 1826 prodrug, with the doxorubicin moiety replaced by a [^{18}F]fluoroalkylamine group (Fig.1). This tracer has proven to be selectively cleaved by β-GUS *in vitro*.

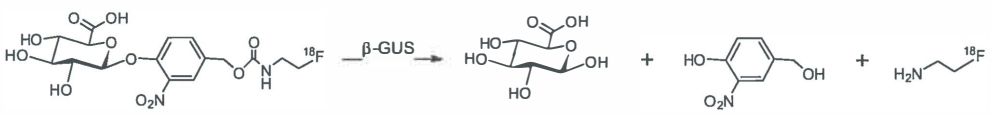

Figure 1. Cleavage of [^{18}F]FEAnGA by β-GUS. The radioactive product [^{18}F]FEA is locally trapped and the released HNBA can be measured photospectrometrically.

A preliminary *in vivo* study in mice bearing genetically modified CT26mβGUS (overexpressing GUS) and CT26 tumors (control) suggests that extracellular β-GUS efficiently cleaves the tracer *in vivo*, resulting in higher radioactivity accumulation in tumors which expresses extracellular β-GUS. Here we present an *in vivo* evaluation of [^{18}F]FEAnGA as a PET tracer for imaging of β-GUS in a less artificial model: i.e. rats bearing C6 gliomas with different dimensions and in a sterile muscle inflammation. The inflammation was induced by injection of turpentine which is known to result in exudation of plasma and infiltration of neutrophils within 24h. The infiltrating leukocytes are thought to release β-GUS in the inflamed muscle. The C6 glioma is a rapidly growing tumor that becomes necrotic when it grows larger than 1 g. In the necrotic tumor areas, β-GUS is released by the necrotic tumor cells and infiltrating white blood cells. Thus, the large C6

tumors and the inflamed muscle, both having increased extracellular β-GUS levels, are expected to show enhanced [^{18}F]FEAnGA accumulation.

MATHERIALS AND METHODS

Reagents and solvents were obtained from commercial suppliers (Sigma-Aldrich and Fluka, Zwijndrecht, The Netherlands and Merck, Darmstadt, Germany) and used without further purification.

Preparation of [^{18}F]FEA. [^{18}F]FEA was prepared by [^{18}F]fluorination of N-[2-(toluene-4-sulfonyloxy)-ethyl]-phtalimide (30 mg, 0.09 mmol) in acetonitrile at 110 °C, followed by deprotection with hydrazine hydrate (50 µl, 1.03 mmol) as described in literature [16]. The tracer was purified by high-performance liquid chromatography (HPLC), using a semi-preparative Prodigy C_{18} reverse-phase column (5µ, 10×250 mm; Phenomenex) with 10 % ethanol in 2.5 mM sodium phosphate buffer as the eluent (flow rate, 4 mL/min; retention time: [^{18}F]FEA= 5 min).

Preparation of [^{18}F]FEAnGA. [^{18}F]FEAnGA was prepared from [^{18}F]fluoroethylamine ([^{18}F]FEA) as described previously [15]. The tracer was purified by HPLC, using a semi-preparative Prodigy C_{18} reverse-phase column (5 µ, 10×250 mm; Phenomenex) with 10 % ethanol in 2.5 mM sodium phosphate buffer as the eluent (flow rate, 4 mL/min; retention time: [^{18}F]FEAnGA= 10 min, [^{18}F]FEA= 5 min). At the end of synthesis (EOS), quality control was performed by HPLC with a Symmetry C_{18} column [5 µm, 4.6×150 mm] with 5% acetonitrile in sodium phosphate buffer 2.5 mM as the eluent (flow rate, 1mL/min; retention time: [^{18}F]FEAnGA= 23 min). The specific activity of [^{18}F]FEAnGA was 150 ± 60 GBq/µmol and the radiochemical purity was always > 95%.

Culturing of C6 rat glioma cells. C6 rat glioma cells obtained from the American Type Culture Collection were maintained in DMEM supplemented with 7.5 % fetal bovine serum in 25 cm^3 culture flasks. All cells were grown in a humidified atmosphere containing 5% CO_2 and passaged every 3-4 days.

Cellular uptake of [^{18}F]FEAnGA in C6 glioma cells. For uptake experiments, cells were plated in triplicate in a 12-well plate at a density of 7×10^5 cells per well. After 24 h,

the medium was discarded and 1 mL of PBS-GMC buffer (5.6 mM D-glucose, 0.49 mM $MgCl_2$ and 0.68 mM $CaCl_2$ in 100 mL phosphate-buffered saline (PBS)) per well was added, followed by the addition of 200 μL [^{18}F]FEAnGA (ca. 250 kBq) or 10 μL [^{18}F]FEA (ca. 125 kBq). In two series of 3 wells, an excess of E. coli β-GUS (740U) or bovine liver β-GUS (340U) was added, respectively. After 60 min of incubation at 37 °C, the medium was collected, the cells washed with cold PBS (3×1 mL/well), harvested with trypsin (250 μL) and resuspended in 1750 μL of DMEM. The cell suspensions as well as the supernatant fractions were collected separately for each well and the radioactivity was measured using a gamma counter. For each well, the medium was analyzed for conversion of [^{18}F]FEAnGA into [^{18}F]FEA by Radio-TLC (R_f FEA= 0.37, R_f FEAnGA= 0.54) (eluent: MeOH/CH_2Cl_2 2:8 + 0.1% Et_3N). After elution, the TLCs were analyzed by phosphor storage imaging. The screens were scanned with Cyclone phosphor storage system (PerkinElmer) and the percentage of conversion of [^{18}F]FEAnGA as a function of the incubation period was calculated by ROI analysis using OptiQuant software.

Efflux analysis of [^{18}F]FEA in C6 glioma cells. C6 glioma cells were plated in triplicate in a 12-well plate at a density of 7×10^5 cells per well. After 24 h, the medium was discarded and 1 mL of PBS-GMC buffer per well was added, followed by the addition of 10 μL [^{18}F]FEA (ca. 1.3 MBq). After 60 min of incubation at 37 °C, the medium was discarded, the cells washed with cold PBS (3×1 mL/well), and 1 mL of PBS-GMC buffer per well was added. At different time points the medium was collected and the cells harvested with trypsin (250 μL) and resuspended in 1750 μL of DMEM. The cell suspensions as well as the supernatant fractions were collected separately for each well and the radioactivity was measured using a gamma counter.

Induction of subcutaneous C6 tumors in Wistar rats. Wistar rats (6-8 weeks old) were obtained from Harlan (Lelystad, The Netherlands). The animals were provided with standard laboratory chow and tap water *ad libitum*. All studies were carried out in compliance with the local ethical guidelines for animal experiments. The protocols were approved by the Animal Ethics Committee of University of Groningen. The tumor-inflammation model was described previously by van Waarde *et al.* [17]. Briefly, C6 glioma

cells [2-3 × 10^6 in a 1:1 mixture of Matrigel and Dulbecco's minimal essential medium containing 7.5 % fetal bovine serum] were subcutaneously injected into the right shoulder of male Wistar rats. At day 12, 0.1 mL of turpentine was intramuscularly injected into the thigh of the left hind leg of the same animal.

Biodistribution (BD) studies in health Wistar rats. A group of healthy Wistar rats (n=5) was anesthetized with 2% isoflurane (Pharmachemie BV, The Netherlands) in medical air. The unconscious animals were injected into the penile vein with 5.04 ± 1.80 MBq of [^{18}F]FEAnGA. The animals were sacrificed 60 minutes post injection by extirpation of the heart, while still being under deep anesthesia. The main tissues were excised (table 1). Blood was collected, and plasma and red cells were obtained from the blood sample by centrifugation (10 min at 6000 rpm). All samples were weighed and the respective amount of radioactivity was determined with a gamma counter (LKB Wallac, Turku, Finland). Tracer uptake is expressed as standardized uptake value (SUV), which is defined as: [Tissue activity concentration (MBq/g) × body weight (g) / injected dose (MBq)].

PET imaging of tumor accumulation of [^{18}F]FEAnGA. In the tumor-inflammation model (n= 8), PET scans were performed in the same animal on day 8 (tumor only) and on day 13 (tumor + inflammation). The rats were anesthetized with 2% isoflurane (Pharmachemie BV, The Netherlands) and positioned in the small animal PET camera (Focus 220) with the tumor in the field of view. The linear spatial resolution in the center of the field-of-view of the camera is <1.3 mm, corresponding to a volumetric resolution <2.5 µl. A transmission scan of 515 seconds with a Co-57 point source was obtained for the correction of attenuation and scatter by tissue. After the transmission scan was completed 12.5 ± 4.7 MBq of the PET tracer [^{18}F]FEAnGA was injected via the penile vein. Simultaneously with the injection of the PET tracer an emission scan of 60 minutes was started. After completion of the emission scan on day 8, the animals were placed back in their cages and allowed to wake up. After the scan on day 13, the rats bearing a C6 tumor and sterile inflammation were sacrificed by extirpation of the heart, while still being under deep isoflurane anesthesia. The complete tumor was removed and separated from muscle and skin. Inflamed muscle could be distinguished from the surrounding tissue by its pale

color and the strong odor of turpentine. The inflamed region was excised from the affected thigh. Tumor, control and inflamed muscle were weighed and the respective amount of radioactivity was measured with a gamma counter.

PET imaging and pharmacokinetics of [^{18}F]FEAnGA in tumor-bearing rats. In a group of Wistar rats (n= 13) bearing a C6 tumor (8 days after inoculation) or a C6 tumor and inflammation (13 days after inoculation) a canula was inserted into the femoral artery for collecting blood samples. A dynamic PET scan was performed as described above. During the PET scan, blood samples of 0.1 mL were taken at 15, 30, 45, 60, 75, 90, 120, 150, 300, 450, 600, 1800, 3600 seconds after tracer injection. After a blood sample was taken, 0.1 mL of heparinized saline was injected via the artery canula to prevent large changes in blood pressure. The blood samples were centrifuged at 6000 rpm for 10 minutes and 50 µL of plasma were collected. The activity in plasma was measured with a gamma counter (LKB Wallac, Turku, Finland). The plasma-activity curves were corrected for decay. The rats were sacrificed after the scan and the tumors, inflamed and healthy muscles were excised and weighed. The radioactivity in the tissues was measured with a gamma counter and converted into SUV.

PET data reconstruction and data analysis. The list mode data of the emission scans was separated into 17 frames. Emission sinograms were iteratively reconstructed (OSEM2D, 4 iterations, 16 subsets) after being normalized, corrected for attenuation, and corrected for radioactive decay. Three-dimensional regions of interest (3D-ROIs) were generated automatically based on Intensity threshold method using Inveon Research Workplace software (Inveon, Siemens, USA) [18;19]. Briefly, the last 9 frames (10-60 min) were summed and a ROI of the viable part of the tumor was generated automatically with a 50 % threshold using a region growing method, i.e. only pixels were included with tracer uptake greater than 50 % of the maximum value within the lesion. The resulting ROIs were used on the original data to create the corresponding time-activity curves (TACs). A second ROI was drawn around the whole tumor to obtain the total tumor volume (V_t; cm^3), using standard software (Inveon, Siemens, USA). In those animals where plasma input curves were obtained through arterial sampling, pharmacokinetic modeling of the

tissue TACs was performed using standard software (Inveon, Siemens, USA). The graphical Logan Model was used to determine the distribution volume, DV_T, and a 2 tissue-compartment model (2TCM) fit were used to calculate the K_1-k_4 with a free blood volume. The binding potential (BP_{ND}) was defined as k_3/k_4. The kinetic modeling was performed using the metabolite plasma radioactivity curve as input function.

Metabolite analysis of [^{18}F]FEAnGA in plasma. 2.5 µL of each plasma sample was collected and applied on a TLC plate (Merck F-254 silica gel plates) and eluted with acetonitrile/water (7:3) (R_f [^{18}F]FEA= 0.57, R_f [^{18}F]FEAnGA= 0.89). After elution, radioactivity on TLC plates was analyzed by phosphor storage imaging. Exposed screens were scanned with a Cyclone phosphor storage system (PerkinElmer) and the percentage of conversion of [^{18}F]FEAnGA as a function of the tracer distribution time was calculated by ROI analysis using OptiQuant software.

***Ex vivo* analysis of the conversion of [^{18}F]FEAnGA to [^{18}F]FEA by measurement of the release of HNBA.** Part of the tumors (0.08 ± 0.04 g), inflamed muscle (0.11 ± 0.05 g) and healthy muscle (0.09 ± 0.03 g), excised from the sampled animals was homogenized in 2 mL of phosphate buffered saline (PBS). The homogenates were centrifuged (10 min, 3000 rpm, 4 °C) and the supernatant was collected and kept on ice. To the supernatant, 2 mL of cold MeCN was added to precipitate the remaining proteins. The samples were vortexed for 30 s and centrifuged at 3000 rpm for 10 min at 4 °C. A volume of 1.5 mL of the supernatant was added to 1.5 mL of cold NaOH 0.25M and UV absorption was measured (Waters 2487 dual wavelength absorbance detector, 412nm). Absorption was converted in concentration, using a HNBA calibration curve, and corrected for the weight of the tumor sample. The measurements were performed in duplicate.

***Ex vivo* analysis of tracer specificity by inhibition of β-GUS.** To prove that of [^{18}F]FEAnGA cleavage is mediated by β-glucuronidase, inhibition experiments were performed using the specific β-glucuronidase inhibitor D-glucaro-1,4-lactone (saccharolactone). Tumors were excised and directly homogenized in 1 mL of PBS. Either 1 mL of 50 µM of saccharolactone in PBS (β-GUS inhibition) or 1 mL of PBS alone (control) were added to the homogenates. After 5 min at 37 °C, approximately 250 kBq of

[^{18}F]FEAnGA was added and the homogenates were incubated at 37 °C for another hour. During this period, samples were taken at different time points and analyzed by radioTLC, as described above for the metabolite analysis.

Histology of tumor necrosis. The frozen excised tumors were cut serially in sections of 20 µm thickness. Central sections of the tumor (containing a mixture of the rim and the necrotic core) were stained with haematoxylin and eosin using standard procedures and photographed with an Olympus photomicroscope.

Statistical analysis. Statistical analyses were performed using Excel 2003 (Microsoft) and SigmaPlot (version 10.0; SPSS, Inc.). Tumors were divided in two groups based on their sizes, using the mean volume of all tumors (1.5 cm^3, n= 15) as discriminator. Tumor size ranged from 0.4 to 1.4 cm^3 for the small tumor group (n= 8) and from 1.5 to 3.8 cm^3 for the large tumor group (n= 7).

Interestingly, PET images of tumors larger than 1.5 cm^3 showed non-viable areas with poor perfusion, whereas such areas were not observed in tumors smaller than 1.5 cm^3. Differences in tracer accumulation between both groups of C6 tumors were analyzed using the two-sided unpaired Student *t*-test. Differences in tracer accumulation between inflamed and healthy muscle were studied in the same animal to reduce variability between animals and therefore were analyzed using the two-sided paired Student *t*-test. Significance was reached when the p value was $p< 0.05$. Correlations were calculated with the linear regression algorithm in SigmaPlot and were considered statistically significant whenever $r^2> 0.5$ and $p< 0.05$.

RESULTS

Cellular uptake of [^{18}F]FEAnGA in C6 glioma cells. C6 glioma cells were incubated with [^{18}F]FEAnGA or [^{18}F]FEA for 60 minutes at 37 °C, in the presence of either E. coli β-GUS (740 U) or Bovine liver β-GUS (340 U) or in absence of the enzyme (control). As depicted in figure 2, the cell associated radioactivity was 6 times higher when C6 cells were incubated with [^{18}F]FEA than when the C6 cells were incubated with [^{18}F]FEAnGA in the absence of β-GUS. There was no significant difference in the cell associated radioactivity of C6 cells incubated with [^{18}F]FEA in the presence or absence of β-GUS. However, when C6 cells were incubated with [^{18}F]FEAnGA the cell associated radioactivity increased 4 and 1.5 times in the presence of E. coli β-GUS and bovine liver β-GUS, respectively.

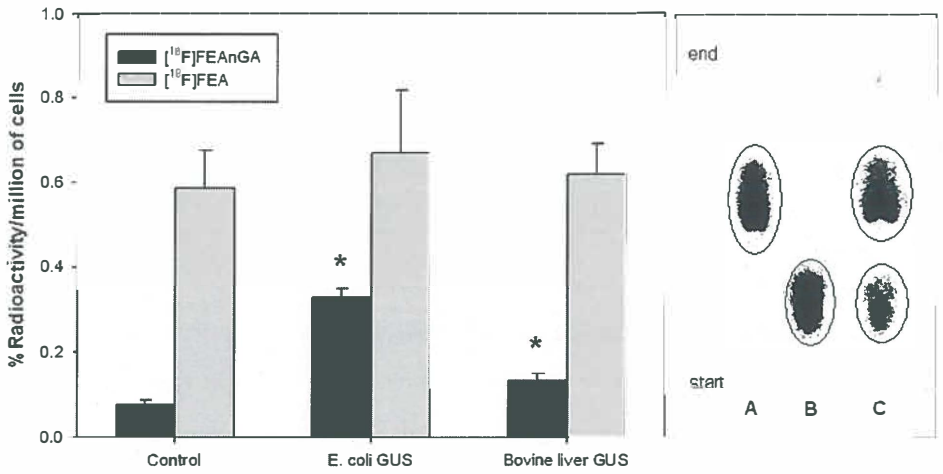

Figure 2. Cell associated radioactivity of [^{18}F]FEAnGA and [^{18}F]FEA in control C6 cells and in C6 cells in the presence of E.coli β-GUS and bovine liver β-GUS. Data are expressed as % Radioactivity/million cells and are mean values of triplicate samples ± SD.* $p < 0.05$, unpaired bidirectional Student *t* test (Left side). Radio-TLC of (A) medium sample of C6 control cells; (B) medium sample of C6 cells with E. coli β-GUS; (C) medium sample of C6 cells with bovine liver β-GUS (right side)

In addition, the radio-TLC of the medium samples showed that in the presence of E. coli β-GUS the conversion of [^{18}F]FEAnGA into [^{18}F]FEA is 99%, while with bovine liver β-

GUS there was only 37 % of conversion into [^{18}F]FEA. These results indicate that the increase in cell-associated radioactivity is associated with the conversion of [^{18}F]FEAnGA into [^{18}F]FEA.

From the efflux analysis of [^{18}F]FEA in C6 cells it was found that in the absence of radioactivity in the medium, 50% of the radioactivity remained trapped in the cells. The other 50 % of the cell-associated radioactivity appeared to be loosely bound to the extracellular domain. This loosely bound activity decreased exponentially with a half-life of 64 minutes (Fig. 3).

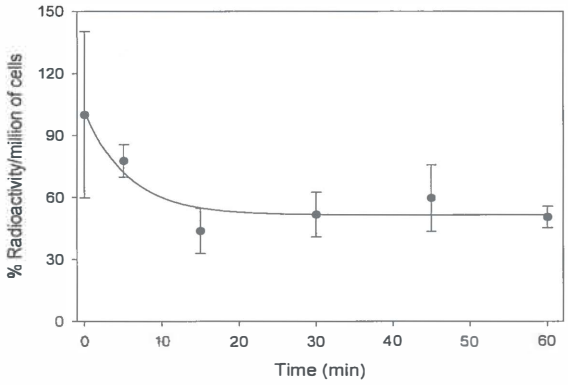

Figure 3. Cell associated radioactivity of [^{18}F]FEA in C6 cells. Data are expressed as % Radioactivity/million cells and are mean values of triplicate samples ± SD. The efflux follows an exponential decay ($y= 51.47 + 50.06\ e^{(-0.18x)}$, $r^2= 0.90$; $p= 0.03$).

Biodistribution of [^{18}F]FEAnGA in healthy Wistar rats. The normal biodistribution of [^{18}F]FEAnGA was evaluated in healthy Wistar rats at 60 min post injection. Data is displayed in table 1. [^{18}F]FEAnGA exhibits low uptake in all investigated organs, with the highest uptake in kidneys (SUV 0.53 ± 0.24) and liver (SUV 0.15 ± 0.04). These findings suggest that the tracer is rapidly excreted mainly through the renal pathway, resulting in low background.

Table 1. *Ex vivo* biodistribution of [^{18}F]FEAnGA in healthy Wistar rats (5 animals), expressed as standardized uptake values (SUV; mean ± SD).

	[^{18}F]FEAnGA (n=5)
Bone	0.02 ± 0.01
Colon	0.07 ± 0.02
Heart	0.04 ± 0.02
Kidney	0.53 ± 0.24
Liver	0.15 ± 0.04
Lung	0.05 ± 0.01
Pancreas	0.07 ± 0.06
Spleen	0.06 ± 0.01
Red blood cells	0.03 ± 0.01
Plasma	0.08 ± 0.02
Muscle	0.04 ± 0.02

PET studies. Two microPET scans were performed on each animal (8 animals), on day 8 and on day 13, in order to evaluate tracer uptake in small and large tumors, respectively. Small tumors are known to have low expression of extracellular β-GUS, as compared to larger tumors that are known to have higher levels of extracellular β-GUS [4-6]. In the PET images, the small C6 gliomas (V_t<1.5 cm^3) revealed a low and homogeneous tracer uptake while in the large tumors (V_t>1.5 cm^3) a higher tracer uptake in the viable part of the tumor and a low uptake in non-viable part of the tumor are clearly visible (Fig. 4).

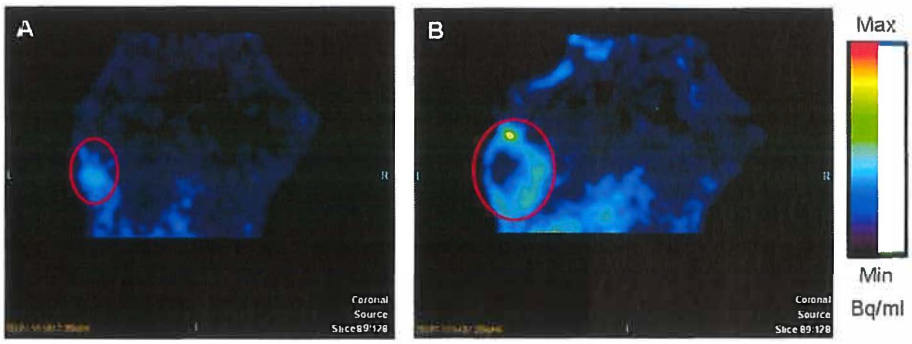

Figure 4. MicroPET images of a rat made on day 8 **(A)** and day 13 **(B)** after inoculation of C6 cells. Position of the tumor is indicated by the ellipse.

The time activity curves of the tumors revealed different kinetics of [^{18}F]FEAnGA in larger tumors (>1.5 cm^3) as compared to smaller tumors (<1.5 cm^3). The accumulation of radioactivity in smaller C6 tumor reached a maximum at 1.5 min post injection and afterwards decreased exponentially with a half-life of 12 ± 3 min, while in large C6 tumors the accumulation of radioactivity in the viable part of the tumor decreased with a half-life of 24 ± 13 min (Fig. 5). These differences in accumulation of radioactivity between tumors are significant at intervals ≥ 25 min after the injection of [^{18}F]FEAnGA ($p < 0.05$). Furthermore, the area under the curve (AUC) of [^{18}F]FEAnGA in large tumors is 1.7 times higher when compared to the AUC of [^{18}F]FEAnGA in small tumors ($p = 0.05$).

At the end of the second scan (day 13) excision of the tumors, inflamed and control muscles was performed to evaluate the accuracy of the PET experiments and to evaluate whether there was any difference in radioactivity accumulation in inflammation lesions as compared to control muscle. In the excised C6 tumors (large tumors only), [^{18}F]FEAnGA uptake (SUV) was 0.13 ± 0.09 at 1 h after injection. The accumulation of radioactivity in the excised inflamed muscle (0.07 ± 0.05) was significantly higher than in healthy muscle (0.04 ± 0.03, $p < 0.05$).

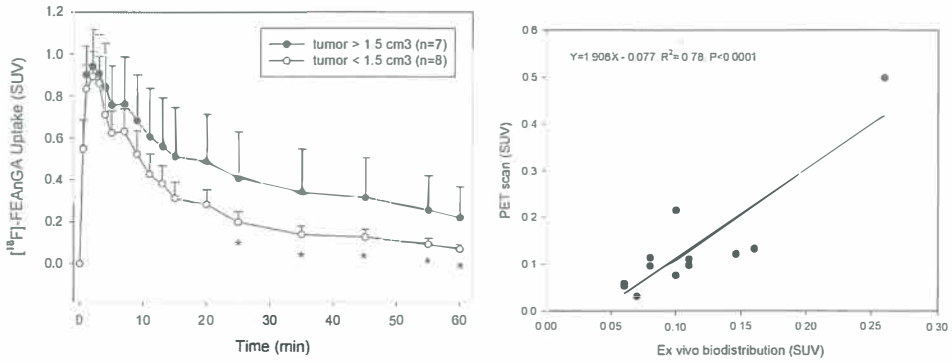

Figure 5. Kinetics of [^{18}F]FEAnGA-derived radioactivity in the viable part of the tumors of different sizes. *p< 0.05 as compared to small C6 tumors (left side). Correlation between tumor uptake of radioactivity (SUV) determined *in vivo* by PET (viable part of the tumor) and *ex vivo* (whole tumor) by gamma counting (right side).

Pharmacokinetic modeling. The sampled rats were divided in two groups (one group with V_t < 1.5 cm^3 and a second group with V_t > 1.5 cm^3) to evaluate the tracer's pharmacokinetics in large heterogeneous and small homogenous tumors, respectively.

By applying 50 % of SUV_{max} as the threshold, a ROI was obtained corresponding to the viable part of the tumor in order to obtain [^{18}F]FEAnGA time activity curves of the viable part of the tumor. The standardized uptake values of [^{18}F]FEAnGA in the viable part of the tumor, obtained from the last 10 minutes of the PET scan correlated well with the *ex* vivo biodistribution of [^{18}F]FEAnGA in the whole tumor (including necrosis) (y=1.9058x - 0.077, r^2= 0.78, p< 0.0001). However, this correlation depends strongly on a single point on the top right-hand side of the graph (Fig. 5). If this point is excluded, only a much weaker correlation is observed (y=0.8246x + 0.0179, r^2= 0.32, p= 0.04). These TACs together with individual metabolite-corrected plasma radioactivity curve were used for pharmacokinetic modeling.

As an initial approach towards pharmacokinetics modeling, Logan and Patlak graphical analysis were applied in order to evaluate the reversibility of [^{18}F]FEAnGA uptake in the viable part of C6 tumors. It was visually found a better fit of [^{18}F]FEAnGA TACs of the

viable part of the tumor to the Logan analysis, when compared to the Patlak analysis (delay time 10 minutes from injection, data not shown).

The distribution volume, DV_T, of [^{18}F]FEAnGA in the viable part of C6 tumors > 1.5 cm^3 (0.64 ± 0.13) obtained with the Logan analysis, was found to be 1.6 times higher than the distribution volume of [^{18}F]FEAnGA in smaller tumors (<1.5 cm^3) (0.39 ± 0.08, p= 0.001).

The distribution volume of [^{18}F]FEAnGA on the viable part of the tumors was also obtained from the reversible 1 and 2 tissue compartment model. Tracer kinetics could be better fitted with a reversible two-tissue compartment model (2TCM) than with a reversible one-tissue compartment model (1TCM), as the Aikake information criterion (AIC) [20] values were found to be lower for the 2TCM when compared to the 1TCM (Table 2).

The distribution volume of [^{18}F]FEAnGA on the viable part of the tumors obtained with the 2 tissue compartment modeling (2TCM) was found to be 1.8 times higher (p= 0.0002) in larger tumors when compared to smaller tumors. Figure 6A shows no overlap in of the estimated distribution volumes between both groups. Furthermore, the DV_T estimated with the 2 TCM correlated well with the DV_T estimated with Logan graphical analysis (Y=1.0309x - 0.0388, r^2= 0.98, p< 0.0001) (Fig. 6B).

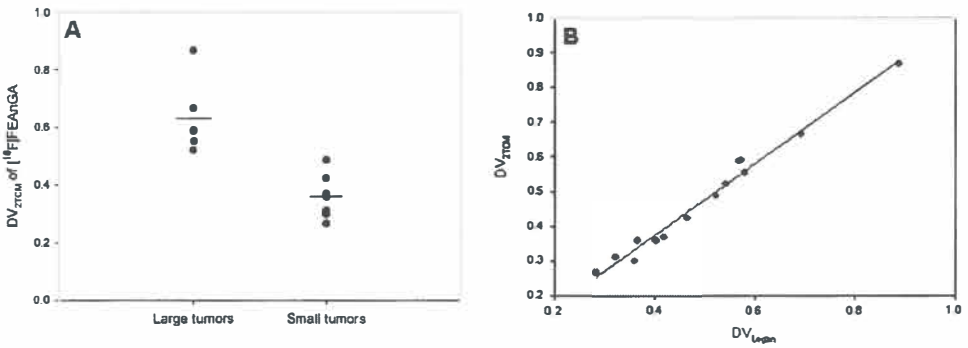

Figure 6. A) Tracer distribution volume (DV_T) in the viable part of the tumors calculated from a 2-tissue compartment model (2TCM) fit. **B)** Correlation between DV_T calculated from a 2TCM fit and estimated by Logan graphical analysis of PET data.

No statistically significant differences were found in the influx of [^{18}F]FEAnGA (K_1) in 1 tissue compartment (1TCM) as well as in K_1/k_2 in the 2TCM in any sampled tumors. A significantly higher [^{18}F]FEAnGA binding potential (k_3/k_4) was found in the tumors > 1.5 cm^3 (1.4 ± 1.1) than in tumors < 1.5 cm^3 (0.6 ± 0.2, p< 0.05).

Table 2. [^{18}F]FEAnGA kinetics in C6 gliomas (mean ± SD). *p< 0.05 as compared to gliomas < 1.5 cm^3, ** p< 0.001 as compared to gliomas < 1.5 cm^3. § p< 0.001as compared to AIC of 1TCM.

Parameters		C6 gliomas > 1.5 cm^3 (n=6)	C6 gliomas < 1.5 cm^3 (n=8)
Logan	DV_T (mL/g)	0.64 ± 0.13*	0.39 ± 0.08
1 TCM	K_1	0.06 ± 0.02	0.04 ± 0.02
	DV_T (mL/g)	0.58 ± 0.12**	0.33 ± 0.07
	AIC	242 ± 23	228 ± 8
2TCM_Reversible	K_1/k_2 (mL/g)	0.30 ± 0.12	0.24 ± 0.06
	DV_T (mL/g)	0.63 ± 0.13**	0.36 ± 0.07
	BP_{ND} (k_3/k_4)	1.4 ± 1.1*	0.6 ± 0.2
	AIC	214 ± 7§	214 ± 13

Measurement of β-GUS activity. β-GUS activity can be assessed by measurement of the release of the spacer, HNBA, or the radioactive moiety [^{18}F]FEA. However, due to the lack of activity at the end of the experiments it was not possible to measure the released [^{18}F]FEA and therefore, the β-GUS activity was only assessed by measurement of the release of HNBA from [^{18}F]FEAnGA. β-GUS activity was analyzed from the homogenates of the excised tumors, inflamed and control muscles. The conversion was 1.5 times higher in tumors > 1.5 cm^3 (4.33E-04 ± 1.33E-04) than in tumors < 1.5 cm^3 (2.95E-04 ± 0.7E-04).

Furthermore, there was a significant correlation between HNBA formation and the distribution volume in the viable part of the tumors (Y=1118x + 0.08, r^2= 0.65, p= 0.0005) (Fig. 7A). The conversion of [^{18}F]FEAnGA in muscle was found to be 1.7 times higher in inflamed muscle (2.40E-04 ± 0.88E-04), when compared to healthy muscle (1.42E-04 ± 0.23E-04). Moreover, there was a significant correlation between HNBA

formation and radioactivity accumulation (SUV) in inflamed muscle (Y=333x - 0.02, r^2= 0.65, p= 0.005) (Fig. 7B).

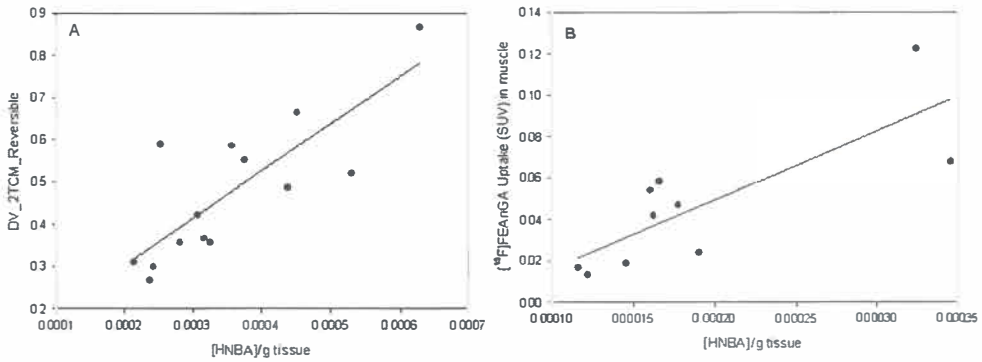

Figure 7. Correlation between **A)** DV_T of [^{18}F]FEAnGA in the viable part of the tumors calculated from a model fit, or **B)** uptake of [^{18}F]FEAnGA in inflamed muscle tissue (SUV), and rate of tracer cleavage determined in tissue homogenate.

To prove that [^{18}F]FEAnGA conversion is β-GUS mediated, tumor homogenates were incubated in the presence or absence of the specific β-GUS inhibitor, saccharolactone. In the absence of saccharolactone, 56 ± 5 % of [^{18}F]FEAnGA in the tumor homogenate was converted into [^{18}F]FEA after 1 h of incubation., In contrast, the formation of [^{18}F]FEA was completely blocked in presence of 50 μM of saccharolactone (Fig. 8). Therefore, nonspecific cleavage of the tracer can be excluded.

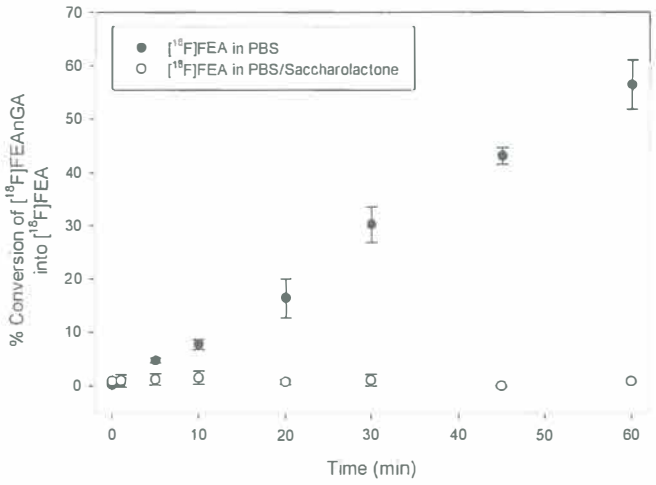

Figure 8. Conversion of [^{18}F]FEAnGA into [^{18}F]FEA in tumor homogenates in the presence or absence of the specific β-GUS inhibitor saccharolactone.

Histology of the C6 tumor. Histological examination of the excised C6 tumors presented very distinct profiles in large and small tumors (Fig. 9). In the large tumors, extensive necrotic regions were found. These regions are characterized by the loss of the integrity of the nuclei, while in smaller tumors the nuclei remain intact, indicating no signs of necrosis.

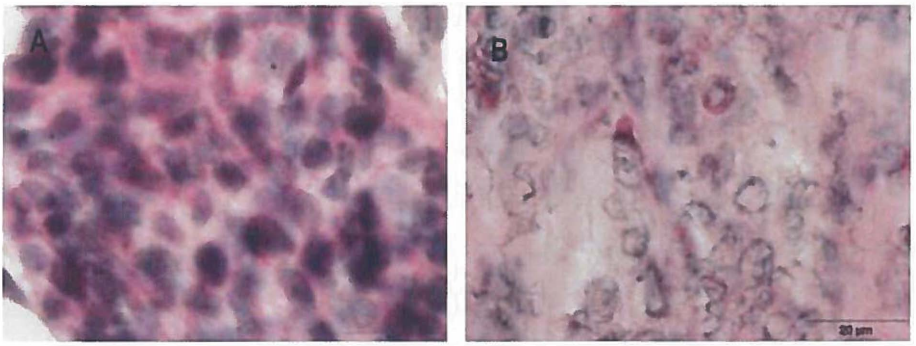

Figure 9. Microscopic image of a specimen of rat tumor: **A)** smaller and **B)** larger than 1.5cm^3 (hematoxylin and eosin, ×400).

DISCUSSION

The extracellular β-GUS in tumors has been exploited as target for new prodrug therapies. In spite of encouraging preclinical results, this therapy has still not been applied in a clinical setting. A major obstacle for clinical usefulness is the interindividual and intertissue variability of β-GUS activity. With a proper PET tracer, it could be possible to evaluate the extent and distribution of extracellular β-GUS activity, providing more information about the factors that modulate the enzyme's expression and activity.

Our previous study, in which we tested [^{18}F]FEAnGA as microPET probe in β-GUS expressing tumors (CT26mβGUS), showed a preferential radioactivity accumulation in these β-GUS overexpressing tumors when compared to normal CT26 tumors [15]. Our results were in agreement with the results obtained with the ^{124}I-PTH-G probe synthesized by Roffler's group, indicating that glucuronide probes are good candidates for the evaluation of β-GUS expression in tumors. In previous work by Roffler *et al.* and us, an increase in radioactivity accumulation in normal CT26 tumors where necrosis was present was also found, suggesting that [^{124}I]PTH-G and [^{18}F]FEAnGA might also be used to evaluate extracellular β-GUS activity in normal tumors [14;15]. Thus the aim of this study was to explore whether [^{18}F]FEAnGA could be a suitable PET tracer to detect physiological β-GUS levels present in solid tumors. Furthermore, we also tested this probe in inflammatory lesions to evaluate whether in this situation the release of β-GUS could also be detected by [^{18}F]FEAnGA.

In vitro accumulation of [^{18}F]FEAnGA and [^{18}F]FEA was performed in C6 cells in the presence or absence of β-GUS to evaluate whether both tracers show the same outcome when incubated with glioma cells as when incubated with the murine adenocarcima cells (CT26 and CT26mβGUS). As despicted in figure 2, the cell-associated radioactivity was 6 times higher when C6 cells were incubated with [^{18}F]FEA than when incubated with [^{18}F]FEAnGA in the absence of β-GUS. As expected, there was no significant difference in the cell associated radioactivity of C6 cells incubated with [^{18}F]FEA in the presence or absence of β-GUS. However, when C6 cells were incubated with [^{18}F]FEAnGA the cell-associated radioactivity increased 4 and 1.5 times in the presence of

E. coli β-GUS and bovine liver β-GUS, respectively. The higher tracer uptake in the presence of E. coli β-GUS compared to the uptake in the presence of bovine liver β-GUS could be explained by the fact that the catalytic rate of bovine liver β-GUS towards [^{18}F]FEAnGA is 13 times lower than the catalytic rate of E. coli β-GUS, which was confirmed by metabolite analysis of the medium with radio-TLC.

For a good PET tracer not only tracer uptake, but also its retention is important. To evaluate whether the tracer after cleavage of β-GUS was retained by C6 cells, the efflux of [^{18}F]FEA was investigated (Fig. 3). The efflux analysis indicated that 50 % of the cell-associated radioactivity was bound loosely to the extracellular domain. Nevertheless, it was observed that in the absence of radioactivity in the medium, still 50 % of the radioactivity remained trapped in the cells.

In this study, two microPET scans were performed in each animal on different days (8 and 13 after C6 cells inoculation), in order to evaluate whether there were any significant changes in the uptake of [^{18}F]FEAnGA in tumors with different sizes. The present PET study showed that tumors could clearly be visualized in the PET images due to the low background in normal tissues. The TACs of the viable parts of the tumors revealed that tumors greater than 1.5 cm^3 exhibit 2 times longer tracer retention than tumors smaller than <1.5 cm^3. In addition, the lack of metabolites in plasma and the increased conversion of [^{18}F]FEAnGA to HNBA and [^{18}F]FEA in large tumors, suggests that this increased retention could be ascribed to: i) the higher conversion of the tracer to [^{18}F]FEA in large tumors that contain more extracellular β-GUS and ii) the ability of [^{18}F]FEA to be better retained in tumors than the intact tracer. Retention of [^{18}F]FEA in the cells was demonstrated in the *in vitro* efflux experiments. In our *in vivo* pilot study, where 3 Wistar rats bearing a C6 tumor where injected with [^{18}F]FEA, a rapid accumulation of [^{18}F]FEA in the tumor and remaining organs in the first 10 min post injection was observed. This accumulated activity remained constant throughout the remaining 50 min of the PET scan (data not shown).

The standardized uptake values in small C6 gliomas obtained from the last 10 min of the PET scan were on average lower than the values obtained from *ex vivo*

biodistribution. This apparent discrepancy is probably caused by partial volume effects due to the limited spatial resolution of the PET scanner (1.35 full width at half maximum, FWHM, in the center of the field-of-view) [19]. Partial volume effects can lead to a spread out of local high activity to surrounding areas, resulting in an underestimation in the measurements of [^{18}F]FEAnGA uptake. However, in the group of large C6 gliomas, where some tumors presented large necrotic areas, the apparent uptake values obtained by PET of the viable part of the tumors were on average higher than the values obtained in the biodistribution. This discrepancy could be explained by the fact that the biodistribution data represents the total tumor uptake including the viable part of the tumor (high uptake) and the necrotic areas (low uptake). Consequently biodistribution shows lower tracer uptake in these tumors than PET.

In the present *ex vivo* study, it was shown that the standardized uptake value of [^{18}F]FEAnGA was significantly higher not only in the large C6 tumors, but also in the inflamed muscle as compared to control muscle. This increased uptake in inflamed muscles correlated well with the conversion of the tracer to HNBA and [^{18}F]FEA, suggesting that this increased release of the tracer is due to the increased release of β-GUS within 24h after the induction of the sterile inflammation. This is in accordance with literature reports showing that in the presence of stimulated neutrophils or injured cells β-GUS is released into the surrounding tissue when inflammation occurs. β-GUS is highly active at the sites of inflammation, where the tissue fluid has a low pH (which is favorable for β-GUS).

Although the standardized uptake value is widely used to quantify the uptake of tracers, it does not correct for the activity in plasma and thus not for tracer delivery to the tissue. This could lead to a wrong interpretation of the data when comparing the tracer in different conditions. Ideally, the binding potential or distribution volume of the tracers should be determined using plasma input on different time points during the scan. Thus, in the present study we further explored quantification of [^{18}F]FEAnGA uptake by pharmacokinetic modeling.

From the graphical analysis (Logan versus Patlak) we visually found a better fit of the tracer's TACs of the tumor to the Logan analysis than to the Patlak analysis, indicating that the tracer has a more reversible behavior than binding irreversibly to the tumor. This was confirmed by the *in* vitro efflux study where we found that in the absence of radioactivity in the medium, 50 % of [^{18}F]FEA was released from the cells.

The compartment analysis was consistent with the Logan graphical analysis. The estimated DV_T from kinetic analysis with Logan plot analysis and the 2TCM were well correlated, which indicated that both methods provided a stable estimation of the DV_T.

The result of curve-fitting by the 2TCM was more accurate than that of the 1TCM, indicating that the state of equilibrium between free and bound tracer cannot be considered to be reached instantly. The values of AIC were significantly lower for the 2 TCM, which was therefore selected for further analysis. As shown in Fig. 5, the estimated DV_T from kinetic analysis with the 2TCM was found to be significantly different in the two groups (small tumors vs. large tumors).

Moreover, analysis of tumor homogenates revealed 1.5 times higher amount of cleaved spacer, HNBA in larger tumors when compared to smaller tumors. The amount of HNBA correlated well with the distribution volumes in the viable part of the tumors obtained from Logan plots as well as the 2-tissue-compartment model, suggesting that the DV_T reflects β-GUS activity. Since metabolite analysis indicated that [^{18}F]FEAnGA is stable in plasma, with 90% of the tracer remaining unmetabolized during the time of the PET scan, we can only attribute this enhanced cleavage of [^{18}F]FEAnGA to HNBA and [^{18}F]FEA to the release of β-GUS into the extracellular space of the tumors. Furthermore, complete blocking of the conversion of the tracer in tumor homogenates with saccharolactone demonstrated that the conversion of [^{18}F]FEAnGA into HNBA and [^{18}F]FEA is specifically mediated by β-GUS.

CONCLUSION

In the present study, we were able to demonstrate that despite relatively low absolute uptake, [^{18}F]FEAnGA is a PET tracer able to detect an increased released of β-GUS in large solid tumors as well as in inflammatory lesions. Therefore, [^{18}F]FEAnGA could help to obtain a better understanding of the metabolic conversion of glucuronide prodrugs in tumors or in inflammatory diseases.

ACKNOLEDGMENT

We gratefully thank J.W.A. Sijbesma, V. Di Gialleonardo, J. Doorduin for all the help in the *in vivo* studies, K. Stojanov for providing the C6 glioma cells and J. Georgieva for performing the histochemical staining.

REFERENCES

1. De Graaf M, Pinedo HM, Oosterhoff D, van der Meulen-Muileman IH, Gerritsen WR, Haisma HJ, and Boven E (2004) Hum. Gene Ther. 15:229-238.
2. George J (2008) Biochem. Cell Biol. 86:235-243.
3. Boyer MJ and Tannock IF (1993) Adv. Cancer Res. 60:269-291.
4. Chen X, Wu B, and Wang PG (2003) Curr. Med. Chem. Anticancer Agents 3:139-150.
5. De Graaf M, Boven E, Scheeren HW, Haisma HJ, and Pinedo HM (2002) Curr. Pharm. Des 8:1391-1403.
6. De Groot FM, Damen EW, and Scheeren HW (2001) Curr. Med. Chem. 8:1093-1122.
7. Bosslet K, Straub R, Blumrich M, Czech J, Gerken M, Sperker B, Kroemer HK, Gesson JP, Koch M, and Monneret C (1998) Cancer Res. 58:1195-1201.
8. Houba PH, Boven E, van der Meulen-Muileman IH, Leenders RG, Scheeren JW, Pinedo HM, and Haisma HJ (2001) Br. J. Cancer 84:550-557.
9. Prijovich ZM, Chen BM, Leu YL, Chern JW, and Roffler SR (2002) Br. J. Cancer 86:1634-1638.
10. Sperker B, Murdter TE, Schick M, Eckhardt K, Bosslet K, and Kroemer HK (1997) J. Pharmacol. Exp. Ther. 281:914-920.
11. Sperker B, Werner U, Murdter TE, Tekkaya C, Fritz P, Wacke R, Adam U, Gerken M, Drewelow B, and Kroemer HK (2000) Naunyn Schmiedebergs Arch. Pharmacol. 362:110-115.
12. Antunes IF, Haisma HJ, and de Vries EF (2008) Nucl. Med. Commun. 29:845-846.
13. Brady F, Luthra SK, Brown GD, Osman S, Aboagye E, Saleem A, and Price PM (2001) Current Pharmaceutical Design 7:1863-1892.
14. Tzou SC, Roffler S, Chuang KH, Yeh HP, Kao CH, Su YC, Cheng CM, Tseng WL, Shiea J, Harm IH, Cheng KW, Chen BM, Hwang JJ, Cheng TL, and Wang HE (2009) Radiology 252:754-762.
15. Antunes IF, Haisma HJ, Elsinga PH, Dierckx RA, and de Vries EF (2010) Bioconjug. Chem 21:911-920.
16. Tewson TJ (1997) Nuclear Medicine and Biology 24:755-760.
17. Van Waarde A, Jager PL, Ishiwata K, Dierckx RA, and Elsinga PH (2006) J. Nucl. Med. 47:150-154.
18. Krak NC, Boellaard R, Hoekstra OS, Twisk JW, Hoekstra CJ, and Lammertsma AA (2005) Eur. J. Nucl. Med. Mol. Imaging 32:294-301.
19. Soret M, Bacharach SL, and Buvat I (2007) J. Nucl. Med. 48:932-945.
20. Akaike H (1992) No To Hattatsu 24:127-133.

Chapter

In vivo evaluation of [^{18}F]FEAnGA-Me: a PET tracer for imaging β-glucuronidase (β-GUS) activity in a tumor & inflammation rodent model

Inês F. Antunes, Hidde J. Haisma, Philip H. Elsinga, Jurgen W. A. Sijbesma, Aren van Waarde, Antoon T. M. Willemsen, Rudi A. Dierckx, Erik F. J. de Vries

Submitted for publication

ABSTRACT

The PET tracer, 1-O-(4-(2-fluoroethyl-carbamoyloxymethyl)-2-nitrophenyl)-O-β-D-glucopyronuronate ([^{18}F]FEAnGA), was recently developed for non-invasive imaging of extracellular β-glucuronidase (β-GUS). However, [^{18}F]FEAnGA exhibited rapid renal clearance, which resulted in a relatively low tracer uptake in the tumor. To improve the pharmacokinetics of [^{18}F]FEAnGA, we now describe its more lipophilic methyl ester analog (called [^{18}F]FEAnGA-Me). [^{18}F]FEAnGA-Me is anticipated to remain longer in plasma than [^{18}F]FEAnGA and consequently its delivery to the tumor is expected to be increased, resulting in better PET images. [^{18}F]FEAnGA-Me was obtained by alkylation of the O-protected glucuronide methyl ester precursor with [^{18}F]-fluorethylamine ([^{18}F]FEA), followed by removal of the acetate protecting groups with NaOMe/MeOH in 5-10% overall radiochemical yield. [^{18}F]FEAnGA-Me is about 10-fold less hydrophilic than [^{18}F]FEAnGA and it is stable in PBS and in the presence of β-GUS for at least 1 h. However, in the presence of esterase or plasma [^{18}F]FEAnGA-Me is converted to [^{18}F]FEAnGA, which is subsequently converted to [^{18}F]FEA by β-GUS. MicroPET studies in Wistar rats bearing a C6 glioma and a sterile inflammation showed similar accumulation of radioactivity in tumors after injection of either [^{18}F]FEAnGA-Me or [^{18}F]FEAnGA. Both, [^{18}F]FEAnGA-Me and [^{18}F]FEAnGA had a rapid two-phase clearance of total plasma radioactivity with a half-life of 1 and 8 min. The circulating half-life of [^{18}F]FEAnGA fraction generated from [^{18}F]FEAnGA-Me by *in vivo* hydrolysis had a half-life of 1 and 11 min in plasma. The distribution volume in the viable part of the tumor after [^{18}F]FEAnGA-Me injection was similar to the distribution volume in the viable part of the tumor after [^{18}F]FEAnGA injection. In conclusion, the overall imaging properties of [^{18}F]FEAnGA-Me were not significantly better than those of [^{18}F]FEAnGA. Therefore, another strategy should be applied in order to improve the kinetics of these tracers.

INTRODUCTION

Glucuronide-drug conjugates exhibit lower toxicity towards normal cells than the corresponding native drugs. However, glucuronide-drug conjugates are susceptible to enzymatic cleavage by β-GUS, resulting in the *in situ* generation of highly cytotoxic drugs. Since tumors and inflammatory lesions have increased levels of β-GUS, glucuronide conjugates have been investigated as tools to deliver drugs to the target site.

For a better understanding of the mechanisms of action and metabolic conversion of these prodrugs, we have recently synthesized a radiopharmaceutical, 1-O-(4-(2-fluoroethyl-carbamoyloxymethyl)-2-nitrophenyl)-O-β-D-glucopyronuronate ([^{18}F]FEAnGA), for non-invasive PET imaging of extracellular β-GUS activity [1]. MicroPET with [^{18}F]FEAnGA could clearly visualize enhanced β-GUS levels, in particular in large tumors with necrotic areas, whereas uptake in other organs was very low (except kidneys and bladder). The distribution volume (DV_T) of [^{18}F]FEAnGA in tumors correlated well with the conversion of [^{18}F]FEAnGA by the β-GUS enzyme. However, because of the highly hydrophilic character of [^{18}F]FEAnGA (logD = -1.61), the PET tracer is very rapidly excreted via the kidneys into the urine. This rapid renal clearance resulted in a relatively low absolute tracer uptake in the tumor [2].

The disadvantage of rapid renal clearance was also found for prodrugs such as DOX-GA3 and DNR-GA3 [3;4]. To reduce renal clearance, researchers converted DOX-GA3 to its methyl ester (DOX-mGA3), which is substantially less hydrophilic [5]. The glucuronide conjugate is negatively charged at physiological pH, whereas the corresponding methyl ester is a neutral molecule. Slow release of DOX-GA3 through conversion of its methyl ester by esterase activity in blood resulted in a prolonged circulation half-life of DOX-GA3. Intravenous administration of DOX-mGA3 in tumor bearing mice resulted in a 2.7-fold increase in the delivery (area under the concentration versus time curve (AUC) from 0.5 to 2 h) of doxorubicin to the tumor, as compared to administration of DOX-GA3. Therefore, we hypothesized that a similar approach could increase the delivery of [^{18}F]FEAnGA as well. Therefore, we now synthesized its less hydrophilic methyl ester of [^{18}F]FEAnGA,

called [^{18}F]FEAnGA-Me. When administered *in vivo*, the methyl group of [^{18}F]FEAnGA-Me should be removed by carboxylesterase activity in plasma to give the original PET tracer [^{18}F]FEAnGA, which could in turn be activated by β-GUS at the target site (Scheme 1) and release 2-[^{18}F]fluoroethylamine ([^{18}F]FEA). The slow release of [^{18}F]FEAnGA after administration of [^{18}F]FEAnGA-Me might result in improved pharmacokinetics of the PET tracer *in vivo*, resulting in a higher absolute tracer uptake in tumors.

Scheme1. General mechanism of activation of the prodrug tracer

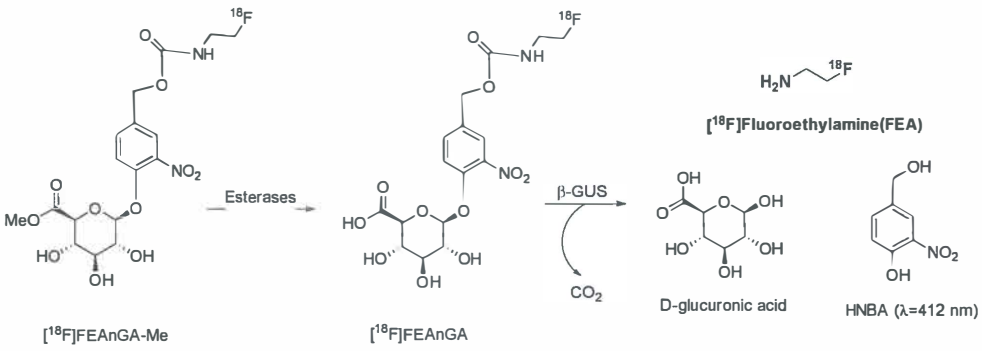

In the present study, we describe the labeling of [^{18}F]FEAnGA-Me and its stability *in vitro*. In addition, we analyzed the *in vitro* conversion of [^{18}F]FEAnGA-Me to [^{18}F]FEAnGA by esterase activity and determined whether [^{18}F]FEAnGA-Me could be converted to [^{18}F]FEAnGA and [^{18}F]FEA *in vivo*. Finally, the PET imaging characteristics of [^{18}F]FEAnGA-Me were compared with the original PET tracer [^{18}F]FEAnGA.

MATERIALS AND METHODS

Reagents and solvents were obtained from commercial suppliers (Sigma-Aldrich and Fluka, Zwijndrecht, The Netherlands and Merck, Darmstadt, Germany) and used without further purification. The reference compounds, FEAnGA-Me and FEAnGA were prepared as previously described [1]. For radiolabeled compounds, the detection on the TLC was performed with Cyclone phosphor storage screens (multisensitive, Packard,

PerkinElmer Life and Analytica Science). These screens were exposed to the TLC strips (60 seconds for *in vitro* experiments and 20 minutes for *in vivo* experiments), subsequently read out using a Cyclone phosphor storage imager (PerkinElmer) and analyzed with OptiQuant software. HPLC purifications were performed with an Elite LaChrom VWR Hitachi L-2130 pump system using a Phenomenex Prodigy C18-column, connected to a UV-spectrometer (Elite LaChrom VWR Hitachi L-2400 UV detector) set at 254 nm and a Bicron frisk-tech radiation detector. Radioactivity measurements for logD determination and cell studies were done using an automated gamma counter (Compugamma, LKB Wallac). Absorbance measurements in the enzyme assays were performed with a UV-spectrophotometer (Waters 2487 dual wavelength absorbance detector).

Radiosynthesis of [^{18}F]FEAnGA-Me (Scheme 2). Aqueous [^{18}F]fluoride was produced via the ^{18}O (p,n)^{18}F nuclear reaction by irradiation of [^{18}O]water with a Scanditronix MC-17 cyclotron. The [^{18}F]fluoride solution was passed through an activated SepPak Light Accell plus QMA anion exchange cartridge (Waters) to recover the [^{18}O]water. The [^{18}F]fluoride was eluted from the cartridge with 1 mL of K_2CO_3 (5 mg/mL) and collected in a vial with 20 mg Kryptofix[2.2.2.]. To this solution, 1 mL acetonitrile was added and the solvents were evaporated at 130 °C. The [^{18}F]KF/Kryptofix complex was dried 3 times by the addition of 0.5 mL acetonitrile, followed by evaporation of the solvent.

[^{18}F]FEA was prepared by fluorination of N-[2-(toluene-4-sulfonyloxy)-ethyl]-phtalimide (30 mg, 0.09 mmol) in 500 µL of acetonitrile at 110 °C, followed by deprotection with hydrazine hydrate (50µl, 1.03 mmol) as described in literature [6]. The resulting amine was distilled at 75 °C into an ice-cold solution of **1** (5 mg, 0.009 mmol) in acetonitrile (0.2 mL). The mixture was allowed to react at room temperature for 30 min. The product was dried at 40 °C for 2 min under a gentle argon flow. Deprotection of the hydroxyl groups was done by addition of 30 µL 0.5 M NAOMe/MeOH and incubation for 7 min at room temperature. The product was neutralized by addition of 20 µL 1 M AcOH, diluted with 2 mL of distilled water and purified by HPLC using a semi-preparative Prodigy C_{18} reverse-phase column (5µ, 10×250 mm; Phenomenex) with 17 % ethanol in 2.5 mM

sodium phosphate buffer as the eluent (flow rate, 4 mL/min; retention time: [^{18}F]FEAnGA-Me= 21 min; [^{18}F]FEAnGA= 6.4 min and [^{18}F]FEA= 4.2 min). The radiolabeled compound [^{18}F]FEAnGA-Me was obtained in 5-10% radiochemical yield from [^{18}F]fluoride (decay corrected) in 150 min. Quality control was performed by HPLC with a Symmetry C_{18} column [5µm, 4.6×150 mm] with 15% acetonitrile in sodium phosphate buffer 2.5 mM as the eluent (flow rate, 1mL/min; retention time: [^{18}F]FEAnGA-Me= 14 min). The specific activity of [^{18}F]FEAnGA-Me was 180 ± 70 GBq/µmol and the radiochemical purity was always > 95%.

Stability of [^{18}]FEAnGA-Me. A sample of radiolabeled [^{18}F]FEAnGA-Me was dissolved in PBS (1mL) and incubated at 37 °C. For 1 hour, the stability of the radiolabeled [^{18}F]FEAnGA-Me was monitored by radio-TLC (R_f FEA= 0.1, R_f FEAnGA= 0.4 and R_f FEAnGA-Me= 1) (eluent: MeCN/H_2O 7:3). After elution, the TLC strips were analyzed by phosphor storage imaging. The screens were scanned with Cyclone phosphor storage system (PerkinElmer) and the percentage of intact [^{18}F]FEAnGA-Me as a function of the incubation period was calculated by ROI analysis using OptiQuant software. The experiment was performed in duplicate.

Distribution Coefficient (Log $D_{7.4}$). To determine the Log $D_{7.4}$ of [^{18}F]FEAnGA-Me an aliquot of 100 µL of HPLC purified [^{18}F]FEAnGA-Me solution was added to a mixture of n-octanol/PBS (4mL:4mL) at pH 7.4. The tubes were vortexed at room temperature for 30 seconds, followed by 30 minutes shaking in a water bath at 37 °C. Aliquots of 1 mL were drawn from both the n-octanol and aqueous phase. Radioactivity in both samples was counted using an automated gamma counter. The experiments were performed in triplicate.

***In Vitro* Hydrolysis of FEAnGA-Me.** To a solution of 0.1% bovine serum albumin (BSA), 200 µL (15U) of carboxylesterase of porcine liver (Sigma-Aldrich) and/or 10 µL (74U) *Escherichia coli* β-GUS (E.coli β-GUS) in 950 µL PBS (pH=7), 50 µL of a 0.004 M solution of FEAnGA-Me was added (total volume 1 mL). The solutions were incubated in a water bath at 37 °C and 100 µL samples were collected at different time points between 1 min and 60 min after the start of incubation. The enzymatic activity was stopped by dilution of the

samples in 300 μL of acetonitrile and cooling of the samples in ice. The release of 4-hydroxy-3-nitrobenzyl alcohol (HNBA) (ε= 3460 $M^{-1}cm^{-1}$) was monitored by measuring the UV absorbance at 412 nm. The experiment was performed in duplicate.

***In Vitro* Hydrolysis of [^{18}F]FEAnGA-Me by plasma.** To a 0.4 mL solution of PBS (pH= 7.4), or rat plasma with or without 10 μL (74U) *Escherichia coli* β-GUS, 0.1 mL of HPLC purified [^{18}F]FEAnGA-Me (2 ± 0.2 MBq) was added. The solutions were incubated in a water bath at 37 °C and 2 μL samples were collected at different time points between 30 seconds and 60 minutes after the start of incubation. The degradation of the radiolabeled [^{18}F]FEAnGA-Me was followed by radio-TLC (eluent: MeCN/H_2O 7:3). After elution, the TLCs were analyzed by phosphor storage imaging as described above. The experiment was performed in duplicate.

Cellular uptake of [^{18}F]FEAnGA-Me. C6 glioma cells were maintained in 5 mL Dulbecco's Modified Eagle Medium (DMEM) supplemented with 7.5% fetal bovine serum (FBS) in 25 cm^3 culture flasks. Cells were grown in a humidified atmosphere containing 5% CO_2 and were passaged every 3-4 days. For uptake experiments, cells were plated in triplicate in a 12-well plate at a density of 7×10^5 cells per well. After 24 h, the medium was discarded and 1 mL of PBS-GMC buffer (5.6 mM D-glucose, 0.49 mM $MgCl_2$ and 0.68 mM $CaCl_2$ in 100 mL phosphate-buffered saline (PBS)) per well was added, followed by the addition of 200 μL [^{18}F]FEAnGA-Me (ca. 250 kBq). In each series of 3 wells, either β-GUS (740U), esterase (15U) or a combination of β-GUS (740U) and esterase (15U) was added. After 60 min of incubation at 37 °C, the medium was collected, the cells washed with cold PBS (3×1 mL/well), harvested with trypsin (250 μL) and resuspended in 1750 μL of DMEM (total volume 2 mL/well). The cell suspensions and the medium were collected separately for each well and the radioactivity was measured using a gamma counter. For each well, the medium was analyzed for conversion of [^{18}F]FEAnGA-Me to [^{18}F]FEA by radio-TLC as described above.

Animal model. Wistar rats (6-8 weeks old) were obtained from Harlan (Lelystad, The Netherlands). The animals were provided with standard laboratory chow and tap water *ad libitum*. All studies were carried out in compliance with the local ethical

guidelines for animal experiments. The protocols were approved by the Animal Ethics Committee of University of Groningen. The tumor-inflammation model was described previously [7;8]. Briefly, C6 glioma cells [2-3 × 10^6 cells in a 1:1 mixture of Matrigel and Dulbecco's minimal essential medium containing 7.5% fetal bovine serum] were subcutaneously injected into the right shoulder of male Wistar rats. At day 12, 0.1 mL of turpentine was intramuscularly injected into the thigh of the left hind leg of the same animal.

PET imaging and *ex vivo* biodistrubution studies. In the tumor-inflammation model (n= 14), PET scans were performed on day 13 after inoculation. The rats were anesthetized with 2% isoflurane (Pharmachemie BV, The Netherlands) and positioned in the small animal PET camera (Siemens, Focus 220) with the tumor in the field of view. Owing to the small field-of-view of our microPET camera, it was not possible to obtain a whole body scan of the rat. Although the camera is equipped with a continuous bed motion option, this method is not suitable to obtain quantitative information, because attenuation correction is not feasible in this mode and the bed motion is relatively slow with respect to tracer kinetics, especially at the early time points. Moreover, imaging of the inflammatory lesions in the leg is difficult due to artifacts created by the high uptake in bladder, which would also be in the field-of-view. For the above mentioned reasons the PET scan was only performed in the tumor region. A transmission scan of 515 seconds with a Co-57 point source was obtained for the correction of attenuation and scatter by tissue. After the transmission scan was completed, [^{18}F]FEAnGA-Me (8.6 ± 0.7 MBq) or [^{18}F]FEAnGA (12.5 ± 2.2 MBq) was injected via the penile vein. Simultaneously with the injection of the PET tracer, an emission scan of 60 minutes was started. After completion of the emission scan, the rats were sacrificed by extirpation of the heart, while still being under deep isoflurane anesthesia. Several tissues, peripheral organs, tumor and inflamed muscle were excised and blood was collected. Plasma and red cells were obtained from the blood sample by centrifugation (20 min at 6000 rpm). All tissue samples and plasma were weighed and the amount of radioactivity was determined with a gammacounter (LKB Wallac, Turku, Finland). Tracer uptake is expressed as standardized uptake value (SUV),

which is defined as: [Tissue activity concentration (MBq/g) × body weight (g) / injected dose (MBq)]. It was assumed that 1 cm^3 of tissue equals 1 g.

Pharmacokinetics studies. In a second group of Wistar rats (n= 21) bearing a C6 tumor, a canula was inserted into the femoral artery for collection of blood samples. A dynamic PET scan was performed as described above. During the PET scan, blood samples of 100 µL were taken at 15, 30, 45, 60, 75, 90, 120, 150, 300, 450, 600, 1800, 3600 seconds after tracer injection. After a blood sample was taken, 100 µL of heparinized saline was injected via the artery canula to prevent large changes in blood pressure. The blood samples were centrifuged at 6000 rpm for 10 minutes and 50 µL of plasma were collected. The activity in plasma was measured with a gamma counter (LKB Wallac, Turku, Finland). The plasma-activity curves were corrected for decay. The rats were sacrificed after the scans and the tumors were excised and weighed. The radioactivity in the tumors was measured with a gamma counter and converted to SUV.

PET image analysis. The list mode data of the emission scans was separated into 17 frames. Emission sinograms were iteratively reconstructed (OSEM2D, 4 iterations, 16 subsets) after being normalized, corrected for attenuation, and corrected for radioactive decay. Three-dimensional regions of interest (3D-ROIs) were generated automatically using the intensity threshold method from Inveon Research Workplace software package (Inveon, Siemens, USA) [9;10]. Briefly, the last 9 frames (10-60 min) were summed and a ROI of the viable part of the tumor was generated automatically with a 50 % threshold using a region growing method, i.e. only pixels were included with tracer uptake greater than 50% of the maximum value within the lesion. The resulting ROIs were used on the original data set to create the corresponding 0-60 min time-activity curves (TACs). A second ROI was drawn around the whole tumor to obtain the total tumor volume (V_t; cm^3), using standard software (Inveon, Siemens, USA). In those animals where plasma input curves were obtained through arterial sampling, pharmacokinetic modeling of the tissue TACs was performed using standard software (Inveon, Siemens, USA). The graphical Logan model was used to determine the distribution volume, DV_T, and a 2 tissue-

compartment model fit was used to calculate the rate constants K_1-k_4 using a free blood volume.

Metabolite analysis. 2.5 µL of each plasma sample was collected, applied on a TLC plate (Merck F-254 silica gel) and eluted with acetonitrile/water (7:3). After elution, TLC plates were analyzed by phosphor storage imaging. Exposed screens were scanned with a Cyclone phosphor storage system (PerkinElmer Life and Analytica Science) and the percentage of conversion of [^{18}F]FEAnGA-Me as a function of time was calculated by ROI analysis using OptiQuant software.

Conversion of [^{18}F]FEAnGA-Me to [^{18}F]FEA with the release of HNBA (scheme 1). Part of the tumors (containing a both the rim and the necrotic core, 0.12 ± 0.04 g) excised from the sampled animals was homogenized in 2 mL of phosphate buffered saline (PBS). The homogenates were centrifuged (10 min, 3000 rpm, 4 °C) and the supernatant was collected and kept on ice. To the supernatant, 2 mL of cold acetonitrile was added to precipitate the remaining proteins. The samples were vortexed for 30 s and centrifuged at 3000 rpm for 10 min at 4 °C. A volume of 1.5 ml of the supernatant was added to 1.5 mL of cold NaOH 0.25M and UV absorption was measured (Waters 2487 dual wavelength absorbance detector, 412nm, aufs=0.01). Absorption was converted in the concentration of HNBA, using a calibration curve. The absorption was corrected for the weight (mg) of the tumor sample. The measurements were performed in duplicate.

Statistical analysis. Statistical analyses were performed using Microsoft Excel 2003 and SigmaPlot (version 10.0; SPSS, Inc.). Differences in tumor accumulation between tracers were analyzed using the two-sided unpaired Student's *t*-test. Differences in tracer accumulation between inflamed and healthy muscle were studied in the same animal to reduce variability between animals and therefore were analyzed using the two-sided paired Student's *t*-test. Significance was reached when the p value was < 0.05. Correlations were calculated with the linear regression algorithm in SigmaPlot and were considered statistically significant whenever $r^2>0.5$ and $p<0.05$. Through out the manuscript values are presented as mean ± SEM.

RESULTS

Labeling of [^{18}F]FEAnGA-Me. [^{18}F]FEAnGA-Me was prepared in analogy to [^{18}F]FEAnGA, by the reaction of [^{18}F]FEA **2** with the imidazolyl intermediate **1**, followed by removal of the acetate protecting groups with NaOMe/MeOH in anhydrous conditions. [^{18}F]FEAnGA-Me was obtained in a 10 ± 5 % overall radiochemical yield (corrected for decay, based on [^{18}F]fluoride) with a total synthesis time of 150 min (Scheme 2). In addition, approximately equal amounts of fully hydrolysed [^{18}F]FEAnGA were formed.

Properties of [^{18}F]FEAnGA-Me. The stability of [^{18}F]FEAnGA-Me in PBS, was evaluated at 37 °C. After 1 hour of incubation, radio-TLC analysis showed that 95% of the tracer was still intact while 5% was hydrolyzed to [^{18}F]FEAnGA. We then determined the lipophilicity of [^{18}F]FEAnGA-Me by measuring its n-octanol/water distribution coefficient (LogD) at pH 7.4. The logD of [^{18}F]FEAnGA-Me was found to be -0.58 ± 0.0002, while the logD of [^{18}F]FEAnGA was found to be -1.61 ± 0.01 [1].

Scheme 2. Radiosynthesis of compound [^{18}F]FEAnGA-Me

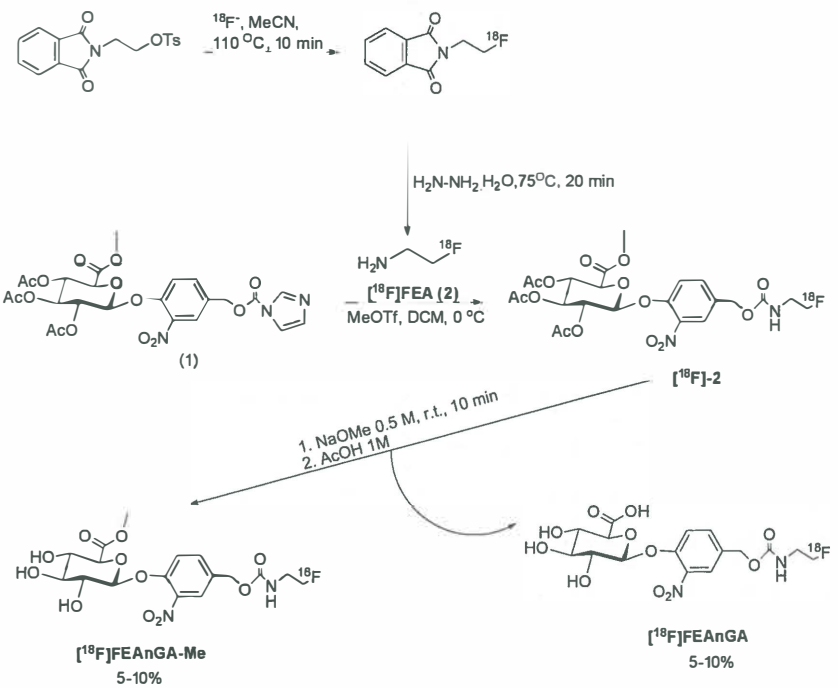

***In Vitro* Hydrolysis of FEAnGA-Me/ [^{18}F]FEAnGA-Me.** The enzymatic processing of FEAnGA-Me was first studied using commercially available bacterial *Escherichia coli* β-GUS and porcine liver carboxylesterase. Figure 1 indicates that incubation of FEAnGA-Me with the combination of esterase and E.coli β-GUS resulted in 80% conversion to FEA and 4-hydroxy-3-nitrobenzyl alcohol (HNBA), while in the presence of E.coli β-GUS alone, only 6% of FEAnGA-Me was for converted to FEA and HNBA. This 6% conversion of FEAnGA-Me to FEAnGA in the absence of esterase was probably due to some spontaneous hydrolysis of the ester to the carboxylic acid. The liberation of 4-hydroxy-3-nitrobenzyl alcohol (HNBA) was measured by UV-spectrophotometry at 412 nm.

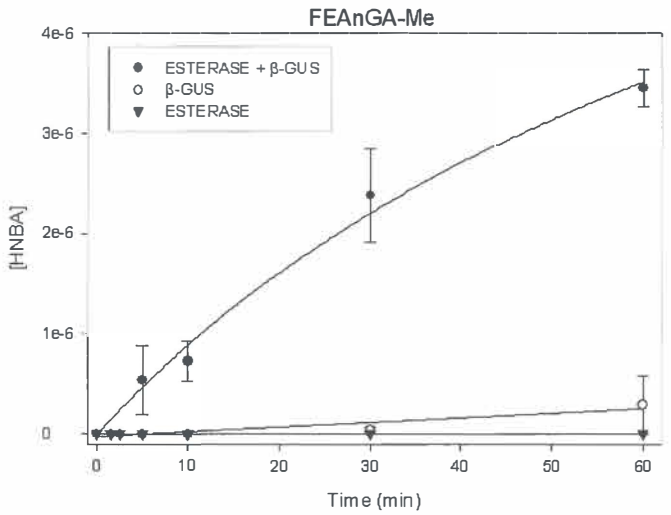

Figure 1. In vitro release of the spacer HNBA from FEAnGA-Me and its quantification by UV absorption due to its yellow color (412nm). FEAnGA-Me was exposed to either esterase or E. coli β-GUS alone, or a combination of both enzymes.

However, monitoring of the conversion of FEAnGA-Me to FEAnGA was not possible, since neither glucuronides show UV absorption at this wavelength. Furthermore, we aimed to demonstrate that esterases in plasma are able to hydrolyze the glucuronide ester to the carboxylic acid. Therefore, we continued the hydrolysis analysis with the radioactive compound, [^{18}F]FEAnGA-Me. Radiolabeled [^{18}F]FEAnGA-Me was incubated in rat plasma. After 30 min, 99% of [^{18}F]FEAnGA-Me was converted to [^{18}F]FEAnGA, while no [^{18}F]FEAnGA was generated in 0.1% BSA in PBS. When [^{18}F]FEAnGA-Me was incubated in

rat plasma supplemented with E.coli β-GUS, 50% cleavage of the tracer to [^{18}F]FEA was observed within 30 min (Fig.2).

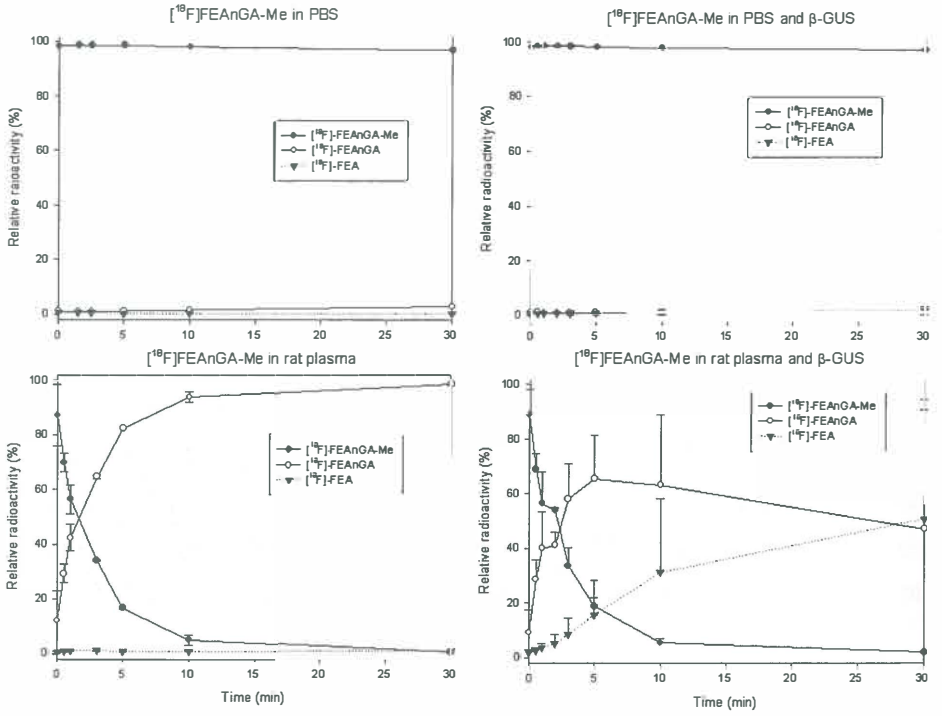

Figure 2. Conversion of [^{18}F]FEAnGA-Me in: PBS (top left side), PBS with E.coli β-GUS (top right side), rat plasma (bottom left side) and rat plasma with E.coli β-GUS (bottom right side).

Cellular uptake of [^{18}F]FEAnGA-Me in C6 glioma cells. As depicted in figure 3, the cell-associated radioactivity was significantly increased by 60%, when C6 cells were incubated with [^{18}F]FEAnGA-Me in the presence of both E. coli β-GUS and esterase. After incubation of C6 cells with [^{18}F]FEAnGA-Me, Cell-associated activity was not affected by either E. coli β-GUS or esterase alone. Furthermore, the radio-TLC analysis of the medium showed that in the presence of both E. coli β-GUS and esterase the conversion of [^{18}F]FEAnGA-Me to [^{18}F]FEA was 99%, while in the presence of E. coli β-GUS alone there was only 7% of conversion to [^{18}F]FEA. These results suggest that the increase in cell

associated radioactivity is related with the conversion of [^{18}F]FEAnGA-Me to [^{18}F]FEA. The latter compound is thought to have a higher tendency to associate to the cells [1].

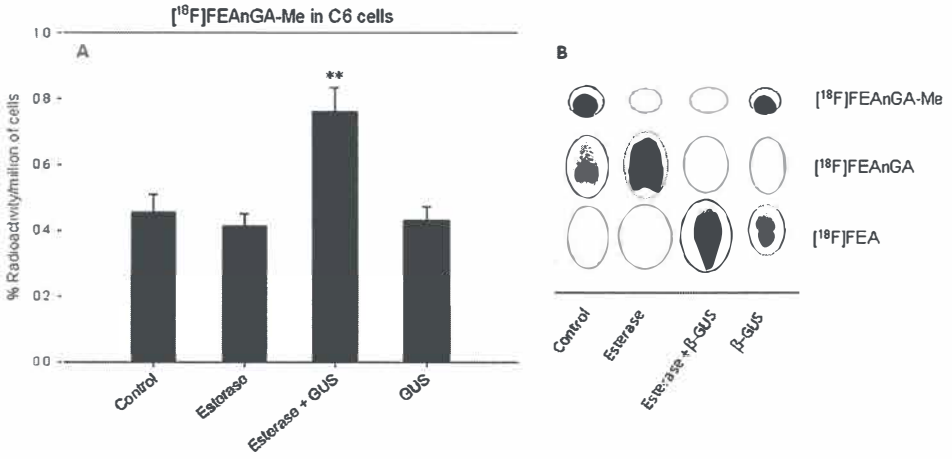

Figure 3. A) Cell associated radioactivity of [^{18}F]FEAnGA-Me in control C6 cells and in C6 cells in the presence of E.coli β-GUS and/or Esterase. Data are expressed as % Uptake per million of cells presented in mean values of triplicate samples ± SEM. ** $p<0.005$, unpaired bidirectional Student's *t* test. **B)** Radio-TLC of medium samples of C6 cells.

***In Vivo* Hydrolysis of [^{18}F]FEAnGA-Me.** The hydrolysis of [^{18}F]FEAnGA-Me to [^{18}F]FEAnGA by plasma was also studied in tumor bearing rats. After injection into the rat, the fraction of [^{18}F]FEAnGA-Me present in plasma decreased rapidly to 50% in the first 2 minutes, followed by a plateau phase. After 10 min, [^{18}F]FEAnGA-Me was more slowly converted to [^{18}F]FEAnGA, with still 26% of the radioactivity in plasma being [^{18}F]FEAnGA-Me at the end of the study (60 min) (Fig. 4A). The fractions of radioactivity in plasma consisting of [^{18}F]FEAnGA and [^{18}F]FEA reached their maximum 60 min post injection (64% and 10%, respectively). When [^{18}F]FEAnGA was injected (Fig. 4B) only 12 % was metabolized to [^{18}F]FEA, which is comparable to the amount of this compound found after injection of the methyl ester.

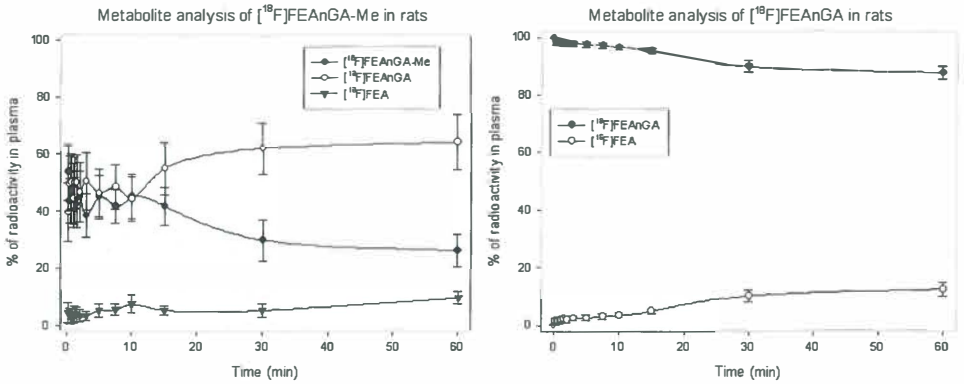

Figure 4. Percentage of [^{18}F]FEAnGA-Me; [^{18}F]FEAnGA and [^{18}F]FEA in the plasma of rats at different time points after injection of **A)** [^{18}F]FEAnGA-Me (left, n=8) or **B)** [^{18}F]FEAnGA (right, n= 14).

The plasma activity curves of [^{18}F]FEAnGA-Me, [^{18}F]FEAnGA and the [^{18}F]FEAnGA fraction generated by *in vivo* hydrolysis of [^{18}F]FEAnGA-Me are shown in figure 5. Exponential curve-fitting analysis of [^{18}F]FEAnGA-Me clearance showed a two-phase clearance with 25% of the injected activity having a half-life $(t_{1/2})_1$ of 1 ± 0.1 min and 75% of the injected activity having a half-life $(t_{1/2})_2$ of 8 ± 1 min (n= 8), which is similar to the plasma clearance of [^{18}F]FEAnGA (27% $(t_{1/2})_1$= 1 ± 0.1 min and 73% $(t_{1/2})_2$= 8 ± 0.8 min, n= 14). In addition, the [^{18}F]FEAnGA fraction generated in-vivo by hydrolysis of [^{18}F]FEAnGA-Me (18% with $(t_{1/2})_1$= 1 ± 0.2 min and 82% with $(t_{1/2})_2$= 11 ± 2 min (n= 8)) had similar plasma clearance as [^{18}F]FEAnGA itself .

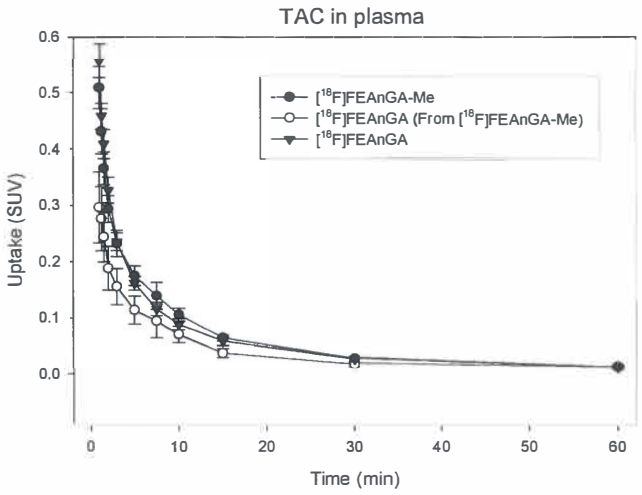

Figure 5. The time activity curves of [^{18}F]FEAnGA-Me and [^{18}F]FEAnGA in plasma as a result of the i.v. administration of either [^{18}F]FEAnGA-Me or [^{18}F]FEAnGA.

The AUC (1-60 min) of [^{18}F]FEAnGA-Me (3.5 ± 0.4) in plasma is similar to the AUC of [^{18}F]FEAnGA (3.3 ± 0.3), whereas the AUC of the [^{18}F]FEAnGA fraction generated *in vivo* by hydrolysis of [^{18}F]FEAnGA-Me (2.3 ± 0.5) was lower that the AUC of [^{18}F]FEAnGA (3.3 ± 0.3) itself, although this difference was not statistically significant.

PET study. To test the potential of [^{18}F]FEAnGA-Me as a PET tracer for detecting β-GUS activity *in vivo*, a PET study was performed in rats bearing a C6 glioma and sterile inflammation. A microPET scan was performed in these rats after injection of either [^{18}F]FEAnGA-Me (n= 6) or [^{18}F]FEAnGA (n= 8), in order to compare both tracers. In the PET images (summed from 10 to 60 min, Fig. 6), [^{18}F]FEAnGA-Me showed a higher background activity when compared to [^{18}F]FEAnGA.

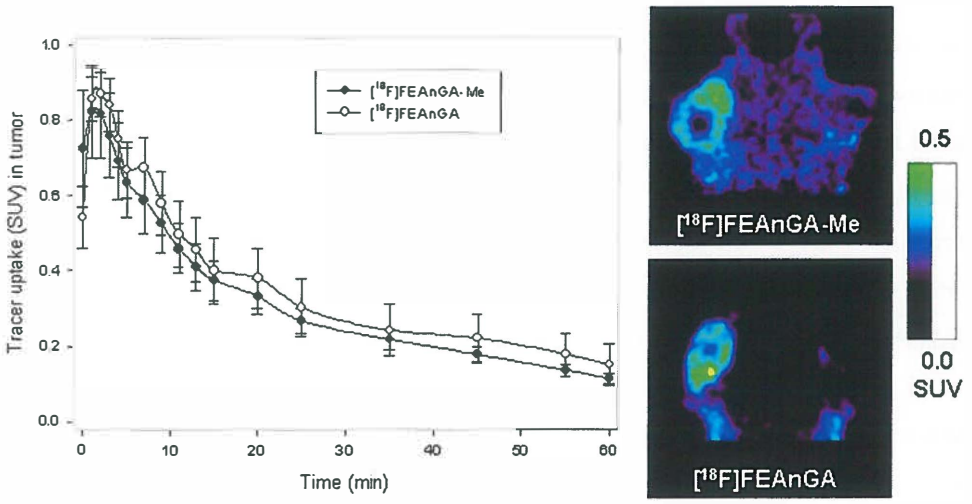

Figure 6. Coronal microPET image of a rat injected with either [18F]FEAnGA-Me or [18F]FEAnGA on day 13 after inoculation of C6 cells (right side). Time activity curves of the tracer uptake (SUV) in the viable part of C6 gliomas after injection with either [18F]FEAnGA-Me or [18F]FEAnGA (left side).

However, the time activity curves of [18F]FEAnGA-Me and [18F]FEAnGA in tumors were similar (Fig. 6). The accumulation of radioactivity in the viable part of the tumors after [18F]FEAnGA-Me injection reached a maximum at 1.5 min post injection and afterwards decreased exponentially with a half-life of 16 ± 2 min, while after [18F]FEAnGA injection, the accumulation of radioactivity in the viable part of the tumors decreased with a half-life of 24 ± 9 min (Fig. 6). In addition, the area under the curve (AUC) of [18F]FEAnGA-Me in tumors (23 ± 6) was similar to the AUC of [18F]FEAnGA in tumors (20 ± 4, p= 0.65).

***Ex vivo* biodistribution.** To compare the distribution after [18F]FEAnGA-Me or [18F]FEAnGA injection, *ex vivo* biodistribution studies of both tracers were performed after the PET scan, i.e. at 60 min post injection. After injection of [18F]FEAnGA-Me the uptake (SUV) in most of the peripheral organs was similar to the uptake in these organs after injection of [18F]FEAnGA. However, uptake in the liver and kidneys was 3 times higher after injection of [18F]FEAnGA-Me than after injection of [18F]FEAnGA ($p<0.05$) (Table 1). In

the excised C6 tumors (2.35 ± 0.42 g), the uptake (SUV) was 0.13 ± 0.02 at 1 h after injection of [^{18}F]FEAnGA-Me, while tracer uptake was 0.13 ± 0.05 and 0.08 ± 0.02 in inflamed and healthy muscle, respectively. When injected with [^{18}F]FEAnGA the uptake was 0.13 ± 0.03 in the excised tumors (2.35 ± 0.65 g) and 0.07 ± 0.02 and 0.04 ± 0.01 in the inflamed and healthy muscles, respectively. The inflammation-to-muscle ratios of both tracers [^{18}F]FEAnGA-Me (1.48 ± 0.22) and [^{18}F]FEAnGA (1.59 ± 0.19) were not significantly different, but the tumor-to-muscle ratios of [^{18}F]FEAnGA-Me (1.85 ± 0.23) were significantly lower than those of [^{18}F]FEAnGA (3.53 ± 0.52, p= 0.02).

Table 1. *Ex vivo* biodistribution 60 min p.i of [^{18}F]FEAnGA-Me or [^{18}F]FEAnGA in Wistar rats bearing a C6 tumor and a sterile inflammation. Tracer uptake is expressed as standardized uptake values (SUV; mean ± SEM). * p<0.05 [^{18}F]FEAnGA-Me when compared to [^{18}F]FEAnGA; ** p<0.05 and *** p< 0.005 when compared to control muscle.

Organs	[^{18}F]-FEAnGA-Me (n=6)	[^{18}F]-FEAnGA (n=8)
Bone	0.05 ± 0.01	0.05 ± 0.02
Colon	0.26 ± 0.07	0.22 ± 0.07
Heart	0.16 ± 0.05	0.14 ± 0.06
Kidney	3.13 ± 0.67*	1.03 ± 0.48
Liver	0.97 ± 0.29*	0.34 ± 0.09
Lung	0.05 ± 0.01	0.12 ± 0.03
Pancreas	0.15 ± 0.08	0.11 ± 0.01
Spleen	0.17 ± 0.08	0.14 ± 0.03
Trachea	0.18 ± 0.07	0.13 ± 0.03
Plasma	0.13 ± 0.03	0.16 ± 0.06
Red blood cells	0.07 ± 0.02	0.06 ± 0.01
Muscle, control	0.08 ± 0.02	0.04 ± 0.01
Muscle, inflamed	0.13 ± 0.05	0.07± 0.02**
Tumor	0.13 ± 0.02**	0.13± 0.03***

Pharmacokinetic modeling. The sampled rats were divided in two groups (injected with either [^{18}F]FEAnGA-Me (7.0 ± 0.9 MBq) or [^{18}F]FEAnGA (7.4 ± 0.5 MBq) to compare the tracers' pharmacokinetics *in vivo*.

By applying 50 % of SUV_{max} as the threshold, a ROI was obtained representing the viable part of the tumor. The TACs of the viable part of the tumor together with individual plasma radioactivity curves, Logan graphical analysis and a 2 tissue reversible compartment model were used for pharmacokinetic modeling.

The tumor distribution volume, DV_T, from the Logan graphical analysis after [^{18}F]FEAnGA-Me injection (0.61 ± 0.06), was not significantly different from the DV_T after [^{18}F]FEAnGA injection (0.50 ± 0.04). The same distribution volumes where also obtain using the 2 tissue compartment modeling (Table 2).

Table 2. Pharmacokinetic parameters of both tracers and their conversion in C6 gliomas.

Parameters	[^{18}F]FEAnGA-Me (n=7)	[^{18}F]FEAnGA (n=14)
DV_{Logan} (mL/g)	0.61 ± 0.06	0.50 ± 0.07
DV_{2TCM} (mL/g)	0.63 ± 0.09	0.48 ± 0.04
[HNBA]/mg tissue	0.35 ± 0.08	0.35 ± 0.03

Measurement of β-GUS activity. β-GUS activity was assessed by measurement of the release of HNBA from [^{18}F]FEAnGA-Me or [^{18}F]FEAnGA. β-GUS activity was analyzed in homogenates of excised whole tumors. The conversion of [^{18}F]FEAnGA to [^{18}F]FEA and HNBA in tumors was found to be similar whether injected with [^{18}F]FEAnGA-Me (0.35 ± 0.07) or [^{18}F]FEAnGA (0.35 ± 0.05).

DISCUSSION

In the last years, interest into the development of radiollabeled markers for the non-invasive evaluation of prodrug-converting enzymes in solid tumors has increased. Knowledge of the prodrug-converting enzyme expression and activity can lead to a better

understanding of the mechanism of action and metabolic conversion of the prodrug and could identify sites that are prone to possible side-effects. Eventually, a suitable PET method might allow the selection of patients eligible for β-GUS mediated prodrug therapy. [^{18}F]FEAnGA is a PET tracer capable of detecting increased release of β-GUS in large solid tumors as well as in inflammatory lesions. However, the renal clearance of [^{18}F]FEAnGA was fast relative to the conversion of [^{18}F]FEAnGA to [^{18}F]FEA resulting in a relatively low tracer uptake in the tumor. Therefore, we synthesized the more lipophilic methyl ester of [^{18}F]FEAnGA, called [^{18}F]FEAnGA-Me and hypothesized that the increase in lipophilicity would prolong the circulation half-life of the tracer which would result in prolonged availability of the tracer for conversion by β-GUS.

The synthesis of [^{18}F]FEAnGA-Me was similar to [^{18}F]FEAnGA, only differing in the deprotection process where NaOMe/MeOH in anhydrous conditions was used instead of aqueous NaOH. This last step was of critical importance with regards to the final yield. In the presence of acetonitrile and NaOMe/MeOH the major compound obtained was [^{18}F]FEAnGA. However, if compound **[^{18}F]-2** was dried before adding NaOMe/MeOH, [^{18}F]FEAnGA-Me was obtained in 5 to 10% yield. In addition, [^{18}F]FEAnGA was concomitantly formed in 5-10% yield. Despite numerous attempts to improve the final yield, we were not able to improve the yield any further. Thus, the final product [^{18}F]FEAnGA-Me was obtained in 5-10% overall radiochemical yield (corrected for decay, based on [^{18}F]fluoride) with a total synthesis time of 120 min (Scheme 2). The identity of [^{18}F]FEAnGA-Me was confirmed by coelution with a sample of the nonradioactive compound by RP-HPLC. [^{18}F]FEAnGA-Me was found to be completely stable in PBS for at least 1 hour.

We anticipated that the methyl group of [^{18}F]FEAnGA-Me could be enzymatically converted to the carboxylic acid of [^{18}F]FEAnGA by esterase in the blood (Scheme 1). Indeed, we showed that [^{18}F]FEAnGA-Me was completely hydrolyzed to [^{18}F]FEAnGA in the presence of bovine liver esterase or rat plasma. Furthermore, intact [^{18}F]FEAnGA-Me itself was not a substrate of E. coli β-GUS. However, only after removal of the methyl group by esterase, complete conversion of the resulting [^{18}F]FEAnGA to [^{18}F]FEA could be achieved

by E. coli β-GUS. This result indicates that the activation of [^{18}F]FEAnGA-Me is a two-step process that requires both esterase and glucuronidase.

In vitro accumulation of [^{18}F]FEAnGA-Me was investigated in C6 glioma cells. The cell-associated radioactivity derived from [^{18}F]FEAnGA-Me was only increased in the presence of both esterase and E. coli β-GUS. There is no significant difference in the cell-associated radioactivity of cells incubated with [^{18}F]FEAnGA-Me alone or in the presence of either E. coli β-GUS or esterase. The radio-TLC analysis of the medium confirmed that this increase in cell uptake is associated with the conversion of [^{18}F]FEAnGA-Me to [^{18}F]FEA, since complete conversion of the tracer to [^{18}F]FEA was only observed when both esterase and β-GUS were present. C6 cells incubated with [^{18}F]FEAnGA-Me, in the presence of both esterase and E. coli β-GUS showed similar accumulation of radioactivity as C6 cells incubated with [^{18}F]FEA (0.8%) and 2 times higher uptake when compared to C6 cells incubated with [^{18}F]FEAnGA, in the presence of E. coli β-GUS (0.4%) [1]. However, the cellular uptake of [^{18}F]FEAnGA-Me in control C6 cells (absence of enzymes) was also higher than the uptake of [^{18}F]FEAnGA, suggesting a lower *in vitro* selectivity of [^{18}F]FEAnGA-Me when compared to [^{18}F]FEAnGA (Fig. 7).

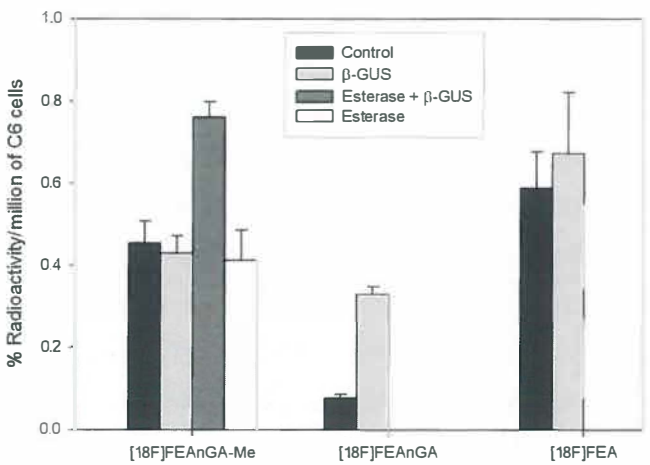

Figure 7. Comparison of the uptake of [^{18}F]FEAnGA-Me; [^{18}F]FEAnGA and [^{18}F]FEA in C6 cells in the presence or absence of esterase and/or E.coli β-GUS.

As expected the lipophilicity of [^{18}F]FEAnGA-Me was found to be 10 fold higher than [^{18}F]FEAnGA. We hypothesized that the administration of the less hydrophilic [^{18}F]FEAnGA-Me would result in a prolonged circulation of [^{18}F]FEAnGA in rats as compared to direct administration of the highly hydrophilic [^{18}F]FEAnGA. However, due to the high esterase activity in rat plasma, the tracer was rapidly converted to [^{18}F]FEAnGA (50%) within the first two minutes post injection. As a consequence no differences in plasma AUC of [^{18}F]FEAnGA-Me and [^{18}F]FEAnGA was observed, nor were differences in the clearance half-life between both tracers observed. Metabolite analysis indicated initially rapid conversion of [^{18}F]FEAnGA-Me to [^{18}F]FEAnGA, but after 8 minutes the fraction of [^{18}F]FEAnGA in plasma stabilized. The late-phase slower conversion of [^{18}F]FEAnGA-Me *in vivo* might be attributed to initial rapid nonspecific uptake of [^{18}F]FEAnGA-Me in tissue (as observed *in vitro* in the cellular uptake experiments in C6 cells), followed by slow redistribution of the methyl ester prodrug tracer into the circulation, where it is converted to [^{18}F]FEAnGA. This slow late phase conversion of the methyl ester prodrug is in agreement with observations by Houba *et al.* for DOX-mGA3.

The *ex vivo* biodistribution of both tracers indicated similar uptake (SUV) in most of the peripheral organs with exception of the liver and kidneys, where the uptake was 3 times higher after injection of [^{18}F]FEAnGA-Me when compared with the uptake after injection with [^{18}F]FEAnGA. The uptake in inflamed muscle was 2 times higher after [^{18}F]FEAnGA-Me injection in comparison with the uptake after [^{18}F]FEAnGA injection. However, the uptake in healthy muscle was also 2 times higher in animals injected with [^{18}F]FEAnGA-Me. Thus, the ratio between inflamed and control muscle for the two tracers was similar. These biodistribution results are in agreement with what we found *in vitro*, where [^{18}F]FEAnGA-Me looses selectivity when compared to [^{18}F]FEAnGA suggesting an increased uptake of the less hydrophilic [^{18}F]FEAnGA-Me in normal tissue. Indeed, also in the pharmacokinetic analysis, no statistical differences were found between the distribution volumes (DV_T) in tumors when injected with one or either tracer.

When injected with [^{18}F]FEAnGA, DV_T in tumors is dependent on the [^{18}F]FEAnGA influx (from the plasma to the extracellular space) and its conversion to [^{18}F]FEA and HNBA

in the presence of extracellular β-GUS. After [^{18}F]FEAnGA-Me injection the DV_T in tumors depends on both [^{18}F]FEAnGA-Me and [^{18}F]FEAnGA influx and the conversion of [^{18}F]FEAnGA to [^{18}F]FEA and HNBA. Therefore, as expected the DV_T in the viable part of the tumors correlated well with the HNBA formation after injection of [^{18}F]FEAnGA but did not correlate well with the HNBA formation when injected with [^{18}F]FEAnGA-Me (Fig. 8).

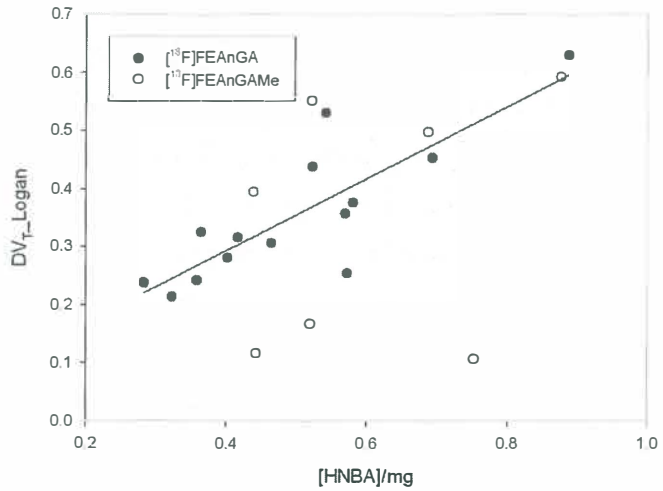

Figure 8. Correlation between distribution volume in the viable part of the tumors calculated from a graphical model fit and rate of tracer cleavage determined in tissue homogenate, after the injection of either [^{18}F]FEAnGA (y=0.04+0.62x, r^2= 0.69, p= 0.0002) or [^{18}F]FEAnGA-Me (y=0.09+0.42x, r^2= 0.11, p= 0.47).

The pharmacokinetic behavior of [^{18}F]FEAnGA-Me is likely more favorable in man considering the lower levels of esterase in the human body as compared to rats which would increase the availability of the tracer for β-GUS. However, this sustained plasma levels of tracer would ultimately increase the background activity and therefore decreasing the contrast between background and targeted region. Therefore, different strategies should be pursued in order to improve the pharmacokinetics of glucuronide PET tracers, such as PET tracers with higher turn over so that the release of the radioactive

moiety is faster than the clearance of the tracer, resulting in higher tracer uptake at the target site without increasing the background activity.

CONCLUSION

[^{18}F]FEAnGA-Me was labeled with [^{18}F]fluoride and had a high *in vitro* stability in PBS. [^{18}F]FEAnGA-Me proved to be a good substrate for plasma esterase and in the presence of both esterase and E. coli β-GUS is converted to [^{18}F]FEA and HNBA. However, the administration of [^{18}F]FEAnGA-Me did not result in a significantly prolonged circulation of [^{18}F]FEAnGA in rats as compared to the direct administration of [^{18}F]FEAnGA. In fact, due to its lower hydrophilicity, nonspecific uptake of [^{18}F]FEAnGA-Me increased, resulting in a lower target to background contrast. In addition, the 2-step prodrug activation strategy further complicates the mode of action of this radiopharmaceutical and thus complicates the interpretation of the imaging results. Therefore, different strategies, such as the use of prodrug with higher β-GUS turnover should likely be pursuit in order to improve the pharmacokinetics and pharmacodynamics of glucuronide PET tracers.

ACKNOWLEDGMENT

We gratefully thank Katica Stojanov and Zhila Mosheini for their help in the C6 glioma cell studies.

REFERENCES

1. Antunes IF, Haisma HJ, Elsinga PH, Dierckx RA, and de Vries EF (2010) Bioconjug. Chem. 21:911-920.
2. Antunes IF, Haisma HJ, Elsinga PH, VAN Waarde A, Willemsen ATM, Dierckx RA, and de Vries EFJ (2011) Molecular Imag., DOI 10.2310/7290.2011.00029
3. Houba PH, Boven E, van der Meulen-Muileman IH, Leenders RG, Scheeren JW, Pinedo HM, and Haisma HJ (1999) Biochem. Pharmacol. 57:673-680.
4. Houba PH, Boven E, van der Meulen-Muileman IH, Leenders RG, Scheeren JW, Pinedo HM, and Haisma HJ (2001) Br. J. Cancer 84:550-557.
5. De GM, Nevalainen TJ, Scheeren HW, Pinedo HM, Haisma HJ, and Boven E (2004) Biochem. Pharmacol. 68:2273-2281.
6. Tewson TJ (1997) Nuclear Medicine and Biology 24:755-760.
7. Van Waarde A, Cobben DC, Suurmeijer AJ, Maas B, Vaalburg W, de Vries EF, Jager PL, Hoekstra HJ, and Elsinga PH (2004) J. Nucl. Med. 45:695-700.
8. Van Waarde A, Jager PL, Ishiwata K, Dierckx RA, and Elsinga PH (2006) J. Nucl. Med. 47:150-154.
9. Krak NC, Boellaard R, Hoekstra OS, Twisk JW, Hoekstra CJ, and Lammertsma AA (2005) Eur. J. Nucl. Med. Mol. Imaging 32:294-301.
10. Soret M, Bacharach SL, and Buvat I (2007) J. Nucl. Med. 48:932-945.

Chapter

[^{18}F]FEAnGA for PET imaging of β-glucuronidase activity in neuroinflammation

Inês F. Antunes, Janine Doorduin, Hidde J. Haisma,
Philip H. Elsinga, Aren van Waarde, Antoon T. M. Willemsen,
Rudi A. Dierckx, Erik F. J. de Vries

Parts of this chapter have been accepted in J Nucl Med

ABSTRACT

Activation of microglia is a hallmark of inflammatory, infectious and degenerative diseases of the CNS. Several studies indicated that there is an increase in release of β-glucuronidase by activated microglia cells into the extracellular space at the site of neuroinflammation. β-Glucuronidase (β-GUS) is involved in the hydrolysis of glycosaminoglycans on the cell surface and the degradation of the extracellular matrix. Therefore, β-GUS might be a biomarker for microglia cell induced neurodegeneration. In this study, we investigated whether the PET tracer [^{18}F]FEAnGA was able to detect β-GUS release during neuroinflammation in a rat model of herpes encephalitis. Male Wistar rats were intranasally inoculated with HSV-1 (HSE) or PBS (control). [^{11}C]-*(R)*-PK11195 and [^{18}F]FEAnGA microPET scans were acquired for 60 minutes. Logan graphical analysis was used to calculate [^{18}F]FEAnGA distribution volumes (DV_{Logan}) in various brain areas. After administration of [^{18}F]FEAnGA, the area under the activity concentration versus time curve (AUC) of the whole brain was 2 times higher in HSV-1 infected rats than in control rats. In addition the DV_{Logan} of [^{18}F]FEAnGA was most increased in the frontopolar cortex, frontal cortex, bulbus olfactorius, cerebral cortex, cerebellum and brainstem of HSV-1 infected rats, when compared to control rats. The conversion of [^{18}F]FEAnGA to HNBA was found to be 1.6 times higher in HSV-1 infected rats than in control rats and it correlated with the DV_{Logan} of [^{18}F]FEAnGA in the same areas of the brain. Furthermore, the DV_{Logan} of [^{18}F]FEAnGA also correlated with β-GUS activity in the same brain regions. It was also found that DV_{Logan} of [^{18}F]FEAnGA tended to correlate better with the [^{11}C]-*(R)*-PK11195 uptake in rats inoculated at day 5 rather than at day 7. Despite relatively low tracer uptake in the brain, [^{18}F]FEAnGA PET was able to detect an increased release of β-GUS during neuroinflammation.

INTRODUCTION

Neurological disorders are often debilitating diseases, in which the symptoms can be treated, but the disease cannot be cured. Despite the large differences between neurological disorders, neuroinflammation is involved in both acute pathology, such as stroke and encephalitis, and chronic neurodegenerative diseases, such as Parkinson's and Alzheimer's disease (AD).

Microglia are the predominant population of macrophages in the brain and are responsive to injury or infection of brain tissue. Upon activation, microglia undergo dramatic morphological changes, metamorphosing from the ramified resting state to the amoeboid activated state. In addition to morphological changes, activation of microglia results in the upregulation of molecules such as the peripheral benzodiazepine receptors (PBR), that is located in the outer mitochondrial membrane [1]. Furthermore, activation of microglia leads to an increase in the production of cytokines and several hydrolases [2]. Functions of microglia cells in the central nervous system (CNS) appear to be complex as they exhibit both neuroprotective and neurotoxic properties [3]. Rather than being a response solely to neuronal insult, microglial activation is thought to precede neurodegeneration during pathogenesis.

Given the role of microglia in mediating neurodegeneration, a great deal of effort has been made to investigate the mechanism and mediators by which microglia can lead to neurodegeneration. There is some evidence that certain types of degeneration in the CNS are accompanied by large increases in lysosomal β-glucuronidase (β-GUS) activity. β-GUS is involved in the hydrolysis of glycosaminoglycans on the cell surface and the degradation of the extracellular matrix. It is known that β-GUS is present extracellularly in necrotic areas of solid tumors. In inflammation, β-GUS is known to be released from granulocytes, including neutrophils, that are highly present at the sites of inflammation [4-6]. Furthermore, studies in experimental animals have shown that brain lysosomal hydrolase activities increase after infection with viruses [7] and after the slow virus mediated diseases scrapie [8], Creutzfeldt-Jakob disease [9] and multiple sclerosis [10;11].

Elevated levels of β-GUS have been reported in the temporal cortex of Alzheimer's disease (AD) patients and the putamen of patients with Huntington's disease [12]. McGeer *et al.* [13;14] indicated that the apparent correlation between low [^{18}F]FDG uptake in AD patients and β-GUS activity determined *post mortem* is consistent with previous suggestions that the decreases in metabolism reflects local neuronal loss and gliosis. According to Koshiya *et al.*, β-GUS is associated with gliosis and its activity in the cells is enhanced with glial proliferation [15]. Taken together, the studies in humans as well as in experimental animal models suggest that β-GUS activity may be a useful biochemical indicator of cellular injury in the brain that accompanies a neurotoxic response of activated microglia.

Recently our group designed a PET tracer, 1-O-(4-(2-fluoroethyl-carbamoyloxymethyl)-2-nitrophenyl)-O-β-D-glucopyronuronate ([^{18}F]FEAnGA) for β-GUS imaging. This tracer has a glucuronide-prodrug based structure similar to the known prodrug HMR 1826, but with the doxorubicin moiety being replaced by the radioactive [^{18}F]fluoroethylamine group. In tissues with high levels of extracellular β-GUS, [^{18}F]FEAnGA is selectively cleaved by β-GUS at the glucuronic acid moiety and after self-immolation of the spacer, the less hydrophilic [^{18}F]fluoroethylamine is released and trapped in the target tissue (Fig. 1).

In this study, we investigated whether the PET tracer [^{18}F]FEAnGA is able to detect β-GUS, which is released during neuroinflammation, in a rat model of herpes encephalitis [16-18].

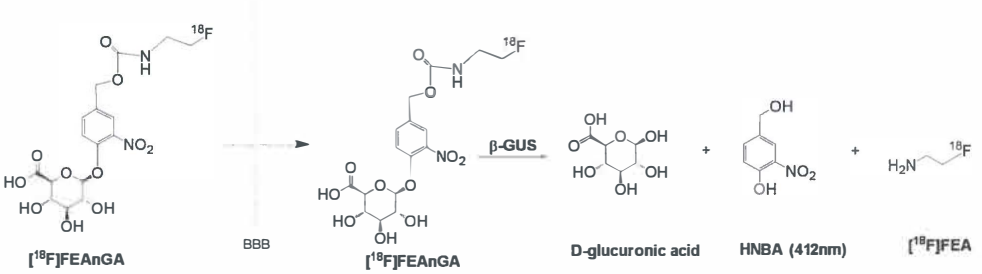

Figure 1. Mechanism of activation of [^{18}F]FEAnGA by β-GUS.

MATERIALS AND METHODS

Synthesis of [^{18}F]FEAnGA. [^{18}F]FEAnGA was prepared as described previously [19]. The tracer was purified by high-performance liquid chromatography (HPLC), using a semi-preparative Prodigy C_{18} reverse-phase column (5µ, 10×250 mm; Phenomenex) with 10 % ethanol in 2.5 mM phosphate buffer as the eluent (flow rate, 4 mL/min; retention time: [^{18}F]FEAnGA= 10 min, [^{18}F]Fluorethylamine ([^{18}F]FEA)= 5 min). At the end of synthesis (EOS), the specific activity of [^{18}F]FEAnGA was 150 ± 50 GBq/µmol and the radiochemical purity > 95% (HPLC with a Symmetry C_{18} column [5µm, 4.6×150 mm] with 5% acetonitrile in phosphate buffer 2.5 mM; flow rate, 1mL/min; retention time: [^{18}F]FEAnGA= 23 min).

Synthesis of [^{11}C]-*(R)*-PK11195. [^{11}C]-*(R)*-PK11195 was labeled by trapping [^{11}C]-methyl iodide [20] in a solution of 1 mg *(R)*-N-desmethyl PK11195 and 10 mg potassium hydroxide in 300 µl dimethylsulfoxide. The reaction mixture was allowed to react for 1 minute at 40 °C, neutralized with 1M HCl and passed through a 45 µm Millex HV filter. The filtrate was purified by HPLC using a µBondapak C18 column (7.8x300 mm) with acetonitrile/25 mM NaH_2PO_4 (pH 3.5) (55/45) as the eluent (flow 5 ml/min). To remove the organic solvents from the product, the collected HPLC fraction (retention time 7 min) was diluted with 100 ml of water and passed through an Oasis HLB 30 mg (1 cc) cartridge. The cartridge was washed twice with 8 ml of water and subsequently eluted with 0.7 ml of ethanol and 5 ml of water. The product was sterilized by filtration over a 0.22 µm Millex LG filter. The product was obtained in 33 ± 15% radiochemical yield (corrected for decay). Quality control was performed by HPLC, using a Novapak C18 column (150x3.9 mm) with acetonitrile/25 mM NaH_2PO_4 (pH 3.5) (60/40) as the eluent at a flow of 1 ml/min. The radiochemical purity was always >95% and the specific activity was 51 ± 18 GBq/µmol.

Animals. Male Wistar rats were obtained from Harlan (Lelystad, The Netherlands). The rats were individually housed in Macrolon cages (38x26x24 cm) on a layer of wood shavings in a room with constant temperature (21 ± 2 °C) and a fixed, 12-hour light-dark regime. Food (standard laboratory chow, RMH-B, Hope Farms, The Netherlands) and water were available *ad libitum*. After arrival, the rats were allowed to

acclimatize for at least seven days. All experiments were approved by the Animal Ethics Committee of the University of Groningen, The Netherlands.

HSV-1 inoculation. A herpes simplex virus-1 (HSV-1) strain was obtained from a clinical isolate, cultured in Vero-cells and assayed for plaque forming units (PFU) per milliliter. The rats were slightly anesthetized with isoflurane (5% for induction and 2% for maintenance) and inoculated with HSV-1 by the application of 100 µL of phosphate-buffered saline (PBS) with $1x10^7$ PFU of virus in the nostrils (50 µL per nostril) with a micro pipette. Control rats were treated similarly by the application of 100 µL PBS without virus. Clinical symptoms in all rats were scored daily after the inoculation by the same observer.

MicroPET Imaging of [^{18}F]FEAnGA. PET scans were preformed when robust clinical sign of infection appeared, which was on day 7 or 8 after the inoculation with HSV-1. The rats were anesthetized with 2% isoflurane (5% for induction and 2% for maintenance) and a canula was inserted into the femoral artery. After cannulation, the rats were positioned in the small animal PET camera (Focus 220) with their heads in the field of view. A transmission scan of 515 seconds with a Co-57 point source was obtained for the correction of attenuation and scatter by tissue. After the transmission scan was completed, the PET tracer [^{18}F]FEAnGA (6.9 ± 3.1 MBq) was injected via the penile vein. Simultaneously with the injection of the PET tracer an emission scan of 60 minutes was started and blood samples of 0.1 mL were taken at 15, 30, 45, 60, 75, 90, 120, 150, 300, 450, 600, 1800, 3600 seconds after the injection. After a blood sample was taken, 0.1 mL of heparinized saline was injected to prevent large changes in blood pressure. The blood samples were centrifuged at 6000 rpm for 10 minutes and 25µL of plasma was collected. The activity in plasma was measured with a gammacounter (LKB Wallac, Turku, Finland). The plasma-activity curves were corrected for decay.

The list mode data of the emission scans was separated into 21 frames (8×30, 3×60, 2×120, 2×180, 3×300 and 3×600 seconds). Emission sinograms were iteratively reconstructed (OSEM2d, 4 iterations, 16 subsets) after being normalized, corrected for attenuation, and corrected for radioactive decay.

MicroPET imaging of [^{11}C]-*(R)*-PK11195. Activation of microglia cells was studied in the rat model of herpes encephalitis with [^{11}C]-*(R)*-PK11195. The PET scans were acquired on either day 5 or day 7 [17] post inoculation with HSV-1. The rats were anaesthetized by 5% isoflurane (Pharmachemie BV, The Netherlands) that was mixed with medical air at a flow of 2 ml/min, which was maintained at 2% isoflurane during the PET scan. Following induction of anaesthesia, the rats were positioned in the small animal PET camera (Focus 220, Siemens Medical Solutions USA, Inc.) in transaxial position with their heads in the field of view. After the transmission scan was completed, the PET tracer [^{11}C]-*(R)*-PK11195 (44 ± 16 MBq) was injected via the penile vein. Simultaneously with the injection of the PET tracer a dynamic emission scan of 60 min was started. The list-mode data of the emission scans was separated into 4 frames of 15 minutes. Emission sinograms were iteratively reconstructed as described above.

MicroPET image analysis. PET image analysis was conducted with the Inveon Research Workplace software (IRW, Siemens, version 3.0). Regions of interest (ROIs) were drawn around the whole brain, bulbus olfactorius, frontopolar cortex, frontal cortex, hippocampus, striatum, thalamus, parietal/temporal/occipital cortex, brainstem, midbrain and cerebellum in a template MRI scan that was co-registered with the PET scan of interest by image fusion. The time activity curves (TAC) per region of interest were determined in Bq/cm^3 units and converted into standardized uptake values (SUV), defined as: [tissue activity concentration (Bq/cm^3)]/[injected dose (Bq)/body weight (g)]. It was assumed that 1cm^3 of brain tissue equals 1 gram.

The plasma time activity curves in Bq/cc were used for pharmacokinetic modeling with Inveon Research Workplace software (IRW, Siemens, version 3.0). Distribution volumes (DV_{Logan}) were calculated using the linear model developed by Logan [21].

Metabolite analysis. A total of 2.5 µL of each plasma sample was collected and applied on a TLC plate, which was subsequently eluted with acetonitrile/water (7:3) (R_f [^{18}F]FEA= 0.57, R_f [^{18}F]FEAnGA= 0.89). After elution, radioactivity on TLC plates was analyzed by phosphor storage imaging. Exposed screens were scanned with a Cyclone phosphor storage system (PerkinElmer) and the percentage of conversion of [^{18}F]FEAnGA

as a function of the tracer distribution time was calculated by ROI analysis using OptiQuant software

***Ex vivo* analysis of the conversion of [^{18}F]FEAnGA to [^{18}F]FEA by measurement of the release of HNBA.** The ability of [^{18}F]FEAnGA to detect extracellular β-GUS is based on the retention of [^{18}F]FEA and the yellow-colored spacer, 4-hydroxy-3-nitrobenzyl alcohol (HNBA), as a result of selective cleavage by the extracellular β-GUS present in inflamed regions (Fig. 1).

For analysis of *in vivo* tracer conversion by β-GUS, the two brain regions (cerebellum and brainstem) where inflammation is expected to be most active [18;19;22] were homogenized in 1mL of PBS. The homogenates were centrifuged (5 min, 6000 rpm) and the supernatant was collected. To 0.5 ml of the supernatant, 1 ml of acetonitrile was added to precipitate the remaining proteins. The samples were vortexed for 30 s and centrifuged at 9000 rpm for 5 min. A volume of 1 ml was taken for UV absorption (412 nm) analysis to quantify the amount of HNBA released in infected and control animals. A ROI of both the cerebellum and the brainstem was created in the PET images by fusion of the ROIs of the two individual brain regions. The DV volume of the cerebellum-brainstem was calculated and compared with the release of HNBA.

β-GUS assay. To 0.5 mL of the supernatant of brain homogenate (see above), 1.5 mL of a solution containing 0.1% BSA in PBS (pH=7.4) was added. To 1 mL of the diluted solution 50 μL of the substrate for β-GUS, 4-nitrophenyl- β-D-glucuronide (PNPG, ε= 7578 $M^{-1}cm^{-1}$) (0.1M) was added while the other 1 mL of the diluted solution received 50 μL of PBS (Blank). All tubes were incubated at 37 °C for 10 minutes. The reaction in each tube was stopped by adding 1.5 mL of 0.1M NaOH and UV absorption was measured at 412 nm. UV absorption of PNPG containing samples was corrected for UV absorption of blank samples. Absorption was converted in micrograms, using a 4-nitrophenyl (PNP) calibration curve. The measurements were performed in duplicate. The β-GUS activity is determined in units (U), defined as: micromoles of PNP liberated per minute [23].

Statistical analysis. All data are expressed as mean ± standard deviation. Differences between groups were determined with the two-sided unpaired Student *t*-test (Microsoft Office Excel 2003). Significance was reached when the p value was ≤ 0.05. Correlations were assessed with Pearson's product moment correlation coefficient (r) using SigmaPlot 10 and were considered statistically significant when $r^2 \geq 0.5$ and $p < 0.05$.

RESULTS

Small animal PET imaging. The [^{18}F]FEAnGA PET images and the whole brain (WB) time-activity curves are displayed in figure 2. The images showed a low brain uptake of the tracer in infected and control animals. The time-activity curves showed that [^{18}F]FEAnGA followed a rapid two-phase decline in uptake (SUV) in the whole brain. From HSV-1 infected brains, 15% of the activity was cleared with a half-life $(t_{1/2})_1$ of 0.7 ± 0.6 min and 85% of the activity with a half-life $(t_{1/2})_2$ of 14 ± 11 min (n= 8). In control rats, 17% of the activity was washed out of the brain with a half-life $(t_{1/2})_1$ of 0.4 ± 0.1 min and 83% of the activity with a half-life $(t_{1/2})_2$ of 8 ± 3 min (n= 8). In addition, the area under the curve (10-60 min) in the whole brain of HSV-1 infected rats is 2 times (9 ± 4) higher, when compared to control rats (5 ± 1, p= 0.05).

In contrast to control animals, HSV-1 infected animals showed brain radioactivity uptake that was significantly higher than plasma radioactivity levels.

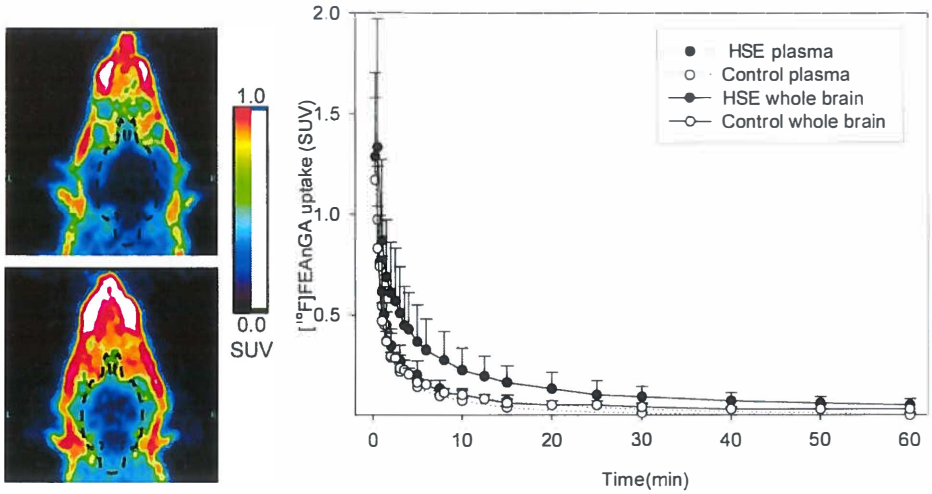

Figure 2. A) Coronal view of the head of a control rat (Top left) and a HSV-1 infected rat (bottom left). The images represent tracer uptake between 10 and 60 minutes after injection of [^{18}F]-FEAnGA. **B)** Whole brain and plasma time–activity curves of [^{18}F]FEAnGA, expressed as standardized uptake values (SUV, mean ± standard deviation), of control rats (n= 4) and HSV-1 infected rats (HSE) (n=8) (Right side).

Pharmacokinetic modeling. Metabolite analysis was performed in the plasma samples that were taken during the [^{18}F]FEAnGA PET scan. Figure 3 indicates that [^{18}F]FEAnGA is very stable for the duration of the scan since no radioactive metabolites were found in plasma (at 60 min, 98 ± 4% intact tracer). Therefore, no metabolite correction was required for pharmacokinetic modeling and the total activity in plasma was used as the input function.

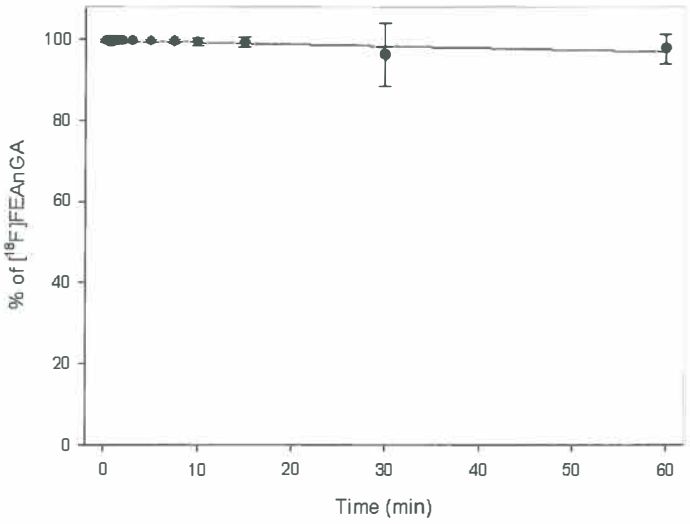

Figure 3. Percentage of the intact [^{18}F]FEAnGA determined by metabolite analysis of the plasma samples that were taken over time (n= 11).

Exponential curve-fitting analysis of [^{18}F]FEAnGA showed a two-phase plasma clearance in infected rats with 22% of the injected activity having a half-life $(t_{1/2})_1$ of 0.5 ± 0.2 min and 78% of the injected activity having a half-life $(t_{1/2})_2$ of 7 ± 3 min (n= 8), which was similar to the plasma clearance of [^{18}F]FEAnGA in control rats (23% $(t_{1/2})_1$= 0.5 ± 0.1 min and 77% $(t_{1/2})_2$= 8 ± 3 min, n= 4).

Logan analysis, using a delay time of 10 min, was used to evaluate the distribution volume (DV_{logan}) of [^{18}F]FEAnGA in the whole brain as well as in individual regions of the brain. The whole brain DV_{logan} of [^{18}F]FEAnGA was found to be 53% higher (p= 0.02) in HSV-1 infected rats than in control rats. Furthermore, the DV_{Logan} was found to be the highest in the frontopolar cortex (0.20 ± 0.02, p= 0.06), frontal cortex (0.17 ± 0.02, p= 0.02) and bulbus olfactorius (0.17 ± 0.02, p= 0.02), followed by the Cerebral cortex (0.13 ± 0.03, p= 0.02), cerebellum (0.12 ± 0.03, p= 0.05) and brainstem (0.11 ± 0.03, p= 0.01) (Table 1). DV_{logan} was significantly higher in most of the individual brain regions of HSV-1 infected animals than in the corresponding regions in controls, with the exception of cerebellum and frontopolar cortex.

Table 1. Distribution volume of [^{18}F]FEAnGA (mL/mg) in different regions of the brain in control rats (n= 4) and rats infected with HSV-1 (HSE) (n= 8). Data are presented as mean ± standard deviation. *p<0.05 when compared to controls.

Regions of the brain	HSE (n=8)	Control (n=4)
Whole Brain	0.12 ± 0.03*	0.08 ± 0.01
Striatum	0.09 ± 0.03*	0.04 ± 0.02
Frontal Cortex	0.17 ± 0.02*	0.13 ± 0.03
Hippocampus	0.10 ± 0.02*	0.05 ± 0.03
Parietal/Temporal/Occipital Cortex	0.13 ± 0.02*	0.09 ± 0.01
Bulbus Olfactorius	0.17 ± 0.02*	0.14 ± 0.02
Cerebellum	0.12 ± 0.03	0.07 ± 0.02
Frontopolar Cortex	0.20 ± 0.02	0.17 ± 0.04
Brainstem	0.11 ± 0.03*	0.06 ± 0.02
Thalamus	0.08 ± 0.03*	0.03 ± 0.01
Midbrain	0.10 ± 0.02*	0.05 ± 0.03

***Ex vivo* analysis of β-GUS activity:** We further quantified the *in vivo* [^{18}F]FEAnGA conversion to [^{18}F]FEA and the spacer HNBA (Fig. 1) in the two brain regions (cerebellum + brainstem) where inflammation was expected to be most active [18;19;22] and therefore most likely would have elevated levels of extracellular β-GUS. Thus, a new ROI was created including both the brainstem and the cerebellum. The DV_{Logan} of the brainstem-cerebellum was found to be 70% (p= 0.04) increased in infected rats when compared to control rats. The *in vivo* formation of HNBA was also increased 65% (p= 0.02) in infected rats (Fig.4). In addition, the DV_{Logan} of the brainstem-cerebellum correlated with the amount of HNBA present in these brain regions ($y=383.23x + 0.01$, $r^2= 0.63$, p= 0.002) (Fig. 4). The increased β-GUS activity was confirmed in an *in vitro* β-GUS enzyme assay, which measures the conversion of the glucuronide PNPG. This *in vitro* β-GUS assay showed 3.4 times higher enzyme activity in brainstem-cerebellum of HSV-1 infected animals than in controls (p= 0.03). In addition, this enzyme activity found in the brainstem-cerebellum tends to correlate with the DV_{Logan} of [^{18}F]FEAnGA in the same region ($y=0.002x + 0.06$, $r^2= 0.52$, p= 0.007).

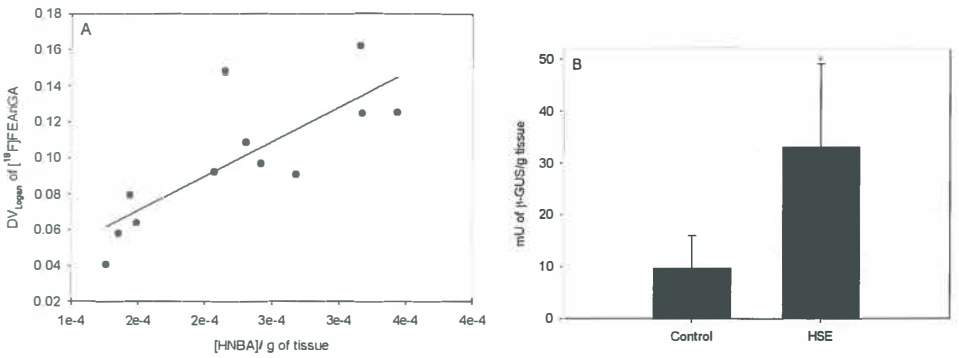

Figure 4. A) Correlation between the distribution volume (DV_{Logan}) of [^{18}F]FEAnGA determined in the cerebellum-brainstem region and the release of the spacer HNBA from [^{18}F]FEAnGA. **B)** β-GUS activity (U/mg tissue) in the cerebellum-brainstem region of control and HSV-1 infected rats, as determined by a PNPG conversion assay. (*p<0.05 as compared to controls).

Comparison of [^{18}F]FEAnGA and [^{11}C]-*(R)*-PK11195 accumulation: Microglia cells are the predominant population of macrophages in the brain and are responsive to injury or infection of brain tissue. Activation of microglia cells results in the upregulation of molecules, such as peripheral benzodiazepine receptors (PBR) that are located on the outer mitochondrial membrane. [^{11}C]-*(R)*-PK11195, which is a ligand of the peripheral benzodiazepine receptors, is the most widely PET tracer used for imaging activated microglia, representing neuroinflammation. In a previous study, we have used [^{11}C]-*(R)*-PK11195 for imaging of neuroinflammation in the rat model of herpes encephalitis [17]. Activation of microglia leads to an increase in the production of cytokines and several hydrolases, such as β-GUS [2]. Thus a comparison between both tracers might give an indication if microglial activation precedes neurodegeneration during pathogenesis, as measured with [^{18}F]FEAnGA, rather than being a response solely to neuronal insult.

The distribution volume of [^{18}F]FEAnGA which was found to be significantly higher in almost all areas of the brain 7 days after HSV-1 inoculation did not correlate with the uptake of [^{11}C]-*(R)*-PK11195 in the same brain areas 7 days after HSV-1 inoculation ($y=5.06x + 0.13$, $r^2= 0.30$, $p= 0.07$) [17;18]. This lack of correlation was due to the high uptake of [^{11}C]-*(R)*-PK11195 in the brainstem compared to the smaller distribution volume

of [^{18}F]FEAnGA in the same region (Fig. 5). However, when the brainstem region was omitted from the analysis, we found a fair correlation of y=5.04x + 0.06, r^2= 0.51, p= 0.01.

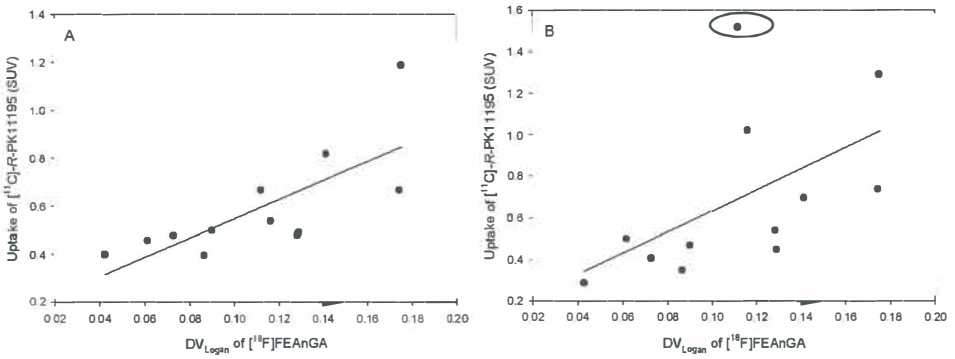

Figure 5. Correlation between the distribution volume (DV_{Logan}) of [^{18}F]FEAnGA in all brain regions of control and HSV-1 infected rats and the uptake of [^{11}C]-*(R)*-PK11195 in the same brain regions. **A)** Correlation between DV_{Logan} of [^{18}F]FEAnGA 7 days post inoculation and [^{11}C]-*(R)*-PK11195 uptake 5 days post inoculation, in different brain regions (y=3.97x +0.15, r^2= 0.54, p= 0.006). **B)** Correlation between DV_{Logan} of [^{18}F]FEAnGA 7 days post inoculation and [^{11}C]-*(R)*-PK11195 uptake 7 days post inoculation, in different brain regions (y=5.06x + 0.13, r^2= 0.30, p= 0.07). The big circle represents the outliner in the correlation between the DV_{Logan} of [^{18}F]FEAnGA in the brainstem of HSV-1 infected animals and the uptake of [^{11}C]-*(R)*-PK11195 in the same region of infected animals.

Since we anticipated that activation of microglia precedes the release of β-GUS, an addition study was performed to evaluate the [^{11}C]-*(R)*-PK11195 in the same brain areas 5 days after HSV-1 inoculation. To quantify the uptake of [^{11}C]-*(R)*-PK11195, the SUV from the last 10 minutes of the PET scan was calculated from the examined brain areas (Table 2).

Table 2. [^{11}C]-*(R)*-PK11195 brain uptake in control and HSV-1 infected rats (5 days after HSV-1 inoculation). The values represent the standardized uptake values (SUV, mean±SD) from the last 10 min of the PET scan. *p<0.05 or **p<0.005 as compared to control.

Regions of the brain	HSE (n=7)	Control (n=7)
Striatum	0.50 ± 0.07*	0.40 ± 0.05
Frontal Cortex	0.67 ± 0.07**	0.49 ± 0.07
Parietal/Temporal/Occipital Cortex	0.48 ± 0.07*	0.40 ± 0.05
Bulbus Olfactorius	1.19 ± 0.18**	0.82 ± 0.09
Cerebellum	0.54 ± 0.09	0.48 ± 0.05
Brainstem	0.67 ± 0.19*	0.46 ± 0.07
Thalamus	0.41 ± 0.04**	0.31 ± 0.06
Midbrain	0.36 ± 0.06	0.34 ± 0.09

The highest uptake of [^{11}C]-*(R)*-PK11195 was found in the bulbus olfactorius ($p<0.001$), frontal cortex ($p= 0.001$), parietal/temporal/occipital cortex ($p= 0.02$), brainstem ($p= 0.02$) and cerebellum ($p> 0.05$) in rats infected with HSV-1 (5 days post inoculation), when compared to control animals. These [^{11}C]-*(R)*-PK11195 uptake values are consistent with the [^{11}C]-*(R)*-PK11195 uptake values obtained in infected rats 7 days post inoculation, with the exception of the cerebellum and brainstem regions where it was found to be 2 times lower in HSV-1 rats 5 days after inoculation, than in the HSV-1 infected rats 7 days after inoculation. In addition, the uptake of [^{11}C]-*(R)*-PK11195 in different brain areas 5 days after HSV-1 inoculation correlated better with the distribution volume of [^{18}F]FEAnGA in the same brain regions (7 days after HSV-1 inoculation) ($y=3.97x +0.15$, $r^2= 0.54$, $p= 0.006$). Thus, the release of β-GUS follows the activation of microglia.

DISCUSSION

The aim of this study was to evaluate whether [^{18}F]FEAnGA PET could be a suitable method to detect β-glucuronidase in the HSV-1 infected brain. Such an imaging method could be employed to gain more insight into neurodegenerative processes. β-GUS is a lysosomal enzyme that is released in reactive astrocytes and microglia. β-GUS is involved in the hydrolysis of glycosaminoglycans on the cell surface and the degradation of

the extracellular matrix and, therefore, its activity may give some indication of the degree of gliosis. In several neurological diseases, there has been evidence of an increase in β-GUS. Whether this increase is due to an earlier response of invading macrophages to digest the infected tissue, or to the release in β-GUS from activated microglia in response to neuroinflammation is not certain. Nevertheless, it is known that in neurological diseases associated with neuroinflammation and neurodegeneration, extracellular β-GUS is present. Extracellular β-GUS expression could be a target for imaging the process of neuroinflammation-mediated neurodegradation. Previously, we have shown that extracellular β-GUS could be monitored by [^{18}F]FEAnGA PET in mice bearing genetically modified β-GUS expressing tumors [19]. Furthermore, β-GUS could also be monitored with [^{18}F]FEAnGA PET in a normal necrotic tumor and in inflammation in rats [24].

The present PET study showed that [^{18}F]FEAnGA uptake in the brain was low. This low brain uptake can be attributed to the hydrophilic characteristics of the tracer, which hampers its penetration of the blood-brain barrier. Nevertheless, PET showed a significant enhancement of the distribution volume of the tracer in the brains of HSV-1 infected rats compared with brains of uninfected rats. Because of the hydrophilic character of [^{18}F]FEAnGA, theoretically the increased tracer uptake in HSV-1 infected rats could be explained by inflammation induced leakage of the blood brain barrier (BBB), rather than increased β-GUS activity. To prove that the increase of [^{18}F]FEAnGA uptake is not only due to enhanced tissue perfusion, we quantified [^{18}F]FEAnGA uptake in cerebellum and brainstem, where inflammation is expected to be most active [18;19;22] and therefore most likely highest increase in levels of extracellular β-GUS will be present. Analysis of the brain homogenates of HSV-1 infected rats revealed a 1.6 times higher amount of the spacer, HNBA that was formed after hydrolysis of the tracer, when compared to brain homogenates of control rats. In addition, β-GUS activity was 3.3 times higher in brain homogenates of infected rats than in controls. Moreover, the distribution volume in this brain region (cerebellum+brainstem) correlated well with the release of HNBA and β-GUS activity. Thus, the distribution volume seems to reflect β-GUS activity, rather than increased BBB permeability. Since metabolite analysis indicated that there was only

[^{18}F]FEAnGA present in the plasma, we can only attribute the presence of the spacer, HNBA, derived from the hydrolysis of the tracer, to the release of β-GUS in the infected regions.

Interestingly, the distribution volume of [^{18}F]FEAnGA (7 days post inoculation of HSV-1) tended to correlate with the uptake of [^{11}C]-*(R)*-PK11195 (PET tracer for imaging microglia activation) 5 days post inoculation of HSV-1 in the same brain areas. However, when compared with the [^{11}C]-*(R)*-PK11195 uptake in the same brain areas 7 days post inoculation of the HSV-1, the correlation was reduced mainly due to a much higher uptake of [^{11}C]-*(R)*-PK11195 in the brainstem than the distribution volume of [^{18}F]FEAnGA in HSV-1 infected animals (7 days post inoculation of HSV-1), suggesting that the release of β-GUS follows the activation of microglia with a delay of a few days. These findings are in agreement with earlier reports, in which β-GUS activity was found to be enhanced during gliosis [12]. To get a better understanding of the relation between microglia activation and β-GUS activity a future study should be performed investigating both microglia activation and β-GUS activity in the same animal in a longitudinal study.

CONCLUSION

Despite relatively low brain uptake, [^{18}F]FEAnGA was able to detect an increased release of β-GUS during neuroinflammation. Further studies should be performed to reveal the exact role of the increased β-GUS activity in neuroinflammatory and neurodegenerative disorders.

ACKNOWLEDGMENT

The authors would also like to thank Sietske Welling Wester and Björge Meijdam of the Department of Medical Microbiology of the University of Groningen, The Netherlands for their help with the HSV-1.

REFERENCES

1. Banati RB, Myers R, and Kreutzberg GW (1997) J. Neurocytol. 26:77-82.
2. Liu J, Hong Z, Ding J, Liu J, Zhang J, and Chen S (2008) J. Proteome. Res. 7:2033-2049.
3. Nakajima K and Kohsaka S (2004) Curr. Drug Targets. Cardiovasc. Haematol. Disord. 4:65-84.
4. Marshall T, Shult P, and Busse WW (1988) J. Allergy Clin. Immunol. 82:550-555.
5. Shimoi K, Saka N, Nozawa R, Sato M, Amano I, Nakayama T, and Kinae N (2001) Drug Metab Dispos. 29:1521-1524.
6. Shimoi K and Nakayama T (2005) Methods Enzymol. 400:263-272.
7. Bowen DM, Flack RH, Martin RO, Smith CB, White P, and Davison AN (1974) J. Neurochem. 22:1099-1107.
8. Mackenzie A, Wilson AM, and Dennis PF (1968) J. Comp Pathol. 78:489-498.
9. Annunziata P and Federico A (1981) J. Neurol. Sci. 49:325-328.
10. Cuzner ML, Barnard RO, MacGregor BJ, Borshell NJ, and Davison AN (1976) J. Neurol. Sci. 29:323-334.
11. McMartin DN, Koestner A, and Long JF (1972) Acta Neuropathol. 22:275-287.
12. Cross AJ, Crow TJ, Dawson JM, Ferrier IN, Johnson JA, Peters TJ, and Reynolds GP (1986) J. Neurochem. 47:882-889.
13. McGeer EG, McGeer PL, Akiyama H, and Harrop R (1989) Can. J. Neurol. Sci. 16:511-515.
14. McGeer EG, McGeer PL, Harrop R, Akiyama H, and Kamo H (1990) J. Neurosci. Res. 27:612-619.
15. Koshiya K, Kato T, Tanaka R, and Kato T (1984) Brain Res. 324:261-270.
16. Buursma AR, de Vries EF, Garssen J, Kegler D, van Waarde A, Schirm J, Hospers GA, Mulder NH, Vaalburg W, and Klein HC (2005) J. Virol. 79:7721-7727.
17. Doorduin J, Klein HC, Dierckx RA, James M, Kassiou M, and de Vries EF (2009) Mol. Imaging Biol. 11:386-398.
18. Doorduin J, Klein HC, de Jong JR, Dierckx RA, and de Vries EF (2010) Nucl. Med. Biol. 37:9-15.
19. Antunes IF, Haisma HJ, Elsinga PH, Dierckx RA, and de Vries EF (2010) Bioconjug. Chem. 21:911-920.
20. Larsen P, Ulin J, Dahlstrom K, and Jensen M (1997) Applied Radiation and Isotopes 48:153-157.
21. Logan J, Fowler JS, Volkow ND, Wolf AP, Dewey SL, Schlyer DJ, MacGregor RR, Hitzemann R, Bendriem B, Gatley SJ, and . (1990) J. Cereb. Blood Flow Metab 10:740-747.

22. Doorduin J, de Vries EF, Willemsen AT, de Groot JC, Dierckx RA, and Klein HC (2009) J. Nucl. Med. 50:1801-1807.

23. Fishman WH, Springer B, and Brunettei R (1948) J. Biol. Chem. 173:449-456.

24. Antunes IF, Haisma HJ, Elsinga PH, VAN Waarde A, Willemsen ATM, Dierckx RA, and de Vries EFJ (2011) Molecular Imag., DOI 10.2310/7290.2011.00029

Chapter

Induction of β-glucuronidase release by cytostatic agents in small tumors evaluated with [^{18}F]FEAnGA PET

Inês F. Antunes, Hidde J. Haisma, Philip H. Elsinga,
Valentina Di Gialleonardo, Aren van Waarde,
Antoon T. M. Willemsen, Rudi A. Dierckx, Erik F. J. de Vries

Submitted for publication

ABSTRACT

Extracellular β-glucuronidase (β-GUS) in tumors has been investigated as a target enzyme for prodrug therapy. However, despite encouraging preclinical results, animal studies also indicate that the success of prodrug therapy might be limited by the insufficient prodrug-converting enzyme activity, especially in small tumors. We hypothesized that a single dose of a cytostatic drug might induce the release of β-GUS in small tumors, resulting in increased levels of extracellular β-GUS and consequently a higher efficacy of the prodrug treatment. Here we examine the extend of β-GUS release in small C6 glioma tumors after a single treatment of Doxorubicin (DOX), Carmustine (BCNU) and Tumor Necrosis Factor α (TNF-α) with the PET tracer [^{18}F]FEAnGA, which has proven to be selective for extracellular β-GUS. Induction of β-GUS release was investigated in cultured C6 glioma cells. In addition, [^{18}F]FEAnGA uptake and pharmacokinetics studies were performed in C6 tumor-bearing rats 48h after a single treatment with different cytostatics. The *in vitro* and *in vivo* studies indicated that all treatments resulted in a decline of vital cells and an increase of extracellular β-GUS activity. The distribution volume of [^{18}F]FEAnGA in C6 gliomas increased significantly by 10-70% depending on the treatment. In the present study, we were able to demonstrate that a single dose of a cytostatic agent was able to increase the release of β-GUS and that [^{18}F]FEAnGA is a suitable PET tracer to evaluate β-GUS activity. This study may open the way to a two-step chemotherapy-prodrug approach, in which tumors are treated with a single dose of a cytostatic before prodrug treatment.

INTRODUCTION

Chemotherapy is an important treatment option for patients with advanced cancer, but its therapeutic efficacy is often limited. Due to severe dose-limiting side-effects, cytostatic drugs can often not be given in sufficient amounts to completely eradicate the tumor. To increase the therapeutic index, cytostatic drugs can be modified into non-toxic prodrugs that are converted *in situ* to the active drug by a tumor-specific enzyme that is selectively expressed at the target site. β-Glucuronidase (β-GUS) (EC 3.2.1.31) is such a tumor-specific enzyme for activation of glucuronide prodrugs [1]. High levels of β-GUS are released in the extracellular space of tumors by necrotic tumor cells and infiltrating monocytes/granulocytes, whereas the enzyme is virtually absent in circulation and only expressed intracellularly in non-target tissues [2]. Most glucuronide prodrugs are unable to cross the cell membrane due to their hydrophilic character, and therefore, are only activated by extracellular β-GUS in the tumor. Several glucuronide prodrugs have been evaluated as candidates for prodrug monotherapy *in vivo*. Encouraging preclinical results were obtained with the prodrugs DOX-GA3, 9-AC and HMR 1826. These prodrugs were able to release doxorubicin/camptothecin after enzymatic cleavage of the glucuronide moiety by extracellular β-GUS suggesting that bioactivation of glucuronide prodrugs by β-GUS is an attractive approach in prodrug therapy [2-4]. However, the improvement in efficacy was more pronounced in large tumors, which contain higher β-GUS levels, than in small tumors. Therefore, despite the encouraging results, success of prodrug therapy might be hampered by the insufficient prodrug-converting enzyme activity inside smaller tumors. In order to improve the efficacy of β-GUS-mediated prodrug therapy, investigators have searched for ways to increase the concentration of target enzyme in the tumor, which should result in more efficient conversion of the prodrug. The increasing in enzyme concentration inside the tumor can be achieved by transfection of the β-GUS gene in tumor models or by conjugation of the enzyme to an antibody/antibody fragment that is directed at a tumor-specific antigen [5]. However, these approaches lead ultimately to immunogenicity.

Recently, Juan *et al.* investigated the concept that the efficacy of prodrugs can be improved by stimulation of infiltration of innate immune cells [6]. Furthermore, chemotherapeutic drugs can induce necrosis as well as leukocyte infiltration, which will most likely generate an increase in the extracellular β-GUS levels. Previous *in vivo* studies performed with [^{18}F]FDG PET have shown that the non viable fraction of the tumor increased after treatment with doxorubicin (DOX) [7]. Carmustine (BCNU) is a nitrosurea used in treatment of gliomas and leukemia and it has been reported to induce necrosis in tumors. On the other hand, cytokines such as Tumor Necrosis Factor α (TNF-α), which has cytostatic/cytotoxic effects, is characterized by its ability to produce hemorrhagic necrosis and is used in cancer treatment in the isolated limb perfusion (ILP) setting for soft tissue sarcoma (STS), irresectable tumors and melanoma metastases confined to the limb.

Therefore we hypothesize that a single dose of one of these cytostatic drugs might increase the release of β-GUS in small tumors, resulting in enhanced extracellular levels of the prodrug-converting enzyme and as a consequence a higher efficacy of the prodrug treatment. Thus, here we examine the extend of β-GUS release in small C6 glioma tumors after a single treatment of Doxorubicin (DOX), Carmustine (BCNU) and Tumor Necrosis Factor α (TNF-α) with the selective PET tracer for β-GUS, [^{18}F]FEAnGA [8]. In the presence of tissues with high levels of extracellular β-GUS, the prodrug-based PET tracer, [^{18}F]FEAnGA is selectively cleaved at the glucuronic acid moiety by β-GUS, and after self-immolation of the spacer, the less hydrophilic [^{18}F]fluoroethylamine is released and trapped in the target tissue (Fig. 1) [8].

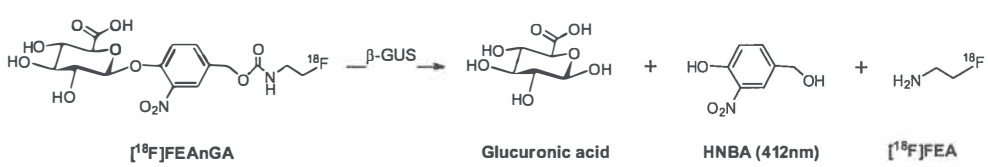

Figure 1. General mechanism of activation of the prodrug tracer

MATERIALS AND METHODS

Reagents and solvents were obtained from commercial suppliers (Sigma-Aldrich and Fluka, Zwijndrecht, The Netherlands and Merck, Darmstadt, Germany) and used without further purification. Doxorubicin was purchased from Pharmachemie (Haarlem, The Netherlands) and Carmusine from Bristol-Myers Squibb B.V. (Woerden, The Netherlands). HrTNF-α and the monoclonal antibodies (CDs) were kindly provided by the department of Oncology (UMCG, Groningen, The Netherlands) and the rat rTNF-α was purchased in Sigma-Aldrich (Zwijndrecht, The Netherlands). Dulbecco's minimum essential medium (DMEM), fetal calf serum (FCS) and trypsin were from Invitrogen.

Synthesis of [^{18}F]FEAnGA. [^{18}F]FEAnGA was prepared as described previously [8]. The tracer was purified by high-performance liquid chromatography (HPLC), using a semi-preparative Prodigy C_{18} reverse-phase column (5μ, 10×250 mm; Phenomenex) with 10 % ethanol in 2.5 mM phosphate buffer as the eluent (flow rate, 4 mL/min; retention time: [^{18}F]FEAnGA= 11 min, [^{18}F]FEA= 5.5 min). At the end of synthesis (EOS), the specific activity of [^{18}F]FEAnGA was 45 ± 11 GBq/μmol and the radiochemical purity > 95% (HPLC with a Luna C_{18} column [5μm, 4.6×250 mm] with 10% acetonitrile in phosphate buffer 2.5 mM; flow rate, 1mL/min; retention time: [^{18}F]FEAnGA= 12 min).

***In vitro* induction of β-glucuronidase release by cytostatics.** C6 rat glioma cells obtained from the American Type Culture Collection were cultured in monolayers in DMEM supplemented with 7.5% fetal bovine serum (FBS) in a humidified atmosphere containing 5% CO_2 at 37 °C. Before each experiment, the cells were seeded in triplicate in a 12-wells plate at a density of 7×10^5 cells per well. After 24 h at 37 °C, monolayers were established. The medium was discarded and 900 μL of PBS-GMC buffer per well was added, followed by the addition of 100 μL of either DOX (1 μM), BCNU (20 μM) or TNF-α (50 ng, 1500-3000 U/ml) in each series of 3 wells. After 24 h of incubation at 37 °C, the medium was collected, the cells washed with cold PBS (3×1 mL/well), harvested with trypsin (250 μL) and resuspended in 1750 μL of DMEM. The cell suspensions were collected separately for each well. A 50 μL sample of the suspension was mixed with 50 μL

of tryphan blue and used for cell counting. Cell numbers were manually determined, using a phase-contrast microscope (Olympus), a Burker bright-line chamber (depth, 0.1 mm: 0.0025-mm^2 squares) and a hand-tally counter.

***In vitro* β-glucuronidase assay.** To a 2.5 mL solution of 0.1M p-nitrophenyl-β-D-glucuronide (PNPG) containing 0.1% BSA in PBS (pH=7.4), 200 μL of the medium/well collected in the aforementioned cell experiment was added. Simultaneously with the addition of the medium, the UV measurements (Waters 2487 dual wavelength absorbance detector, 412nm, aufs= 0.01) of the formation of p-nitrophenol (PNP) (ε= 7578 $M^{-1}cm^{-1}$) was started. Absorption was converted in concentration, using a PNP calibration curve, and corrected for the number of viable cells.

Animal models. Wistar rats (6-8 weeks old) were obtained from Harlan (Lelystad, The Netherlands) or from Charles River (Germany). C6 glioma cells [1-1.5 × 10^6 cells in a 1:1 mixture of Matrigel and DMEM with 5% FBS)] were subcutaneously injected into the right shoulder of male Wistar rats. The animals were provided with standard laboratory chow and tap water *ad libitum*. On day 6, control animals were then injected with PBS (carrier, 1mL, intraperitoneal or 5 μL, intratumoral), whereas treated animals received doxorubicin (8mg/kg of body weight, in 1mL of PBS, intraperitoneal) or Carmustine (50mg/kg of body weight, in 1mL of 10%EtOH/PBS, intraperitoneal) or rTNF-α (5μg/kg of body weight, in 5μL of PBS, intratumoral). All studies were carried out in compliance with the local ethical guidelines for animal experiments. The protocols (DEC number 5549E and 6082A) were approved by the Animal Ethics Committee of Groningen University.

Image acquisition with arterial blood sampling. PET scans were preformed on day 8 (48h after treatment) in Wistar rats bearing a C6 glioma tumor in the right shoulder. The rats were anesthetized with 2 % isoflurane (5 % for induction and 2% for maintenance) and a cannula was inserted into the artery femoralis in rats. After cannulation, the rats were positioned in the small animal PET camera (Focus 220, Siemens) with their shoulders in the field of view. A transmission scan of 515 seconds with Co-57 point source was obtained for the correction of attenuation and scatter by

tissue. After the transmission scan was completed, the PET tracer [^{18}F]FEAnGA (6.3 ± 0.5 MBq) was injected via the penile vein. Simultaneously with the injection of the PET tracer an emission scan of 60 minutes was started and blood samples of 0.1 mL were taken at 15, 30, 45, 60, 75, 90, 120, 150, 300, 450, 600, 1800, 3600 seconds after the injection. After a blood sample was taken, 0.1 mL of heparinized saline was injected to prevent large changes in pressure. The blood samples were centrifuged at 6000 rpm for 10 minutes and 50 µL of plasma were collected. The activity in plasma was measured with a gammacounter (LKB Walla, Turku, Finland). The plasma-activity curves were corrected for decay. Subsequent to the microPET imaging, the animal fixed to the bed were terminated with an excess of anesthesia and positioned in the microCT scanner (MicroCT II, CTI Siemens). A microCT image (exposure time=600 msec; X-Ray voltage= 80 kvp; Anode current= 240 µA; number of rotation steps= 500; total rotation= 360 degrees) was acquired for 10 min for anatomic localization.

PET image reconstruction and data analysis. The list mode data of the emission scans was separated into 21 frames (8×30, 3×60, 2×120, 2×180, 3×300 and 3×600 seconds). Emission sinograms were iteratively reconstructed (OSEM2d, 4 iterations, 16 subsets) after being normalized, corrected for attenuation, and corrected for radioactive decay. The microPET and CT images were then fused using Inveon Research Workplace (Siemens Preclinical Solution, Knoxville, TN). For data analysis, the region of interest (ROI) was manually drawn covering the whole tumor, liver, heart and thymus on the CT images and transferred to the corresponding PET images. The images were summed (last 9 frames; 10-60 min) and a second ROI of the viable part of the tumor was generated automatically with a 50 % threshold using a region growing method, i.e. only included pixels greater than 50 % of the maximum value within the lesion. The resulting ROIs were used on the original (none smoothed) data to originate the corresponding time-activity curves (TACs), using standard software (Inveon, Siemens, USA). Tracer accumulation is expressed as standardized uptake values (SUV), which was defined as: [Tissue activity concentration (MBq/g) × body weight (g) / injected dose (MBq)].

Pharmacokinetic modeling of the tissue TACs was performed using standard software (Inveon, Siemens, USA). The graphical Logan Model was used to determine the distribution volume, DV_T of the tracer in the tumors. The whole blood and plasma activity concentrations were considered to be equal. The plasma-activity curves were corrected for decay and metabolites.

Metabolite analysis of [^{18}F]FEAnGA in plasma. To a 100 µL of each plasma sample, 200 µL of MeCN was added to precipitate the remaining proteins. The samples were centrifuged at 9000 rpm for 5 min. A 2.0 µL aliquot of the supernatant was collected and applied on a TLC plate. The TLC plate was eluted with acetonitrile/water (7:3) (R_f [^{18}F]FEA= 0.57, R_f [^{18}F]FEAnGA= 0.89). After elution, radioactivity on TLC plates was analyzed by phosphor storage imaging. Exposed screens were scanned with a Cyclone phosphor storage system (PerkinElmer) and the percentage of conversion of [^{18}F]FEAnGA as a function of the tracer distribution time was calculated by ROI analysis using OptiQuant software.

Biodistribution (BD) studies. After the CT scan, the tumors were excised, weighted and the amount of radioactivity was determined with a gammacounter (LKB Wallac, Turku, Finland). Tracer uptake is expressed as SUV. These tumors were kept at -80 ^{0}C until further analysis.

***Ex vivo* analysis of the conversion of [^{18}F]FEAnGA to [^{18}F]FEA by measurement of the release of HNBA.** Parts of the frozen excised tumors (0.21 ± 0.10 g, n= 32) were homogenized in 2 mL of PBS. The homogenates were centrifuged (10 min, 3000 rpm, 4 ^{o}C) and the supernatant was collected into new tubes containing 2 mL of cold acetonitrile to precipitate the remaining proteins. The samples were centrifuged once more (10 min, 3000 rpm, 4 ^{o}C) and 1.5 mL of the solution was then added into new tubes containing 1.5 ml of NaOH 0.25M. This final solution was taken for UV absorption (412 nm) analysis.

Flow cytometric analysis. Part of the frozen excised tumors (0.29 ± 0.12 g, n= 10, 2 tumors from each group) were transferred to 60 mm-diameter Petri dishes containing 1 mL of PBS. Tumor sections finely minced to generate cell suspensions. Cell suspensions were then filtered using nylon membranes (41 µm pores). The filtrate was centrifuged at 4

°C (1200 rpm for 5 min). The supernatant was removed and the pellet was washed with 1 mL of PBS. The suspension was centrifuged once again at 4 °C (1200 rpm for 5 min) and the supernatant was removed once again. The pellet was dissolved in 1 mL of PBS and divided in 5 equal parts of 200 µL. To each part, 2 µL (1:100) of a primary antibody was added: CD11b (expressed on the surface of many leukocytes involved in the innate immune system, including monocytes, granulocytes, macrophages, and natural killer cells), CD4 (expressed on the surface of T helper cells, regulatory T cells, monocytes, macrophages, and dendritic cells), CD8 (is predominantly expressed on the surface of cytotoxic T cells, but can also be found on natural killer cells, cortical thymocytes, and dendritic cells), CD33 (expressed on cells of myeloid lineage) and CD15 (expressed on the surface of neutrophils, eosinophils and monocytes), respectively. The cells were incubated on ice for 20 min. After this first incubation, 1 µL of a secondary antibody Alexa Fluor ®488 anti-mouse CD45 (Biolegend, San Diego, USA) was added to all of the samples. After an incubation of 20 min on ice, the cells were centrifuged, washed and ressuspended in 300 µl PBS. The flow cytometry analysis was performed using a FACscan system (BD FACSCalibur).

Histology of tumors. Part of the frozen excised tumors (0.29±0.12 g, n= 10, 2 tumors from each group) were cut serially in sections of 20 µm thickness with a Microtome Leica CM-3050-S Cryostat. Central sections of the tumor (containing a mixture of the rim and the necrotic core) were stained with hematoxylin and eosin using standard procedures and photographed with an Zeiss Axioskop 2 photomicroscope (Pictures with Leica Application Suite software (Leica DFC300FX camera)).

Statistical analysis. Statistical analyses were performed with Excel 2003 (Microsoft) and SigmaPlot (version 10.0; SPSS, Inc.). Differences in tracer accumulation between C6 tumors with and without necrosis were analyzed using the two-sided unpaired Students' *t*-test. Significance was reached when the p value was ≤ 0.05. Correlations were calculated with the linear regression algorithm in SigmaPlot and were considered statistically significant whenever $r^2 > 0.5$ and $p < 0.05$. Through out the manuscript values are presented as mean ± SEM.

RESULTS

***In vitro* induction of β-glucuronidase release with cytostatic agents.** We investigated whether β-glucuronidase release from tumor cells could be induced by treatment with cytostatic drugs. Thus, C6 glioma cells were exposed to DOX (1 μM), BCNU (20 μM), TNF-α (1500-3000 U/ml) for 24 h. At these concentrations, all drugs caused a significant reduction in viable cell number of approximately 25% (Fig. 2A). Extracellular β-glucuronidase activity in these cell cultures was measured by photospectroscopic analysis of the enzymatic conversion of the substrate p-nitrophenyl-β-D-glucuronide (PNPG). DOX, BCNU and TNF-α induced approximately a 2-fold increase in extracellular β-glucuronidase activity. There was a good inverse correlation between the number of cells remaining viable after treatment and the β-glucuronidase activity in the medium (Fig. 2B).

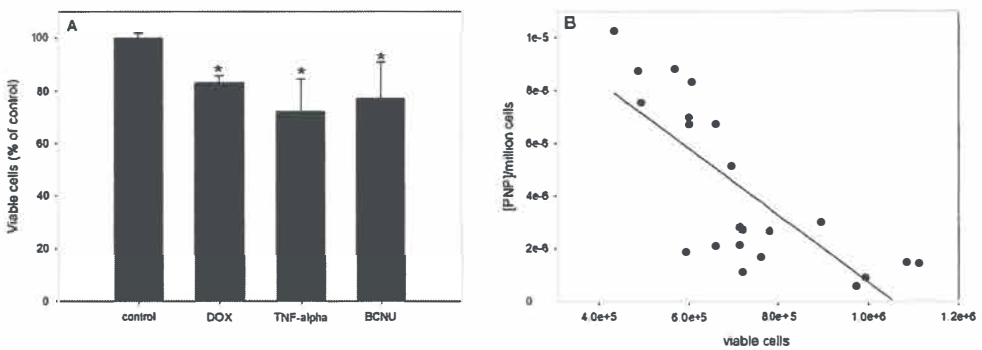

Figure2. A) Decrease in the viable cell number (compared to control) after 24 h of treatment. Data are plotted as mean ± SD. DOX= doxorubicin; TNF-α = tumor necrosis factor α; BCNU = carmustine. **B)** Correlation between β-glucuronidase activity in the medium and the number of viable cells 24 h after treatment. ($Y=1.3E-05 - 1.2E-11$, $r^2= 0.58$, $P< 0.0001$)

PET imaging and pharmacokinetic modeling in the C6 tumors. In the PET images, C6 gliomas were clearly visualized at 1 h post injection (Fig. 3) in treated and control rats. The time activity curves revealed different kinetics of [^{18}F]FEAnGA in tumors treated with BCNU when compared to the time activity curves of [^{18}F]FEAnGA in tumors treated with

DOX or untreated (control, i.p.). The accumulation of radioactivity in the viable part of all C6 tumor reached a maximum at 1.5 min post injection and afterwards decreased exponentially with a half-life of 47 ± 23 min, 27 ± 6 min and 19 ± 3, respectively. In addition, the area under the curve (AUC) of [^{18}F]FEAnGA in tumors treated with BCNU (30 ± 5, p< 0.02) was significantly higher than the AUC of [^{18}F]FEAnGA in control tumors (16 ± 1), while the AUC of [^{18}F]FEAnGA in tumors treated with DOX (18 ± 2, p= 0.27) was similar to the AUC of [^{18}F]FEAnGA in control tumors.

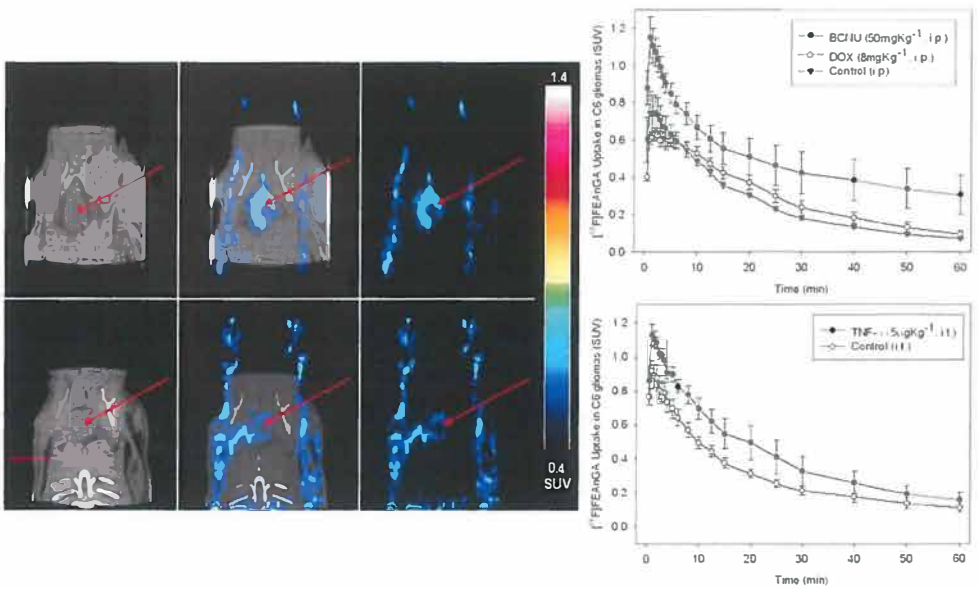

Figure 3. Coronal microCT image, microPET/CT fusion image and microPET image of a rat bearing a C6 glioma (Red arrow): treated with BCNU (top left side) and a Sham rat injected with PBS (Bottom left side). On the right side is presented the average of TACs of [^{18}F]FEAnGA in the C6 gliomas after each treatment.

The time activity curves of [^{18}F]FEAnGA in tumors treated intratumorally with TNF-α were found to be significantly higher at earlier time point (1.5-15 min), when compared to the TAC of [^{18}F]FEAnGA in tumors treated intratumorally with PBS (Control, i.t.). The accumulation of radioactivity of [^{18}F]FEAnGA in the viable part of the tumors

reached a maximum at 1.5 min post injection and afterwards decreased exponentially with a half-life of 22 ± 6 in TNF-α treated tumors and with a half-life of 14 ± 1 min in control tumors (p= 0.21). Furthermore, the area under the curve (AUC) of [^{18}F]FEAnGA in TNF-α (i.t.) treated tumors (27 ± 4) was 2 times higher than the AUC of [^{18}F]FEAnGA in control (i.t.) tumors (18 ± 2, p= 0.06). These TACs together with individual metabolite-corrected plasma radioactivity curve were used for pharmacokinetic modeling.

Logan graphical analysis was used for the pharmacokinetic modeling. From the Logan graphical analysis the distribution volume, DV_T, of [^{18}F]FEAnGA in C6 tumors treated with BCNU (0.83 ± 0.15) was found to be 70% higher than the distribution volume of [^{18}F]FEAnGA in control tumors (i.p., 0.48 ± 0.02, p= 0.044). The Logan distribution volume of [^{18}F]FEAnGA in C6 tumors treated either intraperitoneally with DOX (0.55 ± 0.02, p= 0.03) or intratumorally with TNF-α (0.65 ± 0.01, p= 0.045) was also significantly increased when compared with control tumors (0.48 ± 0.02 (i.p.); 0.50 ± 0.06 (i.t.)).

Biodistribution. The tracer uptake (SUV) in the excised tumors was found to be 0.08 ± 0.01 and 0.09 ± 0.01 in controls (i.p and i.t, respectively) and 0.11 ± 0.02; 0.30 ± 0.11; 0.13 ± 0.03, after treatment with DOX, BCNU and TNF-α, respectively. These values correlated well with the tracer uptake in the tumors obtained from the last 10 min of the scan (50-60 min) which were 0.07 ± 0.01 and 0.11 ± 0.02 in controls (i.p and i.t., respectively) and 0.09 ± 0.02; 0.31 ± 0.10; 0.17 ± 0.04, after treatment with DOX, BCNU and TNF-α, respectively. In addition, tumor size obtained in the biodistribution was in agreement with the PET results (Table 1). Significant difference was only reached in the tracer uptake obtained from the PET scan of tumors treated with BCNU when compared to control tumors (i.p.). At 48 h *post* dosing, tumors from DOX-treated animals were significantly smaller than the tumors of untreated control animals (p< 0.05). Two days after drug administration, BCNU-treated animals also had smaller tumors, whereas TNF-α treated animals had somewhat larger tumors, but these differences in tumor volume were not significantly different from controls.

Table1. Outcome parameters from PET/*ex vivo* analysis. * p< 0.05 when compared to controls. V_P=Partial volume (including only the viable part); V_T=Total volume (including the whole tumor); W_T= Total weigh; SUV= Standardize Uptake Value; BD=biodistribution; HNBA= released spacer (4-hydroxy-3-nitrobenzyl alcohol)

Parameters	Control (i.p.)	DOX (i.p.)	BCNU (i.p)	Control (i.t.)	TNF-α (i.t.)
V_P (PET; cm^3)	0.90±0.10	0.49±0.06*	0.67±0.08	0.49±0.09	0.59±0.11
V_T (PET; cm^3)	0.95±0.13	0.49±0.06*	0.73±0.10	0.49±0.09	0.67±0.10
W_T (BD; g)	0.94±0.12	0.43±0.05*	0.79±0.10	0.53±0.08	0.73±0.11
SUV (PET)	0.07±0.01	0.09±0.02	0.31±0.10*	0.11±0.02	0.17±0.04
SUV (BD)	0.08±0.01	0.11±0.02	0.30±0.11	0.09±0.01	0.13±0.04
DV_{Logan} ($mL.g^{-1}$)	0.48±0.02	0.55±0.02*	0.83±0.15*	0.50±0.06	0.65±0.01*
[HNBA]/mg tumor	0.28±0.03	0.30±0.05	0.60±0.14*	0.11±0.03	0.21±0.03*

Histology and flow cytometry analysis of the excised control and treated C6 tumors. Histological examination of the excised C6 tumors presented very distinct profiles in control and treated tumors. As depicted in figure 5, a tumor treated with TNF-α intratumorally (i.t.) presented a more disorganized cytoarchitecture when compared to the control tumor (i.t.). In addition, the tumor treated with TNF-α showed an area of necrosis accompanied by hemorrhagic vessels with low local inflammatory infiltrates.

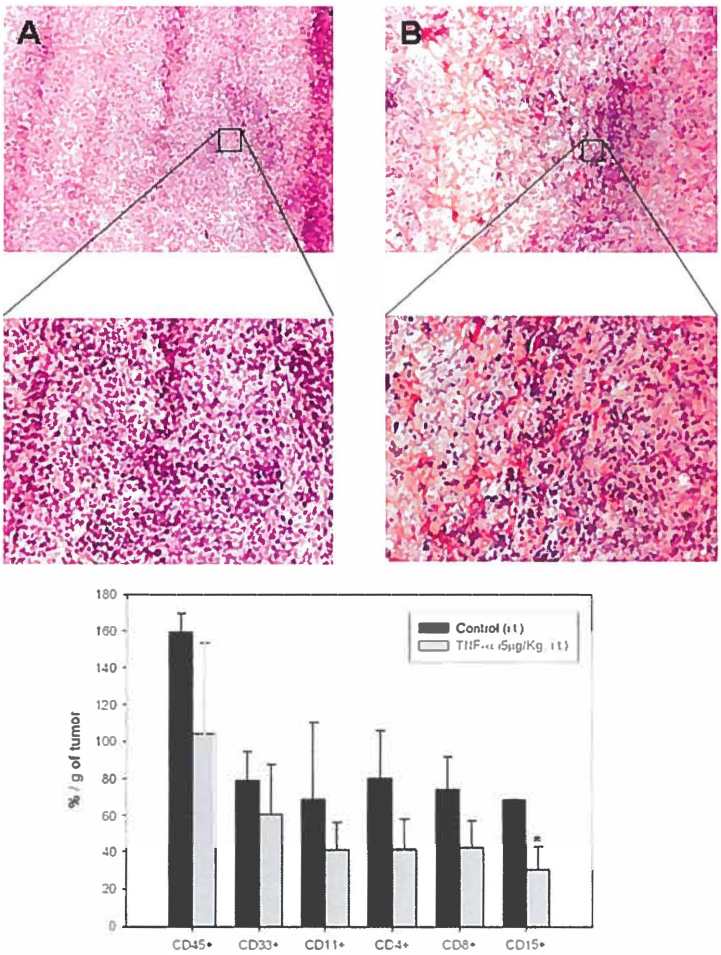

Figure 5. Histological section of: **A)** control (i.t) C6 tumor; **B)** TNF-α-treated C6 tumor, amplified 10× (Top) or amplified 20× (Middle). Flow cytometry analysis (Bottom). Data are plotted as % of marker/g of tumor ± SEM. *p< 0.05 when compared to controls

The tumors that were treated intraperitonealy with PBS, DOX or BCNU also exhibit different morphologies (Fig. 6). The control tumor which was treated with PBS showed a more organized cytoarchitecture with only occasional neutrophils at the margins of the tumor vessels. In comparison, a tumor treated with DOX presented some necrotic regions with a high amount of hemorrhagic vessels. These disrupted vessels also

included neutrophils immediately surrounding the vessels and occasionally in perivascular glioma tissue. In contrast, a tumor treated with BCNU presented a high central tumor necrosis with indefinite or absente cell margins or clear damage to the cytoplasmic membrane. In addition, no evidence of macrophage or polymorphonuclear infiltration was seen.

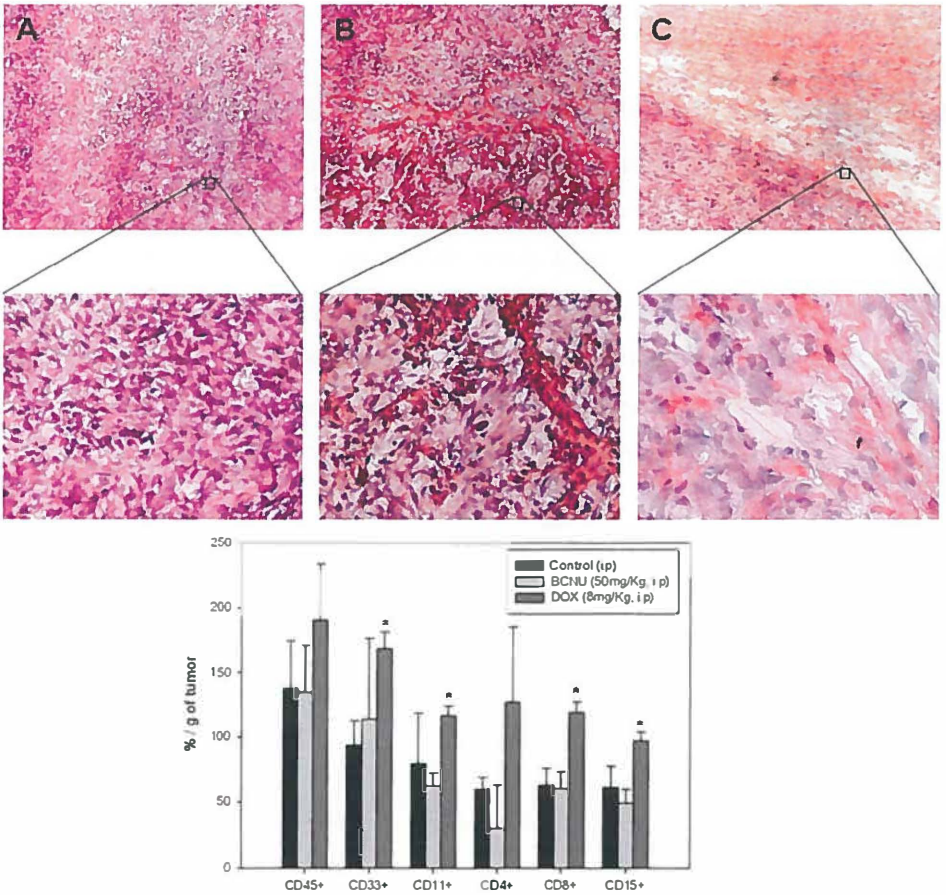

Figure 6. Histological section of: **A)** control (i.p) C6 tumor; **B)** Dox-treated C6 tumor and **C)** BCNU-treated C6 tumor, amplified 10× (Top) or amplified 40× (Middle). Flow cytometry analysis (Bottom). Data are plotted as % of marker/g of tumor ± SEM. *p< 0.05 when compared to controls

PET imaging and pharmacokinetic modeling in heart, liver and thymus. Treatment with cytostatics or cytokines often induces additional toxicity due to the lack of selectivity towards tumor cells. Thus, PET analysis was performed in potential target organs such as heart and liver, which are likely to be affected. We also performed a PET analysis of the thymus in intraperitoneally treated (DOX and BCNU) and control rats, since several reports indicate that chemotherapeutics may also cause hyperplasia of the thymus. Since the distribution volume of [^{18}F]FEAnGA is the parameter which best describes β-glucuronidase activity, we performed a graphical Logan analysis in heart, liver and thymus. There were no significant differences in the distribution volume of the PET tracer in the heart of treated animals when compared to control animals. Although no significant differences in [^{18}F]FEAnGA distribution volume in the liver of treated animals compared to control animals were observed, a different pharmacokinetic profile of the tracer in the livers of rats treated with BCNU was evident (Fig. 7). Interestingly, the DV_{Logan} of [^{18}F]FEAnGA in the thymus of DOX treated animals was found to be significantly different (+65%), when compared to control animals (Table 2).

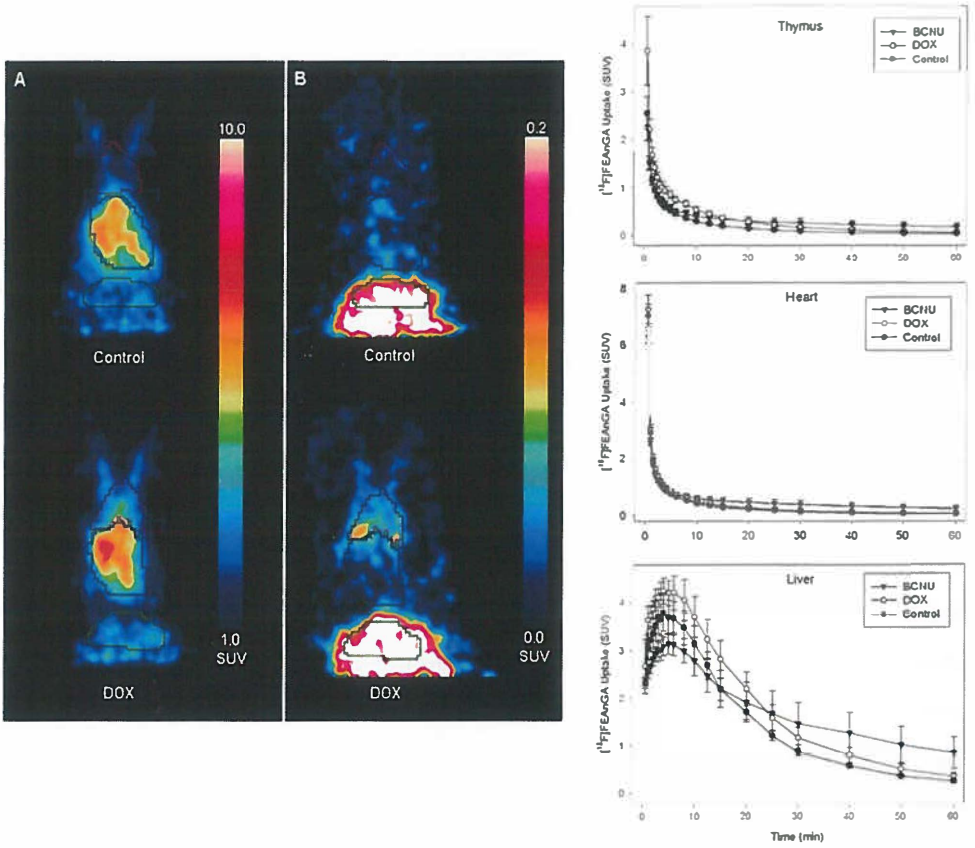

Figure 7. Coronal microPET image of a control (Top left side) and a DOX treated animal (Bottom left side) injected with [^{18}F]FEAnGA: **A)** 1 min post injection; **B)** 40-60 min post injection. [^{18}F]FEAnGA TACs of [^{18}F]FEAnGA uptake (SUV) in the thymus, heart and liver (Right side)

Table 2. Distribution volumes of [^{18}F]FEAnGA in different organs obtained with graphical Logan analysis. * p< 0.05 when compared to controls.

DV_{Logan}	Control (i.p)	DOX	BCNU
Heart	0.56 ± 0.05	0.64 ± 0.09	0.77 ± 0.35
Liver	2.57 ± 0.70	3.32 ± 1.22	2.78 ± 1.74
Thymus	0.35 ± 0.07	0.58 ± 0.08*	0.49 ± 0.17

DISCUSSION

β-Glucuronidase (β-GUS) has been investigated as a target in prodrug therapy for cancer [1]. One of the drawbacks of this approach is that especially small tumors have only relatively low concentrations of extracellular β-GUS. We hypothesized that the efficacy of prodrug treatment can be improved if the extracellular β-GUS levels can be increased prior to prodrug treatment, by for example inducing tumor necrosis and leukocyte infiltration. Thus, the aim of our study was to evaluate the extent and progression of β-GUS release in small C6 glioma tumors after a single treatment of Doxorubicin (DOX), Carmustine (BCNU) and Tumor Necrosis Factor α (TNF-α) with the PET tracer for β-GUS, [^{18}F]FEAnGA [8].

In our *in vitro* study, where C6 glioma cells were incubated with DOX (1 μM), BCNU (20 μM) and TNF-α (1500-3000U), a reduction of approximately 25% in the number of viable cells was found after 24 h of treatment, which is in agreement with the values reported in the literature [9-11]. In addition, there was a good inverse correlation between the number of viable cells and the β-glucuronidase activity in the medium. This correlation was to be expected, since the interventions - through different pathways- cause cell death of a fraction of tumor cells, leading to an increase in β-GUS release. These encouraging *in vitro* results prompted us to perform an *in vivo* study, using [^{18}F]FEAnGA PET to evaluate whether a single treatment with a cytostatic drug could increase the release of β-GUS in the C6 glioma.

Intratumoral treatment with TNF-α

The present PET study, showed that TNF-α (i.t.) treated tumors in male Wistar rats have a higher peak uptake of [^{18}F]FEAnGA-derived radioactivity (SUV_{Max} 20% higher) than control (i.t.) tumors, suggesting increased perfusion in these TNF-α treated tumors. This result is in agreement with the study by Kallinowski and Vaupel, who showed that tumors treated with doses of TNF-α lower than 0.1mg/kg (6.6×10^6 U/mg) show increased perfusion [12].

Histological and flow cytometry analysis indicated a central tumor necrosis with no local inflammatory infiltrates in TNF-α treated tumors. Earlier reports indicated that TNF-α 's proinflammatory effects occur at early time points (within 12 hours after a single

i.t. dose of TNF-α, therefore the absence of inflammatory infiltrates 48 h after the treatment is no surprise [13]. However, the distribution volume of [^{18}F]FEAnGA and its conversion to the spacer HNBA and [^{18}F]FEA (2 parameters related to β-GUS activity) were found to be significantly higher in tumors treated with TNF-α (i.t.) compared to control tumors (i.t.). This increase in β-GUS activity can be ascribed to the release of the enzyme into the extracellular space by the necrotic cells observed in the tumor core. An alternative explanation could be that after administration of low doses of TNF-α, the cytokine binds to specific receptors on the target cell membrane, leading to stimulation in the production of Reactive Oxygen Species (ROS) [10;14]. These intracellular hydroxyl radicals lead to an increase in β-GUS activity inside the lysosomes as well release of the enzyme into the cytoplasm and subsequently into the extracellular space [10].

Intraperitoneal treatment with DOX and BCNU

The kinetics of [^{18}F]FEAnGA suggest a much higher perfusion in BCNU-treated tumors than in controls, which is in agreement the earlier published data [15]. Moreover, the plasma clearance half-life of the tracer is 2.8 times higher in BNCU treated animals ($t_{1/2}$= 18 ± 8 min) than in control ($t_{1/2}$= 7 ± 1 min) or DOX treated animal ($t_{1/2}$= 6 ± 2 min). The increased plasma half-life was accompanied by a higher conversion of [^{18}F]FEAnGA to [^{18}F]FEA in the plasma in BCNU treated animals than in controls or animals treated with DOX. At 60 min post injection, the percentage of intact tracer was 45 ± 11%, 65 ± 8% and 84 ± 5% for BCNU-treated, DOX-treated and control animals, respectively (data not shown). BCNU is known to be able to cause cholestitis within the first 48 hours after administration of the drug. Cholestitis leads to enhancement of the release of β-GUS in the bile and ultimately to elevated levels of β-GUS in the plasma, which could explain the observed elevated hydrolysis rate of [^{18}F]FEAnGA and consequently the increase plasma half-life.

This is a classic example where the standardized uptake value should not be used, since it does not correct for the activity in plasma and thus not for tracer delivery to the tissue. This could lead to a wrong interpretation of the data when comparing the tracer in different conditions. Thus, we also explored quantification of [^{18}F]FEAnGA uptake by

pharmacokinetic modeling to determine the distribution volume of [^{18}F]FEAnGA using plasma input on different time points during the scan. The distribution volume of [^{18}F]FEAnGA in C6 gliomas treated with BCNU was found to be 70% higher than in control (i.p.) animals, while the conversion of [^{18}F]FEAnGA to HNBA and [^{18}F]FEA by β-GUS was 2.2 times higher.

The PET study showed that the TACs of [^{18}F]FEAnGA observed in DOX (i.p.) treated tumors had a lower peak uptake (SUV_{Max} -33%) when compared to control (i.p.) tumors, suggesting a reduction in the tumor blood flow. This result is in line with the observation that anthracycline treatment reduces perfusion in rodent tumors [16;17]. Nevertheless, tumor uptake of [^{18}F]FEAnGA at 60 min post injection was increased by about 30%, 48 h after administration of DOX. In addition, the distribution volume of [^{18}F]FEAnGA obtained from the Logan graphic analysis and its conversion to HNBA and [^{18}F]FEA by β-GUS (2 parameters to describe β-GUS activity) was found to be 10% higher in DOX treated tumors than in control tumors. Interestingly, our previous studies in doxorubicin treated rats showed a decline in [^{18}F]FDG uptake in C6 tumors of circa 30% 48 h after the treatment [7]. This decline in [^{18}F]FDG uptake was attributed to the reduction of proliferating cells within the tumor and an increase in the fraction of the total tumor volume that was necrotic after chemotherapy. The combination of these results suggests that the increase of [^{18}F]FEAnGA uptake in C6 tumors treated with DOX is related to the increase of necrotic areas which consequently releases more β-GUS.

On the other hand, flow cytometry analysis of the DOX treated tumors showed an immune response within the tumors. Besides being a cell proliferation inhibitor by intercalation with DNA, DOX can also provoke tumor infiltration of leukocytes via stimulation of inflammatory cytokines production [18-20]. Recently, it has been shown that DOX promoted the Th1-dominant cytokine response in rats treated with a single dose of the drug. The Th1 response is closely linked with macrophage-mediated immunity [21]. DOX treatment stimulated macrophages to increase their tumoricidal activity. The release of β-GUS in the tumor after DOX treatment is therefore likely also mediated by infiltrating leukocytes [2].

Despite the high doses of cytostatics given to the rats, animal mortality did not occur. Although the animals were terminated only 48 h after the treatment, the high doses of Doxorubicin and BCNU administered intraperitoneally could raise additional toxicity in the heart, liver or even thymus. However, there were no significant differences in [^{18}F]FEAnGA distribution volume in livers and hearts of animals treated with either BNCU or DOX, when compared with controls. This absence in difference of [^{18}F]FEAnGA uptake or DV_{Logan} in the hearts of DOX treated animals is in agreement with previous studies, where the mortality related to DOX cardiotoxicity was only encountered 6 weeks after the DOX treatment [7]. Surprisingly, the distribution volume of [^{18}F]FEAnGA in thymus of DOX treated animals was significantly different from the distribution volume of [^{18}F]FEAnGA in thymus of control animals. Sultana *et al.* recently described that doxorubicin leads to degeneration of the thymus [23] in mice 48h after treatment. This group found that DOX-treated thymus showed a decrease in lymphopoiesis, cortical thymocytes and an increased in Hassall's corpuscles (HC) that may play a role in the appearance of natural regulatory T-cells in human thymic medulla, suggesting that increase of HC in the DOX treated thymus could be considered as an augmentation of protective mechanisms to attempt to avoid further DOX-induced toxicity. The HC are also involved in the clearance of the dead cells. Enlarged HC contain non specific esterase, acid phosphatase and β-glucuronidase [24;25], thus during the acute involution of the thymus induced by DOX, enlarged HC are completely destroyed, and the respective enzymes released. This could explain the fact that β-GUS-selective PET tracer was able to detect the early senescence of the thymus.

CONCLUSION

Taken together, this study shows an increase in β-GUS activity in C6 gliomas in all treatment groups. These preliminary results provide a proof of principle that a single dose of cytostatic can increase the release of β-GUS and that [^{18}F]FEAnGA is a suitable PET tracer to monitor this process. This study may open the way to a two-step chemotherapy-prodrug approach, in which tumors are treated with a single dose of a cytostatic before prodrug treatment.

ACKNOWLEDGMENTS

We gratefully thank Dr. Hetty Timmer for providing the TNF-α and for all the advice given during this study. We also gratefully thank Daniele Faria and Adilson Ferreira for all the help in the histological and flow cytometry analysis.

REFERENCES

1. De GM, Boven E, Scheeren HW, Haisma HJ, and Pinedo HM (2002) Curr. Pharm. Des 8:1391-1403.
2. Bosslet K, Straub R, Blumrich M, Czech J, Gerken M, Sperker B, Kroemer HK, Gesson JP, Koch M, and Monneret C (1998) Cancer Res. 58:1195-1201.
3. Houba PH, Boven E, van der Meulen-Muileman IH, Leenders RG, Scheeren JW, Pinedo HM, and Haisma HJ (2001) Br. J. Cancer 84:550-557.
4. Prijovich ZM, Chen BM, Leu YL, Chern JW, and Roffler SR (2002) Br. J. Cancer 86:1634-1638.
5. De Graaf M, Pinedo HM, Oosterhoff D, van der Meulen-Muileman IH, Gerritsen WR, Haisma HJ, and Boven E (2004) Hum. Gene Ther. 15:229-238.
6. Juan TY, Roffler SR, Hou HS, Huang SM, Chen KC, Leu YL, Prijovich ZM, Yu CP, Wu CC, Sun GH, and Cha TL (2009) Clin. Cancer Res. 15:4600-4611.
7. Van Waarde A, Shiba K, de Jong JR, Ishiwata K, Dierckx RA, and Elsinga PH (2007) J. Nucl. Med. 48:1320-1326.
8. Antunes IF, Haisma HJ, Elsinga PH, Dierckx RA, and de Vries EF (2010) Bioconjug. Chem. 21:911-920.
9. Van Waarde A, Been LB, Ishiwata K, Dierckx RA, and Elsinga PH (2006) J. Nucl. Med. 47:1538-1545.
10. Watanabe N, Yamauchi N, Neda H, Maeda M, Tsuji Y, Okamoto T, Akiyama S, Sasaki H, Tsuji N, and Niitsu Y (1992) Jpn. J. Cancer Res. 83:638-643.
11. Yang J, Yang JM, Iannone M, Shih WJ, Lin Y, and Hait WN (2001) Cancer Res. 61:4010-4016.
12. Kallinowski F, Schaefer C, Tyler G, and Vaupel P (1989) Br. J. Cancer 60:555-560.
13. Wright JL and Merchant RE (1997) Acta Neuropathol. 93:78-86.
14. Bilenko MV, Khil'chenko AV, and Shmit'ko NA (2003) Bull. Exp. Biol. Med. 135:349-352.
15. Steen RG and Graham MM (1991) NMR Biomed. 4:117-124.
16. Denis F, Colas S, Chami L, Louisot P, Le Floch O, Tranquart F, and Bougnoux P (2003) Clin. Cancer Res. 9:4546-4552.
17. Durand RE and LePard NE (1997) Radiother. Oncol. 42:171-179.
18. Ujhazy P, Zaleskis G, Mihich E, Ehrke MJ, and Berleth ES (2003) Cancer Immunol. Immunother. 52:463-472.
19. Orsini FR and Henderson ES (1980) Immunopharmacology 2:375-384.
20. Casares N, Pequignot MO, Tesniere A, Ghiringhelli F, Roux S, Chaput N, Schmitt E, Hamai A, Hervas-Stubbs S, Obeid M, Coutant F, Metivier D, Pichard E, Aucouturier P, Pierron G, Garrido C, Zitvogel L, and Kroemer G (2005) J. Exp. Med. 202:1691-1701.

21. Santos RV, Caperuto EC, de Mello MT, and Rosa LF (2010) Biomed. Pharmacother. 64:579-581.
22. Stolzenbach JC and Larson RE (1990) Cancer Chemother. Pharmacol. 25:227-235.
23. Sultana R, Di Domenico F, Tseng M, Cai J, Noel T, Chelvarajan RL, Pierce WD, Cini C, Bondada S, St Clair DK, and Butterfield DA (2010) J. Proteome. Res. 9:6232-6241.
24. Kotani M and Nawa Y (1991) Arch. Histol. Cytol. 54:551-557.
25. Nakagawa S, Dvorkin B, and White A (1968) Yale J. Biol. Med. 41:120-132.

Chapter

Summary

β-Glucuronidase is a lysosomal enzyme that might be explored in the treatment of several diseases. Especially in those where β-glucuronidase is upregulated in inflammatory lesions (either due to inflammation or infection) or necrotic lesions of large solid tumors. In these pathological conditions, β-glucuronidase-mediated prodrug therapy could be applied. Over the past decades, preclinical studies have shown exciting results, especially for the treatment of cancer, where the treatment with cytostatics is hindered by serious side-effects which can be either by the lack of selectivity or acquired resistance.

Glucuronide-conjugates are substrates for β-glucuronidase, thus they can be used as prodrugs for β-glucuronidase-based prodrug therapy. These prodrug therapy strategies are based on selective activation of the prodrug by the higher β-glucuronidase activity in tumor/inflammatory lesions, called Prodrug monotherapy. The efficacy of glucuronide prodrugs can be further improved by combined use of the prodrugs with a tumor-specific antibody (called Antibody-directed enzyme prodrug therapy, ADEPT) or by transfection of the tumor cells with a gene encoding the desired exogenous enzyme (called Gene-directed enzyme prodrug therapy, GDEPT). Despite the appealing concept of prodrug therapy and the encouraging preclinical results, each of these different strategies has its disadvantages and therefore, the quest for a clinical applicable strategy is continuing. For such specific strategies, knowledge of the expression levels and the distribution of the prodrug-converting enzyme is vital. Therefore non-invasive imaging techniques like positron emission tomography (PET) can be attractive tools to evaluate new enzyme-prodrug combinations and to optimize treatment strategies. Thus, the aim of this thesis was to develop PET tracers for monitoring extracellular β-glucuronidase activity in different disease models, with the intention to use this non-invasive method to support the optimization of β-glucuronidase-mediated prodrug therapy.

In chapter 2, the knowledge of the expression of β-glucuronidase in different diseases is reviewed. In addition, the use of β-glucuronidase as a target for therapy is addressed and an overview of the glucuronide-conjugates used for prodrug therapy in cancer is given. Furthermore, the use of glucuronide-conjugates in inflammatory pathologies such as rheumatoid arthritis and neuroinflammation is also included. From

this study we concluded that glucuronide-conjugates might not only be used for prodrug therapy in cancer but also in inflammation.

When prodrug therapy is based on elevated activity of β-glucuronidase at the target site, the localization and magnitude of expression of β-glucuronidase, are probably the most important factors modulating the target-specificity of the release of the active drug from the glucuronide prodrug. The variability in the activity of β-glucuronidase in different human tissues is high. Thus, the development of non-invasive clinically applicable technologies to monitor and evaluate β-glucuronidase based prodrug therapy has become desirable. A technique that seems especially suited for imaging β-glucuronidase expression is PET. In chapter 3, a brief overview of the reporter probes (tracers) developed for imaging gene/enzyme prodrug systems is given. It was found that most of the PET tracers were developed for monitoring the herpes simplex virus type 1 thymidine kinase (HSVtk)/ganciclovir (GCV), GDEPT system. However at the start of this project PET tracers for monitoring β-glucuronidase activity in either the two steps therapy ADEPT and GDEPT or in monotherapy were still lacking.

Therefore we synthesized a new PET tracer to evaluate extracellular of β-glucuronidase called 1-O-(4-(2-fluoroethyl-carbamoyloxymethyl)-2-nitrophenyl)-O-β-D-glucopyronuronate ([^{18}F]FEAnGA) (Chapter 4). This tracer is a glucuronide-conjugate with a similar structure of the well known prodrug HMR 1826. The main difference is that the active drug doxorubicin was replaced with a radioactive moiety, [^{18}F]fluoroethylamine ([^{18}F]FEA. Kinetic studies indicate that [^{18}F]FEAnGA is a good substrate for E. coli β-GUS and bovine liver β-GUS. Thus, [^{18}F]FEAnGA was first tested *in vitro* and *in vivo* in CT26 adenocarcinoma cells and the CT26mβGUS transfected cells which express membrane-anchored β-GUS on the outer cell membrane. Both *in vitro* and *in vivo* studies indicated an increase tracer uptake in the CT26mβGUS cells/tumors than in the normal CT26 cells/ tumors. This increased uptake was further related to the higher conversion of [^{18}F]FEAnGA to [^{18}F]FEA by the extracellular β-glucuronidase present in CT26mβGUS, indicating that [^{18}F]FEAnGA could be a promising PET tracer for imaging of extracellular β-glucuronidase

activity. In addition, it was also found a high conversion of [^{18}F]FEAnGA to [^{18}F]FEA in big necrotic CT26 tumors, which was ascribed to the released β-GUS in necrotic regions.

To prove our previous hypothesis, we tested whether [^{18}F]FEAnGA could detect differences in expression of β-glucuronidase in an animal model with tumors of different sizes and a sterile inflammation (tumor vs inflammation) in chapter 5. In this rat tumor-inflammation model [^{18}F]FEAnGA uptake was found to be significantly higher in big necrotic tumors (V_T>1.5cm^3) than in small tumors (V_T<1.5 cm^3). The distribution volume of [^{18}F]FEAnGA in the viable part of the tumors was also significantly higher than the distribution volume of [^{18}F]FEAnGA in the viable part of small tumors. In addition, the distribution volume of [^{18}F]FEAnGA correlated well with the cleavage of [^{18}F]FEAnGA to [^{18}F]FEA, indicating that the distribution volume of [^{18}F]FEAnGA seems to be a suitable parameter to evaluate β-glucuronidase activity. In this experiment, [^{18}F]FEAnGA uptake was found to be significantly higher in inflamed muscle than in healthy muscle.

Because [^{18}F]FEAnGA exhibited rapid renal clearance, which resulted in a relatively low tracer uptake in the tumor, we aimed to improve the pharmacokinetic properties of the PET tracers. To this purpose, the more lipophilic methyl ester analog of [^{18}F]FEAnGA, called [^{18}F]FEAnGA-Me, was synthesized and evaluated in chapter 6. [^{18}F]FEAnGA-Me was anticipated to remain longer in plasma than [^{18}F]FEAnGA and consequently its delivery to the tumor and retention in the tumor was expected to be increased, which should result in better PET images. [^{18}F]FEAnGA-Me is activated in two steps. First the ester moiety is hydrolyzed by esterases in plasma, subsequently the prodrug was activated by extracellular β-glucuronidase in the target tissue. [^{18}F]FEAnGA-Me was proven able to detect β-glucuronidase activity. However, [^{18}F]FEAnGA-Me did not have superior properties over [^{18}F]FEAnGA. Therefore, other strategies should be applied in order to improve the kinetics of these tracers.

In inflammation, β-glucuronidase is known to be released from granulocytes, including neutrophils that are highly present at the sites of inflammation. Also in the brain increased levels of extracellular β-glucuronidase are present during neuroinflammation. For example, elevated levels of β-glucuronidase have been reported in the temporal

cortex of Alzheimer's disease patients and the putamen of patients with Huntington's disease. Thus, in chapter 7 the feasibility of [^{18}F]FEAnGA for detecting β-glucuronidase activity in neuroinflammation was explored. To this purpose, rats were intranasally infected with the HSV-1 virus. This rat model of herpes encephalitis better mimics neurological disorders than models, in which a toxic substance is injected into the brain, since it does not involve invasive manipulations, but induces microglia cell activation via a biological process. Our results indicated that the distribution volume of [^{18}F]FEAnGA was enhanced in the whole brain of HSV-1 infected rats, as compared to uninfected rats. *Ex vivo* β-glucuronidase analysis of cerebellum and brainstem showed an enhancement of the enzyme activity and the conversion of the PET tracer [^{18}F]FEAnGA to the corresponding [^{18}F]FEA in these areas. The correlation of the distribution volume of [^{18}F]FEAnGA with the enhancement of β-glucuronidase activity and conversion of the tracer suggested that the distribution volume of [^{18}F]FEAnGA reflects β-glucuronidase activity. In addition, distribution volume of [^{18}F]FEAnGA in rats inoculated with HSV-1 virus on day 7 correlated better with the [^{11}C]-*(R)*-PK11195 uptake (a tracer for activated microglia) in infected rats at day 5 rather than at day 7, suggesting that β-glucuronidase activity is enhanced as a result of microglia activation, rather than an inducer of microglia activation.

One of the potential disadvantages of β-glucuronidase-based prodrug monotherapy is the insufficient prodrug-converting enzyme (β-glucuronidase) activity, especially in small tumors. In order to improve the efficacy of β-GUS-mediated prodrug therapy, investigators have searched for ways to increase the concentration of target enzyme in the tumor, which should result in more efficient conversion of the prodrug. Augmentation of the enzyme concentration inside the tumor can be achieved by transfection of the β-GUS gene in tumor models, by conjugation of the enzyme to an antibody (fragment) that is directed to a tumor-specific antigen or even by stimulation of infiltration of innate immune cells. We hypothesized that a single dose of a cytostatic drug or cytokine might increase the release of β-GUS in small tumors. Thus, in chapter 8 the extend of β-GUS release in small C6 glioma tumors after a single treatment of Doxorubicin

(DOX), Carmustine (BCNU) and Tumor Necrosis Factor α (TNF-α) was examined with our PET tracer for β-GUS, [^{18}F]FEAnGA. Our results indicated that the distribution volume of [^{18}F]-FEAnGA in C6 gliomas increased significantly by 10 – 70% depending on the treatment, proving that a single dose of a cytokine or a cytostatic agent was able to increase the release of β-GUS. This study may open the way to a two-step chemotherapy-prodrug approach, in which tumors are treated with a single dose of a cytostatic drug before prodrug treatment.

Although [^{18}F]FEAnGA does not have the ideal properties of a PET tracer, it was able to selectively detect extracellular β-glucuronidase activity and therefore, it could provide a better understanding regarding β-glucuronidase activity in different disease models and could be used for treatment assessment. Therefore, we may now have a non-invasive technique that can provide crucial information regarding β-glucuronidase expression and prodrug pharmacology. This could lead to a better understanding of the mechanisms of action and metabolic conversion of the prodrug and therefore could be an impetus for the development of new prodrug therapies.

Chapter

Future perspectives

The studies that were described in this thesis have shown that our new PET tracer [^{18}F]FEAnGA was able to monitor β-glucuronidase activity in different pathologies. In addition, this tracer could be useful to facilitate the implementation of new β-glucuronidase-based prodrug treatment strategies. These promising results encourage further research to investigate the potential of this β-glucuronidase activity imaging in different areas.

PET tracer for β-glucuronidase

In this thesis we were able to develop a PET tracer, [^{18}F]FEAnGA to evaluate extracellular β-glucuronidase activity. In chapter 5 we demonstrated that in large necrotic tumors the distribution volume of [^{18}F]FEAnGA corresponded with extracellular β-glucuronidase activity, However, being a glucuronide conjugate, this tracer was rapidly eliminated and, as a result, relatively low uptake in the target areas was obtained. Improvement of the pharmacokinetics of this tracer would allow higher uptake in the target areas and therefore a better tumor-to-backgound ratio. There was an attempt to develop a more lipophilic tracer, [^{18}F]FEAnGA-Me by transforming the glucuronic acid into its methyl ester in order to increase the circulation half-life of the tracer (Chapter 6). However, not only the circulation half-life did not increase (due to the rapid demethylation), but the specificity towards the enzyme was also reduced. Therefore, different strategies should be explored to improve the kinetics of these tracers. One promising strategy would be to accelerate the release of the radioactive moiety from the PET tracer at the target site by increasing the rate of enzymatic conversion of the tracer. It has been hypothesized that glucuronide prodrugs with elongated spacers could decrease steric hindrance to a larger extent than conventional spacers due to the enlarged spacing between the parent drug and the glucuronic acid. In fact, doxorubicin prodrugs with an elongated spacer showed major improvement of enzymatic activation rate (2 to 3 fold higher, when compared with the single spacer) [1]. Thus, by applying a similar spacer in [^{18}F]FEAnGA, its kinetics might be improved, which could even allow sufficient trapping of the tracer in tissues with low levels of extracellular β-glucuronidase, like small tumors.

In this thesis it was also found that the radioactive moiety, [^{18}F]fluoroethylamine is reversibly bounded to the membrane of surrounding cells at the target site. Therefore, another strategy to increase the uptake of the tracer at the target site would be the use of more lipophilic radioactive moieties to improve the retention of the radioactive probe in the tumors. Nevertheless, this strategy might also influence the selectivity of the tracer due to non-specific binding.

On the other hand, imaging of enzymes can be achieved either by the use of a labeled substrate whose product is metabolically trapped at the site of catalysis (such as [^{18}F]FEAnGA) or by the use of a labeled enzyme inhibitor that binds to the enzyme either covalently or non-covalently with relatively slow dissociation. Thus, one could speculate the use of a radiolabeled β-glucuronidase inhibitor for imaging β-glucuronidase that would be independent of the enzymatic activation rate. However, using an inhibitor as a PET tracer for β-glucuronidase would only provide information regarding its expression and not its activity. Therefore this last strategy should not be attempted. Moreover, the enzyme can bind only one inhibitor molecule per protein molecule, whereas it can convert many substrate molecules during the imaging experiment, which leads to signal amplification. Theoretically, a substrate derived PET tracer would therefore be more sensitive than an inhibitor derived tracer.

Disease models

In this thesis, we were able to prove that in both tumor models (CT26 and C6) the uptake or distribution volume of [^{18}F]FEAnGA was increased due to the conversion of the glucuronide tracer to the radioactive product [^{18}F]fluoroethylamine. Nevertheless, this PET tracer should be further tested in more tumor types to confirm its validity. In addition, we do think that in future studies immunohistochemical assays should be performed in order to correlate the uptake of the tracer with the presence of the enzyme.

An important finding in this thesis was that [^{18}F]FEAnGA could also be used in inflammatory lesions confirming Shimoi's earlier reports, where it was suggested that β-glucuronidase released from neutrophils or certain injured cells may hydrolyze

glucuronide conjugates to free aglycones at the site of inflammation [2]. Thus, further studies with [^{18}F]FEAnGA in inflammarory models such a rheumatoid arthritis might give new perspectives regarding the use of glucuronide prodrugs in the treatment of inflammatory diseases.

In addition, in chapter 7 β-glucuronidase activity was found in the brain areas where also microglia activation was found. However, it seems that expression of β-glucuronidase follows activation of microglia cells, suggesting that β-glucuronidase is more involved in the neurodegenerative process than in the activation of microglia. To get a better understanding of the relation between microglia activation and β-glucuronidase activity, future longitudinal studies should be performed, namely by using simultaneously [^{11}C]-*(R)*-PK11195 and [^{18}F]FEAnGA in the same animal, followed by immunohistochemistry of activated microglia and β-glucuronidase. In this way we might be a step closer to understand the mechanism and mediators by which microglia can lead to neurodegeneration.

Prodrug treatment evaluation

As mentioned above, a potential limitation of glucuronide prodrugs in monotherapy is that they are not activated homogenously throughout the tumor tissue, but only at the site of necrosis and inflammatory cell infiltration. In addition, small tumors (1-1.5 g in C6 tumors) do not yet contain necrotic areas. The efficacy of prodrug monotherapy could be increased by induction of β-glucuronidase activity. Possible ways to achieve higher extracellular enzyme concentration might be the reduction of the pH in the tumor areas by local hyperthermia and glucose injection or by the induction of necrosis with radiotherapy. Alternatively, two-steps approaches, such as ADEPT and GDEPT, could be employed fur further increase of the levels of the enzyme in the tumor. However in ADEPT and GDEPT approaches where the exogenous enzyme is either delivered to the tumor or generated in the tumor cells is usually limited by immunogenicity and heterogeneous expression of the enzyme at the target site. Perhaps the most important finding in this thesis was the introduction of a possible new two-step strategy to improve

the efficacy in prodrug therapy. We hypothesized that in the first step of this two-step strategy a single dose of a certain cytostatic drug or cytokine should be given in order to increase the levels of extracellular β-glucuronidase at the target site. After the release of β-glucuronidase into the extracellular domain, the relatively non-toxic prodrug is administered in the second step. By the use of the PET tracer, we were able to see which cytostatic drug produced the highest release of β-glucuronidase in small C6 tumors. Now, further research should be performed to investigate whether the animals that showed increased levels of extracellular β-glucuronidase at the tumor, after a single dose of cytostatic drug benefit in the prodrug therapy. In addition, it should be investigated whether the total adverse effects of this two-step strategy are indeed less than for conventional chemotherapy. However, precautions in interpreting these results are required. Different tumors have different properties, thus a single dose of a certain cytostatic drug might give a different outcome in a different tumor. Therefore, the application of this two-step strategy in different tumor models is warranted. In this respect, the use of PET with a β-glucuronidase specific tracer could be very helpful. When successful in animals, the two-step chemotherapy-prodrug treatment concept proposed in this thesis might be translated to the clinic.

REFERENCES

1. De Groot FMH, Loos WJ, Koekkoek R, van Berkom LWA, Busscher GF, Seelen AE, Albrecht C, de Bruijn P, and Scheeren HW (2001) Journal of Organic Chemistry 66:8815-8830.
2. Shimoi K and Nakayama T (2005) Methods Enzymol. 400:263-272.

Samenvatting

Resumo

SAMENVATTING

Een belangrijke uitdaging voor het vinden van een effectieve behandeling van kanker of bepaalde ontstekingsziekten is het uitroeien van de ziekte zonder schade aan te brengen aan gezonde weefsels van de patiënt. Het gebrek aan effectiviteit van behandelingen is vaak te wijten aan de fysiologische overeenkomsten tussen gezonde cellen en aangedane cellen, waardoor de selectieve therapeutische werking van cytotoxische geneesmiddelen in uitsluitend de zieke cellen niet mogelijk is. Met dit probleem in gedachte werd een nieuw concept ontwikkeld, genaamd prodrug therapie, waarbij het geneesmiddel wordt gemodificeerd tot een minder reactieve of een minder cytotoxische prodrug. De prodrug kan weer worden omgezet in het actieve geneesmiddel door een enzym dat alleen in het beoogde weefsel (zieke cellen) in hoge concentraties voorkomt. Het enzym β-glucuronidase zou een aantrekkelijk enzym kunnen zijn voor deze prodrug benadering. Het is bekend dat in bepaalde ziekten – bijvoorbeeld verschillende soorten kanker, bacteriële en virale infecties, reumatoïde artritis en neurologische aandoeningen – hoge concentraties β-glucuronidase worden gevonden in de ruimte tussen de cellen in aangedane weefsels. In gezonde weefsels daarentegen wordt het enzym uitsluitend gevonden binnenin de cellen in de lysosomen. Selectieve prodrugs voor β-glucuronidase zijn meestal glucuronide verbindingen van het geneesmiddel, die relatief niet-toxisch zijn vanwege het water-oplosbare karakter van glucuronide groep. Dit voorkomt dat prodrugs de cel kunnen binnendringen en daardoor dat de prodrugs worden geactiveerd door β-glucuronidase in de lysosomen in gezonde cellen. In het zieke weefsel daarentegen is het enzym aanwezig buiten de cellen, waardoor de prodrug kan worden omgezet in het toxische oorspronkelijke geneesmiddel dat ter plekke zijn therapeutische effect kan bewerkstelligen.

Wanneer prodrug therapie is gebaseerd op verhoogde activiteit van β-glucuronidase in ongezond weefsel, zijn de locatie en de omvang van de expressie van β-glucuronidase waarschijnlijk de meest belangrijke factoren die weefsel specificiteit van het vrijkomen van het actieve geneesmiddel vanuit de prodrug bepalen. De variatie van β-glucuronidase activiteit in verschillende weefsels en de variatie tussen individuen is echter hoog. Daarom

zou de ontwikkeling van een niet-invasieve, klinisch toepasbare techniek om prodrug therapieën gebaseerd op β-glucuronidase te kunnen volgen en evalueren gewenst zijn. Een techniek die bijzonder geschikt lijkt om β-glucuronidase expressie zichtbaar te maken is positron emissie tomografie (PET)

Positron emissie tomografie is een nucleaire beeldvormende techniek die wordt gebruikt om cellulaire en moleculaire gebeurtenissen in het lichaam af te beelden door injectie van een positron uitzendende, radioactief gelabelde moleculaire speurstof (tracer). Een tracer voor het afbeelden van β-glucuronidase activiteit zou het mogelijk maken om de locatie en omvang van de β-glucuronidase expressie in de tijd te volgen. PET zou daarmee belangrijke informatie kunnen verschaffen over ziekten met verhoogde β-glucuronidase spiegels en de techniek zou kunnen worden toegepast om te voorspellen welke patiënten voordeel zouden kunnen hebben van β-glucuronidase prodrug therapie, waardoor de effectiviteit van de behandeling wordt verbeterd.

Gedreven door het feit dat geen geschikte PET tracers beschikbaar zijn voor het afbeelden van β-glucuronidase, was het doel van het onderzoek dat beschreven is in dit proefschrift om PET tracers voor extracellulaire β-glucuronidase enzym activiteit te ontwikkelen en om deze tracers toe te passen voor het bepalen van β-glucuronidase expressie in diverse diermodellen voor verschillende aandoeningen.

Voor glucuronide verbindingen is aangetoond dat ze selectief worden omgezet door β-glucuronidase. Alle prodrugs voor β-glucuronidase zijn dan ook glucuronide verbindingen. Derhalve zouden glucuronide verbindingen die een radioactieve groep bevatten wellicht geschikte PET tracers voor β-glucuronidase kunnen zijn. In dit onderzoeksproject zijn daarom twee glucuronide bevattende PET tracers, genaamd [^{18}F]FEAnGA en [^{18}F]FEAnGA-Me, ontwikkeld. Wanneer deze tracers het doelweefsel met verhoogd β-glucuronidase spiegels hebben bereikt, zouden ze moeten worden geactiveerd door dit enzym, waarbij de radioactieve groep 2-[^{18}F]fluorethylamine ([^{18}F]FEA) wordt gevormd. Dit radioactieve afbraakproduct zou dan in het aangedane weefsel moeten achterblijven, terwijl het intacte [^{18}F]FEAnGA snel uit het gezonde weefsel zou moeten verdwijnen zonder de cellen binnen te dringen.

Deze glucuronide bevattende PET tracers werden eerst geëvalueerd in-vitro om vast te stellen of ze daadwerkelijk worden geactiveerd in aanwezigheid van β-glucuronidase. Daarna werden de tracers in-vivo onderzocht in muizen en ratten met verschillende type tumoren. De tracers werden ook getest in ratten met een steriele ontsteking en de meest geschikte tracer, [^{18}F]FEAnGA , werd ook getest in ratten met een infectie in de hersenen. Daarnaast werd [^{18}F]FEAnGA PET onderzocht als een niet-invasief hulpmiddel voor de optimalisatie van prodrug therapie. Van prodrug therapie is bekend dat de effectiviteit in kleine tumoren lager is dan in grote vanwege de relatief lage spiegels van extracellulair β-glucuronidase in kleine tumoren. Daarom werd getest of een enkele dosis van een cytostatisch geneesmiddel zou leiden tot een verhoogde afgifte van β-glucuronidase door de tumor, hetgeen de tumor meer gevoelig zou moeten maken voor de daaropvolgende behandeling met een prodrug.

Uit de in-vitro en in-vivo evaluaties van de tracers hebben we kunnen concluderen dat [^{18}F]FEAnGA betere farmacokinetische eigenschappen heeft dan [^{18}F]FEAnGA –Me. [^{18}F]FEAnGA PET is in staat om extracellulaire β-glucuronidase aan te tonen, niet alleen in tumoren, maar ook in ontstekingen. Dit suggereert dat prodrug therapie gebaseerd of β-glucuronidase ook gebruikt zou kunnen worden in ontstekingsziekten. Ten slotte hebben we het principe kunnen bewijzen dat een enkele dosis van een cytostatisch geneesmiddel de afgifte van β-glucuronidase kan doen toenemen en dat [^{18}F]FEAnGA een geschikte tracer is om dit proces af te beelden. Deze studie zou kunnen leiden tot een twee-staps chemotherapie-prodrug benadering, waarin tumoren worden behandeld met een enkele dosis van een cytostatisch geneesmiddel om de β-glucuronidase spiegels te verhogen voor de start van de prodrug behandeling, waardoor de effectiviteit van de prodrug therapie wordt verhoogd.

RESUMO

O principal obstáculo para alcançar um tratamento eficaz no cancro ou em determinadas doenças infecciosas/inflamatórias é a erradicação da doença sem prejudicar as células e órgãos saudáveis do paciente. Esta falta de eficácia é devida principalmente às semelhanças fisiológicas entre células saudáveis e células afectadas (ou células alvo) que impedem a incorporação selectiva dos medicamentos citotóxicos apenas nas células ou orgão alvo. Contudo, existem pequenas diferenças bioquímicas e fisiológicas entre ambos os tipos de células (tal como a actividade de certas enzimas) que podem ser usadas para incorporar selectivamente alguns agentes químicos nas células alvos. Assim sendo, um novo conceito foi introduzido – terapia pró-fármica – onde o fármaco originalmente activo é transformado num pró-fármaco inactivo (ou menos tóxico) que é convertido *in vivo* no fármaco activo, por via enzimática, de forma a exercer um efeito terapêutico apenas no local desejado. A enzima β-glucuronidase é uma óptima candidata para a activação selectiva de pró-fármacos. Sabe-se que em determinadas doenças, por exemplo, vários tipos de tumores, infecções bacteriana ou viral, artrite reumatóide e disfunções neurológicas, elevados níveis de β-glucuronidase são encontrados no espaço intersticial, ao contrário das células saudáveis, onde a enzima só existe nos lissosomas presentes no interior das células. Fármacos glucuronizados são os usuais pró-fármacos selectivos para a β-glucuronidase. Eles são relativamente pouco tóxicos, devido à sua natureza hidrofílica, o que previne que estes pró-fármacos penetrem dentro das células e entrem em contacto com a β-glucuronidase lisossômica. No entanto, nas células alvo, onde a enzima está expressa extracelularmente, o pró-fármaco é convertido no fármaco activo, exercendo o seu efeito apenas no local desejado.

Sendo a terapia pró-fármica baseada na elevada actividade extracelular da β-glucuronidase no orgão-alvo, a localização e magnitude da expressão da β-glucuronidase são provavelmente os factores mais importantes relativamente à conversão específica do pró-fármaco no fármaco activo. A variabilidade na actividade da β-glucuronidase em diversos tecidos, bem como em seres humanos diferentes é elevada, tornando-se imperativo o desenvolvimento de tecnologias não invasivas e clinicamente aplicáveis para

monitorizar e avaliar a terapia pró-fármica com base na β-glucuronidase. Uma técnica que parece especialmente adequada para visualizar a expressão da β-glucuronidase é a Tomografia por Emissão de Positrões (PET). PET é uma sofisticada técnica de imagem usada em medicina nuclear para detectar alterações a nível celular/molecular do organismo por injecção de um radiofármaco emissor de positrões. Assim sendo, havendo um radiofármaco especifico para avaliar a actividade da β-glucuronidase será possível monitorizar a localização, magnitude e persistência dos níveis de β-glucuronidase ao longo do tempo, permitindo a obtenção de informações cruciais relativamente a doenças onde os níveis de β-glucuronidase extracelular são elevados. Podendo ainda ser utilizado para prever quais os pacientes elegíveis para a terapia pró-fármica melhorando a eficácia do tratamento.

A falta de radiofármacos PET para a monitorização da β-glucuronidase extracelular deu origem ao trabalho desenvolvido nesta tese que teve como objectivo a síntese de novos radiofármacos PET específicos para a β-glucuronidase para a avaliação da actividade da β-glucuronidase extracelular em diferentes modelos animais com diferentes enfermidades.

Os novos radiofármacos desenvolvidos nesta tese: [^{18}F]FEAnGA e [^{18}F]FEAnGA-Me, possuem uma estrutura idêntica aos fármacos glucuronizados (selectivos para a β-glucuronidase), onde o composto activo foi substituído por uma cadeia alquílica contendo a radionuclido [^{18}F], denominada de [^{18}F]Fluoroetilamina ([^{18}F]FEA) . Após administração no paciente, e uma vez atingido o orgão-alvo onde a β-glucuronidase se encontra expressa extracelularmente, o radiofármaco deverá ser convertido pela enzima e a fracção radioactiva, [^{18}F]FEA, será selectivamente incorporada no alvo, enquanto que o restante radioafármaco que não foi convertido ([^{18}F]FEAnGA ou [^{18}F]FEAnGA-Me) será rapidamente excretado devido à sua natural hidrofilicidade.

Estes radiofármacos de PET foram inicialmente avaliados *in vitro* para confirmar a sua conversão por intermédio da enzima. Posteriormente, foram avaliados *in vivo*, em ratos, com diferentes tipos de tumores. [^{18}F]FEAnGA e [^{18}F]FEAnGA-Me também foram

testados *in vivo* num modelo de inflamação estéril. Enquanto que o radiofármaco mais promissor, [^{18}F]FEAnGA, foi igualmente testado *in vivo* num modelo de neuroinflamação.

Apesar da terapia pró-fármica ser um conceito bastante promissor também possui desvantagens, tal como a ineficácia no tratamento de pequenos tumores devido à falta de β-glucuronidase extracelular presente no tumor. Por esta razão, tentou-se avaliar se a administração prévia de uma dose única de um citostático aumentaria a libertação de β-glucuronidase, resultando numa maior eficácia do tratamento pró-fármico.

Com todos estes estudos foi possível concluir que o radiofármaco [^{18}F]FEAnGA possui uma melhor farmacocinética *in vivo* que o seu análogo [^{18}F]FEAnGA-Me. [^{18}F]FEAnGA não só consegue detectar a actividade enzimática da β-glucuronidase em tumores como também em lesões inflamatórias. Sugerindo que talvez a terapia pró-fármica também possa ser utilizada no tratamento de doenças inflamatórias. No último estudo *in vivo* foi possível confirmar que uma única dose de um citostático é suficiente para aumentar a libertação de β-glucuronidase e que o radiofármaco [^{18}F]FEAnGA é indicado para seguir este processo. Com este último estudo abriu-se caminho para uma nova estratégia de 2 passos, cujos tumores são previamente tratados com uma dose única de um citostático de modo a aumentar os níveis de β-glucuronidase extracelular antes do tratamento pró-fármico de modo a aumentar a eficácia no tratamento pró-fármico.

Acknowledgments

It is unbelievable that I eventually reached this final chapter of my thesis. Thus, "At last but not the least" I would like to express my gratitude to all of you who made this thesis a reality ☺

First I would like to thank Prof. dr. R.A.J.O. Dierckx (Rudi) for giving me the opportunity to conduct this PhD project. I'm especially grateful to be given the chance to participate in high quality congresses which opened my eyes and mind to the world of Nuclear Medicine. I also would like to thank you, Prof.dr.H.J. Haisma and Prof.dr. P.H. Elsinga, for your priceless support, inspiration, suggestions and comments. Without your guidance, the completion of this thesis would not have been possible.

As for you Erik, I found it very hard to describe in a few words the gratitude, respect and admiration I have for you. You were my supervisor and teacher. Definitely without you guidance and endless help, this thesis would not exist. You were always there when I needed you and you always found time for me in your busy schedule. Your constant optimistic and constructive spirit was very encouraging. A very thank you for never giving up and for believing in me.

I would also like to thank the reading committee, Prof.dr. A. Verbruggen, Prof.dr. G.A.M.S. van Dongen and Prof.dr. G.A.P. Hospers, for taking the time to read this thesis and for their comments.

To the department of Pharmaceutical Gene Modulation from the University Center of Pharmacy, Groningen I would like to thank Janine Buitendijk, Frank Dekker and Marije Scholte for all their help over the last years.

I would like to acknowledge the GUIDE office: Banus and Maaike for helping me with all the papers and formalities and for organizing the courses.

For the CDP I wish to thank Dr. Wiebe Hofstra, Silvia, Arie and Hilda for all your help in the animal studies.

Very warm and big thanks for the entire Nuclear Medicine and Molecular Imaging department (NGMB). Especial thanks for Annie van Zanten, for solving all my administration/financial adversities during these years. My gratitude also goes to Ineke for being my rescuer in the administration world ☺

To Jan, Niels and Klaas Pieter, I will always be grateful for your medical point-of-view given in many occasions.

To Hans Pol, Arja and Erna, thank you for always having a smile and making me feel at home.

To Gert and Jitze, thank you for keep reminding me to work in safety ☺

To Hilde, Berta, Joost, Chantal, Michel, Janet and Ewout, thank you for the many pleasant days we had in the lab. Could not imagine a better place and better colleagues to work with!!! To the rest of the colleagues in the NGMB department, please forgive me for not mentioning all your names but thank you for everything.

To the physicists Prof.dr Anne Paans, Antoon, Johan, Sergiy, Marcel, Noortje, I would like to express my gratitude for all the input you gave in analyzing and interpreting the data, but also for helping me when I most needed.

To Aren a very big thanks for finding time to correct my manuscripts and for all your additional help in the *in vivo* studies. Speaking of *in vivo* studies I could not forget to mention dear Jurgen for all your patients and help in the animal studies and for always having a plan B or C or even D when it was needed.

To my dear former and present "room-girls": Janine, Silvana, Leila, Ania, Valentina, Mershima and Danielle. I'm very grateful that I made this adventurous journey in your company. The fun, support, the exchanged knowledge and of course the chocolate Fridays are some of the special memories that I will keep with me forever (although I'm very happy that the chocolate Fridays became fruit Fridays, right Leila?). To Janine thanks for teaching me so many things during these years. To my dear friend Silvana, thank you for being there when I most needed. You are one of a kind!!! "Scheissa" Leila, couldn't you have taught me a better German word? Ania thank you for not letting my plants die. Vale, can not thank you enough for all your help and friendship. Mershima what would be me without your magnetic field? Danielle muito obrigada pelos nossos momentos lusitanos e

pela tua amizade. To the rest of PhD students, thank you for all the nice moments we shared.

As for my remaining friends from Groningen (Giuseppe, David, Érika, Federica, Reza, Vahid, Hans, Nathalie, Andrea, Zilin, Jorge, Rei, Katica, Chris) thank you for all the amazing moments that we shared over these years.

Of course for you my dear Julia I have to thank you separately. The numerous moments we shared are far too many to be mention in a single paragraph. But I do want to acknowledge all our brainstorming moments (which were a lot) that made the highlight of our meetings whenever we met. Hope you don't go too far so we can keep having these nice brainstorms☺.

I would like to express my gratitude to Dr. Maria dos Anjos Neves for all the knowledge I gained during the time I worked with you. But most importantly, for you believing in me and giving me the courage to apply for this PhD project ☺

To my paranymphs Roel and Bram thank you very much for all your support and help. For you Roel thank you for being my good friend for all theses years and hopefully for many years to come. As for you Bram I can not thank you enough for everything you have done for me. Between the ups and downs of a radiochemist, I found you (or you found me… depending on the point of view). Thank you for your priceless support, for making the impossible things happen, and for your understanding during the hard and stressful moments in this thesis time. Thank you for being my right hand, my best friend and my partner☺.

À minha mãe gostaria de agradecer todo o apoio que me concedeste ao longo desta aventura. Por inúmeras vezes transmitiste-me a confiança necessária para eu ultrapassar todos os meus obstáculos e as minhas dúvidas que me permitiram chegar onde estou hoje.

O mesmo te posso dizer a ti pai. Sem ti todo este trabalho não teria sido possível. O teu apoio incondicional e a tua amizada foram e serão sempre muito importantes para mim.

À minha restante família gostaria de vos agradecer por todo o vosso apoio e compreensão. For my remaining family thank you very much for all your support and a special thanks to Els which knew exactly what to say when I most needed.

Por fim gostaria de agradecer e dedicar esta tese à minha Carolina (Karol). Tu és a minha motivação, fonte de inspiração e, acima de tudo, a minha admiração. Obrigada princesa!

List of Abbreviations

1TCM	One tissue compartment model
2TCM	Two tissue compartment model
AUC	Area under the curve
β-GUS	β-glucuronidase
CNS	Central nervous system
CT	Computed tomography
DMEM	Dulbecco's modified eagle medium
DNR-GA3	*N*-[4-(daunorubicin-*N*-carbonyl-oxymethyl)phenyl]-O-β-glucuronylcarbamate
DOX	Doxorubicin
DOX-GA3	*N*-[4-doxorubicin-*N*-carbonyl(oxymethyl)phenyl] O-β-glucuronyl carbamate
FEA	Fluoroethylamine
FEAnGA	1-O-(4-(2-Fluoroethyl-carbamoyloxymethyl)-2-nitrophenyl)-O-β-D-glucopyronuronate
FEAnGA-Me	Methyl 1-O-(4-((2-fluoroethylcarbamoyloxy)methyl)-2-nitrophenyl)-β-D-glucopyronuronate
FHBG	9-(4-Fluoro-3-hydroxymethylbutyl)guanine
FIAU	2'-Deoxy-2'-fluoro-5-iodo-1-β-Darabinofuranosyluraci
$Glu^{540/451}$	Glutamic acid
HMR 1826	*N*-(4-b-glucuronosyl)-3-nitrobenzyloxycarbonyl-doxorubicin
HNBA	4-Hydroxy-3-nitrobenzyl alcohol
HPLC	High- performance liquid chromatography
i.p.	Intraperitoneal
i.t.	intratumoral
i.v.	intravenous
K_{cat}	catalytic rate of an enzyme
kDa	kilo dalton
K_M	Michaelis constant

LDL	Low-density lipoprotein
LPS	Lipopolysaccharide
min	minutes
NMR	Nuclear magnetic ressonance
p.i.	*post* injection
PET	Positron emission tomography
PMN	Polymorphonuclear cells
PNP	4-nitrophenyl
PNPG	4-nitrophenyl glucuronide
ppm	Parts per million
PTFE	Politetrafluoroethylene
ROI	Region of interest
rpm	Rotations per minute
RP-HPLC	Reverse phase high-performance liquid chromatography
s	seconds
SPECT	Single-photon emission computed tomography
Tyr504	Tyrosine
TLC	Thin-layer chromatography
TMS	Tetramethylsilane
V_{max}	Maximum rate